Compartmental Investigation of Brain Energy Metabolism using Radiotracer Kinetics

---

Dissertation

zur

Erlangung der naturwissenschaftlichen Doktorwürde
(Dr. sc. nat.)

vorgelegt der

Mathematisch-naturwissenschaftlichen Fakultät

der

Universität Zürich

von

Matthias Tasso Wyss

von

Zürich ZH und Alchenstorf BE

Promotionskomitee

Prof. Dr. Kevan Martin (Vorsitz)

Prof. Dr. med. Alfred Buck (Leitung der Dissertation)

Prof. Dr. Jean-Marc Fritschy

Zürich, 2009

for my wonderful princesses

Mirjam, Nada and Noée

The important thing is not to stop questioning. Curiosity has its own reason for existing. One cannot help but be in awe when he contemplates the mysteries of eternity, of life, of the marvelous structure of reality. It is enough if one tries merely to comprehend a little of this mystery every day. Never lose a holy curiosity.

Albert Einstein (1879 - 1955)

List of content

List of figures

Summary

The measurement of metabolism-related processes *in vivo* is a critical prerequisite for a better understanding of brain metabolism and its relationship to the brain at work. For a long time it was supposed that blood-borne glucose was the sole energy substrate of brain cells and that it was metabolized by the neurons and the astrocytes more or less independently.

Only during the last few decades did one begin to appreciate the compartmentalization of energy metabolism between neurons and astrocytes. The finding of an activity-dependent glutamate mediated activation of the astrocytic glycolysis to generate and release lactate has led to the idea of an astrocyte neuron lactate shuttle (ANLS). The ANLS hypothesis claims that neurons take up the astrocytic lactate and use it for oxidation. This hypothesis has provoked a vivid debate about lactate use of neurons as an energy substrate.

This project aimed at measuring the kinetics of positron emitter labeled tracers for the investigation of specific metabolic compartments of the neuron-astrocyte unit. *In vivo* radiotracer studies are useful tools to estimate the exchange of specific substances between different compartments. They can be performed both in animals and humans.

The project was divided into three main parts:

First, astrocytic oxidative metabolism was investigated using 1-^{11}C-acetate. It turned out that this is a promising tracer to investigate astrocytic oxidative metabolism in rats and humans. An increased radioactivity washout was found during brain activation pointing to an increase in astrocytic oxidative metabolism during increased synaptic activity. Different pharmacological interventions supported the hypothesis that the measured acetate turnover is indeed related to oxidative metabolism.

In a second part, we focused on neuronal oxidative metabolism. Inspired by previous reports demonstrating preferential lactate uptake by neurons, we evaluated the newly synthesized radiotracer 1-^{11}C-L-lactate with respect to its kinetic properties in the rodent brain and were able to

demonstrate its feasibility to quantify cerebral lactate oxidation *in vivo*. We could show increased cerebral - most probably neuronal - lactate oxidation during increased brain activity. We further hypothesize, that the kinetics of 1-^{11}C-L-lactate is not only measuring lactate metabolism, but is in addition an indicator of total neuronal oxidative metabolism.

In a final method-oriented part of the project, we introduced a novel high-sensitivity surface probe for the measurement of radiotracer concentration through the intact although thinned skull. We demonstrated its ability to measure glucose utilization and blood flow in the rat cerebral cortex. This new development potentially broadens the field of applications for beta probes compared to conventional intracortical beta scintillators. Due to its decreased invasiveness it was successfully applied in the conscious animal.

In summary, we demonstrated the usefulness of radiotracer methods for the investigation of specific aspects of cerebral energy metabolism and improved the methodology of beta probes.

Zusammenfassung

Mit radioaktiv markierten Substanzen können veschiedene Stoffwechselvorgänge im lebenden Organismus untersucht werden. Ein grosser Vorteil dieser Methode ist ihre Anwendbarkeit in Humanstudien mittels Positronenemissionstomographie. Viele Arbeiten benutzten ^{18}F-Fluorodeoxyglukose, ein radioaktiv markiertes Glukoseanalog, für die Messung des zerebralen Glukoseumsatzes. Dieser stellt ein globales Mass für die Energiestoffwechselvorgänge dar, erlaubt aber keine Aussagen über die involvierten zellulären Kompartimente. In den vergangenen Jahrzehnten wurde aber klar, dass der Hirnstoffwechsel in den Astrozyten und den Neuronen räumlich und zeitlich sequestriert ist. Gleichzeitig besteht eine enge Kooperation zwischen den beiden Zelltypen. Dies wurde mit der Formulierung der sogenannten Astrozyten-Neuronen-Laktat-Shuttle Hypothese unterstrichen. Diese besagt, dass aktivitätsabhängig in den Astrozyten gebildetes Laktat von den Neuronen zur Energiegewinnung verwendet wird.
Ziele dieses Projektes waren A) Charkterisierung der Gewebekinetik von radioaktiv markiertem Azetat und Laktat und B) Anwendung dieser Substanzen zur Untersuchung des astrozytären (Azetat) und neuronalen (Laktat) oxidativen Stoffwechsels.

Es ist bekannt, dass Azetat vorwiegend von den Astrozyten aufgenommen wird. Wir stellten daher die Hypothese auf, dass mit radioaktiv markiertem Azetat der astrozytäre Stoffwechsel untersucht werden kann. Experimente mit verschiedenen pharmakologischen Interventionen zeigten, dass die Auswaschrate des radioaktiven Labels mit grosser Wahrscheinlichkeit ein Mass für die CO_2 Produktion und damit des Sauerstoffverbrauchs ist. Unter elektrischer Stimulation des Infraorbital-Nervs stieg der so gemessene astrozytäre Sauerstoffverbrauch markant an.

In Analogie zu den Azetat Experimenten untersuchten wir in einem zweiten Teil den neuronalen oxidativen Stoffwechsel mit markiertem Laktat (1-^{11}C-L-Laktat). Grundlage dieser Experimente sind Hinweise, dass Laktat präferenziell von den Neuronen aufgenommen wird. Auch bei Laktat ist es wahrscheinlich, dass die Auswaschrate des Labels den oxidativen Stoffwechsel reflektiert. Die

Experimente zeigten wie bei Azetat einen markanten Anstieg der Labelauswaschrate unter Stimulation, welchen wir als gesteigerten neuronalen Sauerstoffverbrauch deuten.

In einem letzten Teil der Arbeit ging es darum, die angewandte Messtechnik weiter zu verfeinern. Wir entwickelten eine Betasonde, mit welcher das Radioaktivitätssignal durch den Schädelknochen hindurch gemessen werden kann. Dieses neue Gerät ist etwa 20-mal sensitiver als das zuvor verwendete System. Dank dieser Sensitivitätssteigerung war es möglich, zwei Injektionen im selben Tier vorzunehmen, womit die Varianz der Daten erheblich gesenkt wurde. Als letztes konnten wir demonstrieren, dass mit der neuen Sonde Messungen am wachen Tier möglich sind.

Acknowledgements

All the work performed during my MD PhD project was done in the lab of Alfred Buck and Bruno Weber at the Department of Nuclear Medicine in the University hospital of Zürich. I'm very grateful to them for their fundamental technical help, their scientific support, for many enlightening discussions and also for various wonderful experiences and activities outside the laboratory environment. Without these two mentors I probably would not have started the MD PhD program. Jean-Marc Fritschy and Kevan Martin I want to thank for being in my MD PhD thesis committee and for their scientific supervision of the project. They observed my work progress and were always available for administrative, technical and scientific support.

I always compare experimental research with team sport. Without a motivated team and the assistance of many others, experiments would not be possible to be performed successfully. I was very lucky to be a member of an enthusiastic and motivated lab team. I want to say thank you to all which were joining the work group during my time working on these projects (Nicolas Späth, Valerie Treyer, Stefan Heer, Florent Haiss, Nicolas Obrist, Cristina Zunzunegui, Novella Calcinaghi, Nadja Olini, Daniele Nolan, Renaud Jolivet, Rajesh Ramaswamy and Johannes Reichold (if somebody got lost 'mea culpa est')).

A large thank you should go to the Radiochemistry staff (Rolf Hesselmann, Gerrit Westera, Konstantin Drandarov, Tibor Cservenyak, Zoran Vujicic, Petra Pavlicek, Cécile Dumas, Angela Llamazares, Matti Mustonen, Ufuk Oezdemir, Bruno Mancuso and Anass Johayem). They never gave up in improving tracer synthesis and increasing radiochemical yield. Regularly they produced radiotracers especially for my studies beside their daily clinical productions. They always fulfilled my special wishes concerning the special requirements for radiotracers used in small laboratory animal experiments.

I would like to thank Gustav von Schulthess and the Clinic for Nuclear Medicine for the enormous support and the access to the imaging facilities of the Nuclear Medicine Dapartment for the human studies in the PET center.

A great thank-you belongs to my parents, my brothers and my friends for their assistance and encouragement I got from them throughout my MD PhD time in particular and during my hitherto life in general. My parents built me a stable basement for my life and provided me the opportunity to get the education I passed. My brothers (Simon, Ueli and Jürg) were always available when I needed them.

A very special thanks for her love and her support belongs to my wife Mirjam. She was a comfort to me in hard and shared happiness in good times. Last but not least I want to mention my two little daughters Nada and Noée who challenged me every day beside all the scientific challenges.

This work was supported by the swiss national science foundation (grants 3100 A0-105804/1 and PP00B-110751/1) and the OPO Stiftung Zürich.

List of definitions

AIC = Akaiche information criterion

A measure for the goodness of fit of an estimated statistical model. In Kinetic modeling it is used as a tool for model selection. Given a data set, several competing models are ranked according to their AIC, with the one having the lowest AIC being the most accurate.

ANLSH = Astrocyte-neuron-lactate-shuttle hypothesis

Present concept about the intercellular organization of brain energy metabolism and its coupling to synaptic activity. See page 19 and ***Figure 2*** for explanation.

AR = Autoradiography

A method to determine the distribution of a radiolabeled ligand on tissue sections. See page 31 for further description of the methodology.

ATP = Adenosine-5'-triphosphate

Beside many other functions it is the most important 'energy currency' transported within cells. Net production during glucose degradation.

BBB = Blood brain barrier

A protective barrier formed by the blood vessels and glia of the brain. It prevents plenty of substances in the blood from entering the brain tissue.

BOLD fMRI =

Functional magnetic resonance imaging relying on the detection of intrinsic changes in haemoglobin oxygenation assumed to imply underlying neural activity.

CBF = Cerebral blood flow

Blood supply to the brain in a given time. In an adult, CBF is typically about 15% of the cardiac output.

CNS = Central nervous system

It consists of the brain and the spinal cord and is enclosed in the meninges. It coordinates the neuronal activity of all parts of the body of a multicellular organism.

EF = First pass extraction fraction

The fraction of a radiotracer which is extracted from the brain during its first passage after injection. The EF is highly dependent on cerebral blood flow expressed by the equation EF = K_1/CBF.

FWHM = Fuel width at half maximum

Image resolution of a PET scanner is determined by the FWHM of a point spread function.

^{18}F-FDG = ^{18}F-fluorodeoxyglucose

Analog of glucose labeled with fluorine-18 often used for the determination of glucose utilization *in vivo* using radiotracer methods such as PET.

GABA = Gamma aminobutyric acid

The main inhibitory neurotransmitter in the mammalian central nervous system. It plays an important role in regulating neuronal excitability throughout the nervous system.

GLAST = Glutamate aspartate transporter

One of the five glutamate transporters identified so far in the brain. It is also often called excitatory amino acid transporter 1 (EAAT1). It is highly expressed in astrocytes allowing them to be responsible for most of glutamate uptake during synaptic transmission. It mediates the transport of glutamate from the synaptic cleft with the cotransport of 3 sodium ions. This co-transport allows the

transport of glutamate against a concentration gradient into the cell. This is an important process to avoid excitatory damage in the brain.

GLT-1 = Glial glutamate transporter

It is also called excitatory amino acid transporter 2 (EAAT2). Like GLAST it is predominantly localized in astrocytes and responsible for sodium-dependent astrocytic glutamate upake.

GLUT = Glucose transporter

Twelve membrane-spanning domains containing proteins enabling the facilitative transport of glucose across cell membranes. Actually 14 members have been identified. GLUT1 (BBB and astrocytes) and GLUT3 (neurons) are the predominant cerebral glucose transporters.

K_1, k_2, k_3, .., k_n = Rate constants

Regularly used in kinetic modeling to describe the transfer of radiotracer between the compartments of a n/2-tissue compartment model. They are assumed to be linearly related to the concentration differences between two compartments. On pages 23 - 30 the principles are further explained.

K_m = Dissociation constant

This is a commonly used parameter to describe the affinity between a ligand and a protein (e.g. receptor, transport protein). The dissociation constant has molar units, which corresponds to the concentration of a ligand at which the binding site is half occupied. The smaller the dissociation constant the higher the affinity of the ligand for its target site.

LC = Lumped constant

This constant calibrates for the differences in transport and phosphorylation rates between the glucose analog fluorodeoxyglucose and glucose in tissue. It is required for rigorous calculation of the glucose metabolic rate from radiotracer experiments using ^{18}F-FDG.

LCMRglu = Local cerebral metabolic rate of glucose

Number to quantify glucose utilization in the brain. Usually given in µmol/100g/min.

LDH = Lactate dehydrogenase

This enzyme catalyzes the conversion of pyruvate to lactate and vice versa. LDH is a rate-limiting enzyme in lactate fluxes. In vertebrates 5 isoforms are so far identified. In brain especially LDH-1 (present in neurons) and LDH-5 (enriched in astrocytes) play an important role.

MCT = Monocarboxylate transporter

Proton-linked transporters located at the plasma membrane responsible for the transport of monocarboxylic acids such as lactate. At least 9 MCTs-related genes have so far been identified in mammals.

MRS = Nuclear magnetic resoncance spectroscopy

A method exploiting the magnetic properties of certain nuclei. It has proven a unique tool for the measurement of metabolic fluxes in brain. Read page 39 for more details.

NAD+/NADH = Nicotinamide adenine dinucleotide

A coenzyme found in all living cells. In metabolism, NAD+/NADH are involved in redox reactions carrying electrons from one reaction to another.

NADPH = Nicotinamide adenine dinucleotide phosphate

In cells of the brain, as in other organs, this reduced substrate provides the reducing power. In addition, NADPH is needed for the scavenging of reactive oxygen species.

PET = Positron emission tomography

A non-invasive nuclear medicine imaging technique often applied in human neuroimaging. It produces three-dimensional images of functional processes. On pages 34 -35 the method is introduced in detail.

RQ = Respiratory quotient

The RQ is calculated from the ratio $CO_{2\ produced}$/ $O_{2\ consumed}$. The range of RQ for humans usually ranges from 1.0 (representing pure carbohydrate oxidation) to ~0.7 (representing pure fat oxidation).

TAC = Time activity curve

Curves obtained by kinetic radiotracer experiments describing the radioactivity concentration in the tissue under study over time.

TCA cycle = Tricarboxylic acid cycle (syn. Krebs' cycle)

Part of the metabolic pathway involved in the oxidative degradation of carbohydrates, fats and proteins into carbon dioxide and water to produce energy. The TCA cycle occurs in the matrix of mitochondria. It is also known as the citric acid cycle.

Introduction

The main function of the brain consists of dealing with information. This involves transfer, processing and exchange of information. The work of the brain is closely linked to metabolism, i.e. changes in the electrical activity of neurons are tightly coupled to changes in metabolic substrate use and local blood flow (for a review see (Raichle and Mintun 2006)). The tight connection of electrical activity to physiological processes such as blood flow was already postulated more than one century ago in a seminal work by (Roy and Sherrington 1890). This relationship forms the basis of functional neuroimaging methods such as positron emission tomography (PET; Reivich et al. 1977; Reivich et al. 1979) and functional magnetic resonance imaging (fMRI; Ogawa et al. 1992). These two techniques are the most widely used methods in the field of brain imaging today, underlined by an enormous number of publications in this field. Whereas fMRI measures signals related to haemodynamics and oxygen consumption – known as blood oxygen level dependent (BOLD) signals, PET is able to investigate a variety of different pathways and compartments. This capability of PET mainly depends on the radiotracers used. For the study of brain energy metabolism especially ^{18}F-fluorodeoxyglucose (^{18}F-FDG) has been used extensively up to date. Originally the method of determining glucose utilization using radiolabeled glucose analogues was introduced by Sokoloff for the use in rodents (1977) together with autoradiography and was later refined for the application in humans using PET (Reivich et al. 1977; Reivich et al. 1979). The approach gives an excellent regional metabolic differentiation, but it does not distinguish between different compartments such as neuronal and glial cells. However, such compartmental differentiation is of major importance to make a step further in the current understanding of mechanisms and relationships underlying brain energy metabolism. Today, it is widely accepted that brain metabolism is compartmentalized not only on a cellular level between neurons and glial cells, but also on a subcellular level e.g. between tricarboxylic acid (TCA) cycle in mitochondria and anaerobic glycolysis in the cytoplasm of the cells (Hertz 2004).

The current thesis project mainly aims at evaluating new approaches to measure distinct metabolic compartments in the brain (i.e. oxidative metabolism in neurons and astrocytes) based on the

measurement of radiotracer kinetics. In this context the following introduction reviews the central concepts and fundamentals about brain metabolism and its measurement using radiotracer methods.

Brain energy metabolism

Benchmark data of the brain

The brain is an organ that displays high metabolic activity, which manifests itself in remarkable numbers. Although it claims only ~2% of body weight, it receives ~15% of the cardiac output and accounts for about 20% of total body oxygen consumption, as well as 25% of total body glucose utilization. Already these proportions demonstrate that cerebral energy metabolism and energy budgeting play an important role. This becomes even clearer if one considers that brain functions arrest after 2 minutes of interrupted blood circulation and that consciousness is lost already after approximately 15 seconds of oxygen deprivation. The size of the endogenous stores of energy substrates is the main reason for this dependence. Compared to their rates of utilization, they are small and their turnover rates are slow (Choi et al. 2003; Watanabe and Passonneau 1973). For example, glycogen reserves are about 10 to 100 times smaller than in the liver (Brown and Ransom 2007).

Present concepts of brain energy metabolism

Glucose: The major energy fuel

The respiratory quotient (RQ), which is calculated from the ratio $CO_{2\ produced}/O_{2\ consumed}$, helps to make a statement about the composition of the diet an organ consumes. The ranges of RQs go from 1.0 (representing complete carbohydrate diet) to ~0.7 (expected for pure fat oxidation). The RQ of the brain is close to 1, indicating that carbohydrates are the main substrates of cerebral oxidative metabolism. For a long time blood-borne glucose was regarded to represent the major and only energy substrate for the brain supporting neuronal activity (Siesjo 1978; Sokoloff 1989). Glucose crosses the vascular endothelial cells and enters the brain cells via specific facilitative glucose transporters (GLUT) along its concentration gradient (McEwen and Reagan 2004; Vannucci et al. 1998; Vannucci et al. 1997). The two main isoforms of glucose transporters found in brain are GLUT1 and GLUT3 (Maher et al. 1993; Maher et al. 1994). GLUT1 is present in two isoforms, namely in a highly glycolysated form (55 kDa) at the blood brain barrier (BBB) and in a less glycosylated form (45 kDa) predominantly present in glial parenchyma (Morgello et al. 1995). The isoform GLUT3 is present mainly in neurons (Maher et al. 1993; Maher et al. 1994). GLUT density and therewith glucose transport increase upon stimulation by glutamate within the range of a few seconds. This represents the fastest stimulation of mammalian glucose transport known to date (Duelli and Kuschinsky 2001; Loaiza et al. 2003). Following this first step in glucose utilization, glucose is processed via the same pathways as in other tissues. This includes its sequential degradation in cytosolic glycolysis and oxidative metabolism in the mitochondria resulting in complete degradation to CO_2 and H_2O (***Figure 1***).

One molecule of glucose yields 38 molecules of the energy fuel adenosine triphosphate (ATP) during complete oxidation. However, the relative contribution of neuronal and astrocytic glycolysis and respective TCA cycle activities to the total cerebral energy budget is not clear at present and highly controversial. Beside its role as energy fuel, glucose also serves as a precursor by entering several biochemical pathways. Glucose plays an important role in the synthesis of the three key neurotransmitters of the brain (gamma amino butyric acid (GABA), glutamate and acetylcholine (anaplerotic reactions)) as well as in the pentose phosphate pathway that provides nicotinamide

adenine dinucleotide phosphate (NADPH) needed for the scavenging of reactive oxygen species.

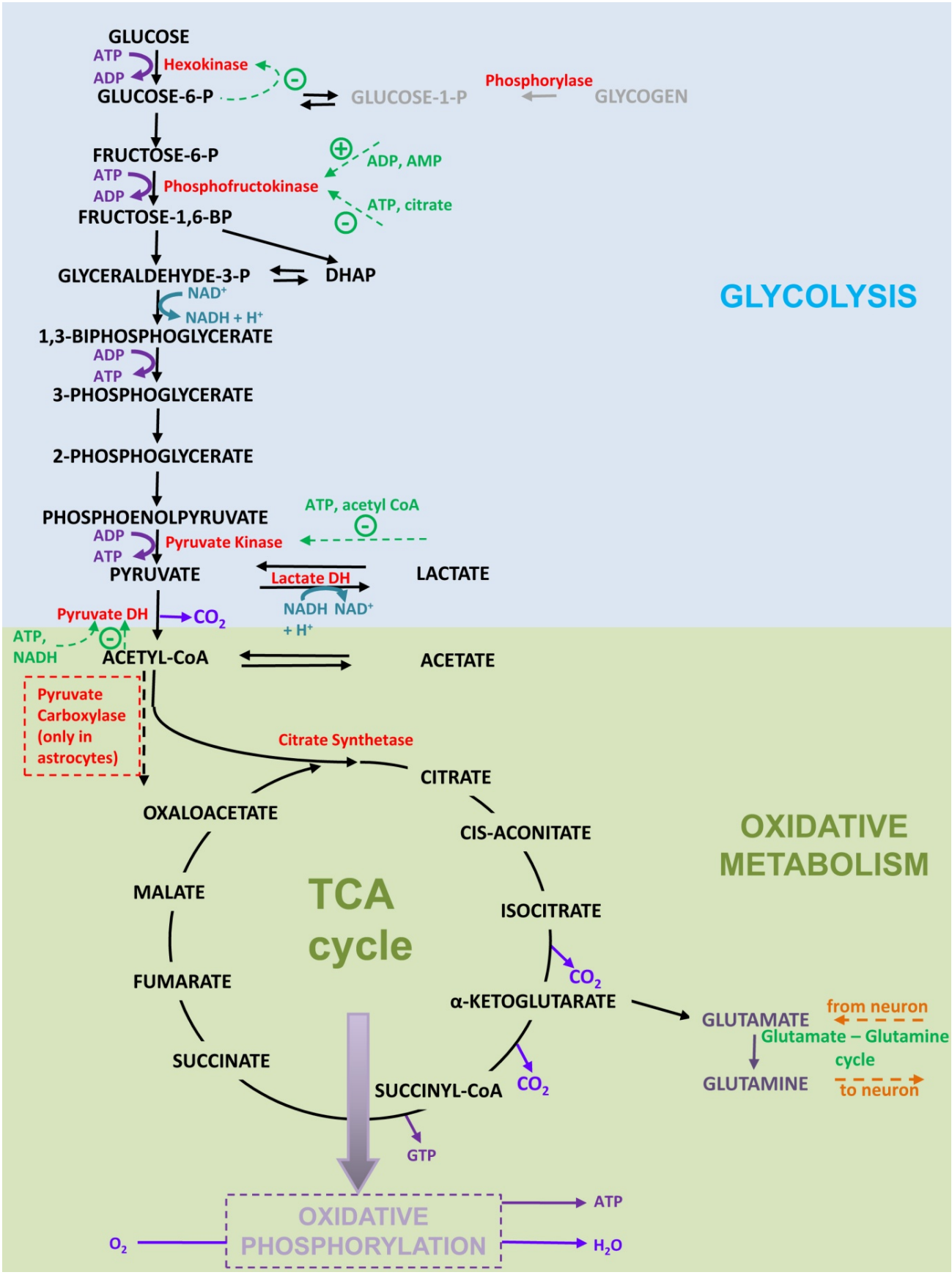

Figure 1. Main metabolic pathways involved in the degradation of glucose for the generation of energy

(See figure legend on the next page.)

In the upper part of the scheme (light blue background) the glycolysis – anaerobic degradation of glucose to pyruvate/lactate - is shown. Phosphorylation to glucose by hexokinase is the first regulation step. This enzyme is inhibited by glucose-6-phosphate. In addition the possibility of glucose storage as glycogen is indicated (in the brain this is only known to occur to a limited extent in astroytes).
Two other important steps in the regulation of glycolysis are the steps catalyzed by the enzymes phosphofructokinase and pyruvate kinase. Their activity is controlled by adenosine triphosphate (ATP), citrate and acetyl CoA. Pyruvate is in equilibrium with lactate catalyzed by lactate dehydrogenase (lactate DH) and regenerating NAD+ which is necessary to sustain glycolysis after glyceraldehyde 3-phosphate.
The lower part of the diagram (light green background) depicts the tricarboxylic acid cycle (syn. Krebs' cycle) with its substrates. Pyruvate dehydrogenase (Pyruvate DH) decarboxylates pyruvate to acetyl CoA, which enters the cycle by reacting with oxaloacetate to citrate. Pyruvate dehydrogenase activity is inhibited by ATP and NADH. In addition, the link to the glutamate/glutamine cycle, which plays an important role in the interplay of astrocytes and neurons, and the oxidative phosphorylation downstream of the TCA cycle are added (for details see main text).

Use of alternative substrates

Under special conditions the brain has the capability to use energy substrates other than glucose. The mammalian brain contains transport mechanisms that allow alternative substrates such as lactate to cross the BBB via specialized monocarboxylate transporters (MCT). Recently an additional Na+-coupled transport system in neurons for L-lactate, short-chain fatty acids and ketone bodies was described (Martin et al. 2006b).

In breast-fed newborns and suckling rats the utilization of ketone bodies and monocarboxylates by the brain is increased (Cremer 1982; Cremer et al. 1979; Dombrowski et al. 1989; Hawkins et al. 1971; Nehlig and Pereira de Vasconcelos 1993). A few studies have also suggested under certain circumstances monocarboxylates and ketone bodies can represent energy substrates for the adult brain. In the case of prolonged starvation and diabetes, an increase in brain ketone bodies utilization has been documented (Gjedde and Crone 1975; Hawkins et al. 1986; Mason et al. 2006) and monocarboxylic acid transport in the brain is increased about twofold in patients with Diabetes Type I during hypoglycaemia (Mason et al. 2006). Net lactate utilization by the brain was also reported during and after exercise-induced (Dalsgaard and Secher 2007; Ide et al. 2000) and artificially induced hyperlactatemia (Smith et al. 2003). The discussion about lactate use of the normal mammalian brain has become especially vivid after the formulation of the astrocyte-neuron lactate shuttle hypothesis (see below).

Compartmentation of brain metabolism

In parallel to the discovery of possible alternative substrate use by brain cells the finding of metabolic compartmentation in the central nervous system (CNS) received increased attention. Already forty years ago distinct compartments in brain metabolism were suggested. It was stated that at least two compartments were involved (two distinct TCA cycles) (Berl et al. 1970; Berl et al. 1968). Using ^{14}C labeled substrates a large and a small glutamate pool were postulated. One TCA cycle metabolizes acetate and is associated with a small pool of glutamate which is the precursor of glutamine, the so-called 'small' compartement (its TCA cycle was termed 'synthetic' with reference to the synthesis of glutamine). The second TCA cycle, more or less inaccessible to acetate and not associated with glutamine synthesis, was termed 'large' compartment (Berl et al. 1970; Berl and Frigyesi 1969; Cremer 1970; Van den Berg et al. 1969; Van den Berg and Ronda 1976). Using immunohistochemical studies the small compartment was identified eventually as astrocytic and the large as neuronal (Martinez-Hernandez et al. 1977; Minchin and Beart 1975a; Minchin and Beart 1975b; Norenberg and Martinez-Hernandez 1979). Moreover, compartmentation was discovered to be at least in part due to the different enzymatic equipment of neurons and astrocytes. Glutamine synthetase was found to be localized specifically in astrocytes (Martinez-Hernandez et al. 1977; Norenberg and Martinez-Hernandez 1979) whereas the enzyme glutaminase is primarily enriched in neurons (Cangro et al. 1984).

During the last decade the evidence about the highly compartmentalized metabolism in brain tissue further increased and the interest in the function of the astrocytes in this interplay entered the scene of neuroscience (Hertz 2004; Hertz et al. 2007; Volterra and Meldolesi 2005). The astrocytes were now regarded as active and important partners of neuronal cells in the metabolic cooperation. It has been found that the metabolic compartments are active in a highly regulated and concentrated manner dependent on neuronal activity. Recently Kasischke et al. were able to resolve metabolic signatures in processes of astrocytes and neurons using an elegant approach with two-photon microscopic fluorescence imaging of nicotinamide adenine dinucleotide (NADH) in brain tissue slices (Kasischke et al. 2004). They found a spatiotemporal separation of glycolytic and oxidative metabolism between astrocytes and neurons during increased neural activity, supporting the idea of a highly regulated team work between neurons and astrocytes. This tight

metabolic cooperation was postulated previously as the astrocyte-neuron lactate shuttle hypothesis.

Astrocyte-neuron lactate shuttle hypothesis

About 15 years ago it was for the first time postulated that lactate, produced preferentially by the astrocytes, is shuttled via specific monocarboxylic acid transporters (MCT) from the astrocytes to active neurons (Magistretti and Pellerin 1999; Magistretti et al. 1999; Pellerin and Magistretti 1994) where it is subsequently oxidized in the TCA cycle (***Figure 2***). This process was termed the astrocyte-neuron lactate shuttle (ANLS) and the ANLS hypothesis provoqued a heated debate in the Neuroscience community that still lasts today (Bonvento et al. 2005; Chih et al. 2001; Chih and Roberts Jr 2003; Kimelberg 2004; Pellerin and Magistretti 2003; Schurr 2005).

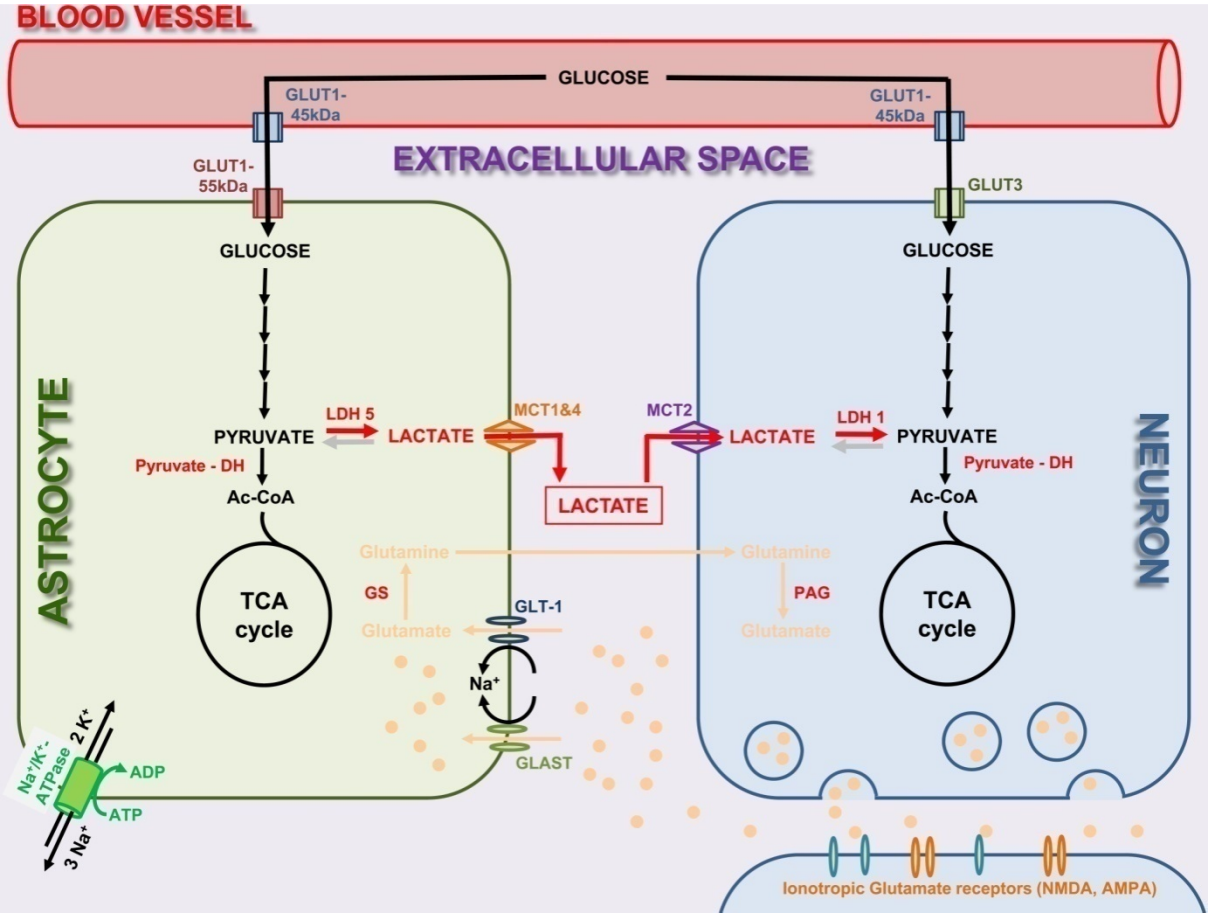

Figure 2. Concept of the astrocyte-neuron lactate shuttle hypothesis (ANLSH)

Simplified schematic of the major mechanisms involved in the tight coupling between neuronal activity and brain metabolism. Activation of glutamatergic afferents leads to presynaptic release of glutamate which activates postsynaptic ionotropic glutamate receptors (NMDA, AMPA). To determine glutamatergic action the

(continuation on page 20)

(continuation from page 19)

neurotransmitter is mainly taken up by astrocytes from the synaptic cleft via the specific glutamate transporters GLT-1 and GLAST (Danbolt 2001). The large accompanying Na+ influx activates the Na+/K+ - ATPase, glucose transport and glucose utilization in astrocytes leading to conversion of pyruvate into lactate. Lactate is released via monocarboxylate transporters (MCT1 and 4) into the extracellular space and from there taken up by the neurons (MCT2) whom it serves as an energy substrate. After uptake into astrocytes glutamate is converted to glutamine by the astrocyte-specific enzyme glutamine synthetase (GS; Martinez-Hernandez et al., 1977) and transported back to neurons. For further details see text. (Further abbreviations in the figure: GLUT1, GLUT3: glucose transporters; LDH1, LDH5: lactate dehydrogenases; TCA cycle: tricarboxylic acid cycle; Ac-CoA: acetyl-CoA; Pyruvate – DH: pyruvate dehydrogenase; PAG: phosphate activated glutaminase)

Basically, the hypothesis summarizes a whole chain of events involved in the coupling of neuronal and metabolic activity. In detail, it describes the following processes: During increased synaptic activity glutamatergic neurons release the neurotransmitter glutamate into the synaptic cleft. From there it is avidly taken up by the astrocytes via specific glial glutamtate transporters (EAAT1 or GLAST and EAAT2 or GLT-1) in cotransport with sodium ions (Danbolt 2001). This cotransport of sodium ions leads to an increase in the intracellular sodium concentration which activates energy-dependent Na+/K+-ATPases. The corresponding hydrolysis of ATP leads to an activation of the astrocytic glycolysis, i.e. the degradation of glucose to pyruvate and via lactate dehydrogenase to lactate. According to the ANLS theory most of the lactate produced in the astrocytes is released via specific MCT into the extracellular space and from there it is taken up by the neurons via a different isoform of MCT (Broer et al. 1999; Broer et al. 1997; Froberg et al. 2001; Gerhart et al. 1998; Gerhart and Leino 1999; Halestrap and Price 1999; Pierre et al. 2002).

The hypothesis is based on numerous findings. Most of them were established in *in vitro* preparations. Already the distribution of the specific MCTs and their affinity for lactate favors export of lactate from astrocytes and uptake by neurons (Debernardi et al. 2003; Pellerin et al. 1998; Pierre and Pellerin 2005). Astroglial cells predominantly express low affinity MCTs (MCT1 with a dissociation constant (Km) for lactate of 3.5 – 8 mmol/l (Broer et al. 1997) and MCT4 with a Km of 35 mmol/l (Dimmer et al. 2000)). In contrast, neurons express predominantly high affinity MCTs (MCT2 with Km of 0.7 mmol/l (Broer et al. 1999)). A second finding that supports the ANLS hypothesis is the distribution of lactate dehydrogenases (LDH). The enzyme catalyzing the reaction from pyruvate to lactate and vice versa exists in different isoforms. The two subtypes found in the brain are LDH1 and LDH5. LDH1 (heart-type LDH; inhibited by pyruvate) which

preferentially catalyzes the reaction from lactate to pyruvate is specific to neurons, whereas LDH5 (muscle-type LDH; present in glycolytic tissues) catalyzes the step from lactate to pyruvate and is predominantly found in astrocytes (Bittar et al. 1996; Laughton et al. 2000). In summary, the equipment of the different players in the neuro-glial cooperation is such, that a lactate flux from astrocytes to neurons is favored.

Support for the ANLS hypothesis also comes from cell culture experiments demonstrating a preferential use of lactate compared to glucose by neurons (Bouzier-Sore et al. 2003b; Itoh et al. 2003; Larrabee 1983; Larrabee 1995; Larrabee 1996; McKenna et al. 2001). In recent days there has been increasing evidence for the ANLS from in situ experiments in brain slices. One of the recent and most often cited works in this context is the aforementioned study by Kasischke et al. which elegantly showed the temporal sequence of several metabolic events using two-photon fluorescence imaging of nicotinamide adenine dinucleotide (2004). The authors were able to demonstrate that neuronal oxidative metabolism is followed by astrocytic glycolysis during focal neural activity.

However, there still is a vivid debate about the contribution of the single compartments and about the validity of the lactate shuttle between astrocytes and neurons in the brain. One of the main reasons for the ongoing controversy is the fact that evidence for the ANLS hypothesis is still based mainly on *in vitro* experimental findings. Results obtained in 'artificial' preparation might not reflect the situation in the intact brain. Since the formulation of the hypothesis more than one decade ago there still is insufficient *in vivo* support for the processes involved in the ANLS. However, there exists some indirect in vivo evidence for the concept. Smith and coworkers used glucose utilization measurements with ^{18}F-fluorodeoxyglucose positron emission tomography in healthy volunteers. An increase of the blood lactate concentration led to a decrease of total cerebral glucose metabolism (Smith et al. 2003). This was interpreted as indirect evidence for the preferential use of lactate by the neurons. At the same time a complementary approach was applied in rats. Using dichloroacetate for the pharmacological activation of the pyruvate dehydrogenase activity, lactate production of astrocytes was decreased which evoked increased baseline cerebral glucose utilization (Itoh et al. 2003). This finding further supports the compartmentalization of the glucose metabolism between astrocytes and neurons. Furthermore, Serres and colleagues presented data

from nuclear magnetic resonance spectroscopy studies demonstrating that there is production of lactate within the brain parenchyma through glycolysis which originates from a cellular compartment other than neurons (Serres et al. 2004; Serres et al. 2005; Serres et al. 2003), but they were not able to clearly identify the exact origin. Just recently a study was published where changes of neuronal, astrocytic and extracellular pH values were taken as evidence for the shuttling of lactate between astrocytes and neurons (Erlichman et al. 2008). In addition, in other tissues, such as testis and skeletal muscle, lactate shuttles also have been described some years ago (Brooks 2002) indicating that lactate shuttles may present a more general principle in organisms.

However, all these studies offer only indirect support for the shuttling of lactate from the astrocytes to the neurons and new approaches for investigating aspects of brain energy metabolism are desirable.

Common *in vivo* neuroimaging methods in the field of brain metabolism

Theoretical considerations about radiotracer experiments and their analysis

In the first part of this section the theoretical and technical principles of radiotracer experiments and the most common radiotracer techniques (positron emission tomography (PET), beta probe studies, autoradiography (AR) are explained in detail because their theory forms the basis of this work. Radiotracer methods can measure organ distributions (AR, PET) and time courses (PET, beta probe studies) of local tracer concentrations. Using PET and beta probes in vivo experiments can be performed. This leads to more realistic experimental conditions than in isolated organ preparations, which are occasionally used to generate kinetic tracer data. In *in vivo* experiments not only the effect of tracer recirculation but also the influence of other body organs is included (e.g. metabolism of the radiotracer in the liver, binding of radiotracer in other organs etc.), which can strongly affect tracer kinetics in the organ under investigation. In general, experiments in the intact organism provide a more realistic environment for testing the adequacy of a model to describe tracer kinetics.

Beside radiotracer methods there obviously exist several other methodologies to investigate aspects of brain metabolism. Examples are nuclear magnetic resonance spectroscopy, A-V difference measurements and microdialysis studies. Some of these methods will be compared to the radiotracer methods in the second part of this chapter and major issues will be discussed.

General requirements for a radiotracer

To exploit the quantitative capabilities of radiotracer kinetic measurements, data has to be analyzed using appropriate methods. In the next sections an overview will be given about the

concepts applied to analyze radiotracer kinetic data. Besides the obvious requirement to cross the BBB, there are several further general prerequisites which a new tracer must fulfill to be feasible for brain studies. Firstly, the tracer must be related predominantly to the process of concern. Secondly, the kinetics of the tracer in the tissue must be within the time window of the measurement and the radioactivity decay time of the labeling isotope. In addition, ideally there should be no metabolism of the labeled compound in blood. Finally, radiotracers have to be produced with high specific activity allowing the application of very small amounts to avoid unwanted pharmacological side effects.

Concept of compartmental modeling for data analysis

Data acquired with both PET and beta probes represent tracer concentration per tissue volume (kBq/cc). In most cases, tracer concentration cannot be directly transformed into quantitative parameters such as substrate utilization in µmol per tissue volume per minute or perfusion in ml per minute per 100 ml of tissue. However, such absolute quantification is superior to other quantification methods for e.g. group comparisons or monitoring of treatment effects. Beside an optimal tracer for the process studied and an optimized acquisition protocol, adequate data analysis tools are needed. Compartment models are widely used to describe biological processes in living organisms. ***Figure 3*** shows the visualization of three different configurations of the classical compartment model using diagrams with rectangles to symbolize compartments and arrows representing the exchange of the tracer between the compartments. Linear compartmental models are the most commonly used tracer kinetic models for the analysis of radiotracer data. Compartments in the field of radiotracer imaging refer to a volume of the tissue, in which properties such as concentrations, metabolism and transport characteristics can be assumed to be homogeneous. That is, within a compartment the rate of exchange of a tracer is fast compared to the rate of exchange between different compartments and thus the tracer is instantaneously mixed within the compartment. Examples of frequently used compartments include:

- Tracer in the arterial plasma

- Free tracer in tissue that can be bound or that may diffuse back into the blood
- Tracer in the tissue that has been unspecifically bound to other than the targeted cell components
- Tracer in tissue that has been specifically bound to the targeted cell component (e.g. receptor sites, enzymes)

Blood compartment

The first compartment in most models is the arterial blood. It is necessary to know the tracer concentration in the blood over time. After intravenous injection the tracer is transported to the heart where it is well mixed with blood and distributed throughout the body by the arterial circulation. Assuming that after this mixing all the arterial blood has the same tracer concentration, the concentration of tracer delivered to capillaries can be determined from any peripheral artery. Blood sampling at timed intervals is initiated with the onset of the tracer administration. In studies applying manual blood sampling, short intervals are chosen at the beginning to avoid missing the peak concentration of the tracer in arterial blood (10 – 20 second intervals). Sampling is continued at less frequent intervals later in the experimental period (up to 15 – 30 minute intervals). Arterial blood samples are then centrifuged to separate plasma from cells and measured using an appropriate device to determine the plasma concentration of the tracer. Tracer in the plasma is the fraction which is available for transfer into tissue and its dynamics is called arterial input curve. The time course of native tracer in plasma (= input curve; C_{pl}) is the driving force of tracer delivery to tissue and an important prerequisite for data analysis (see below). An increased number of studies use on-line blood sampling, which dramatically reduces the number of blood samples to be collected.

The models assume first-order processes. This has the consequence that the change of tracer concentration in one of the compartments is a linear function of the concentrations in all other compartments. As mentioned above, it is also assumed that the observed system is not disturbed by the injected radioligand. This prerequisite is fulfilled by most tracer studies, because detection

devices used for radiotracer imaging studies have sensitivities of 10^{-11} – 10^{-12} mol/l, offering the possibility to inject tiny amounts of the tracer.

Tissue compartment(s)

Looking at a one-tissue compartment model (***Figure 3A***), the dependence of the concentration in the tissue compartment on the concentration of tracer in plasma can be illustrated. The tracer concentration in tissue increases due to the extraction of tracer from plasma. As this process is described by a first-order process, the transfer of material is proportional to the concentration in plasma (C_{pl}). At the same time it is reduced by a backward transfer, which is proportional to the concentration in the tissue (C_{tiss}). Both processes compete, so that the change of the tracer concentration in the tissue over time ($dC_{tiss}(dt)/t$) can be expressed by the following differential equation:

$$\frac{dC_{tiss,1}(t)}{dt} = K_1 C_{pl}(t) - k_2\, C_{tiss,1}(t) \qquad (1)$$

The two rate constants (also called transfer coefficients), K_1 and k_2, have a somewhat different meaning, indicated by the use of capital and small letters. K_1 includes a perfusion dependent component and has units of milliliter per minutes per milliliter of tissue, whereas k_2 indicates the fraction of mass transferred per time (min^{-1}). For example, if k_2 has the value 0.1 min^{-1}, the material leaves the compartment at a rate of 10% per minute.

In addition, the more complex models shown in ***Figure 3B*** and ***3C*** distinguish different forms of tracer in tissue. After entering a cell, the tracer is available in a free form at a concentration $C_{tiss,1}$. From this form, it can directly be bound to its target component of the cell $C_{tiss,2}$ (e.g. target receptor site, intracellular macromolecules etc.), but it also may bind to unspecific cell components, $C_{tiss,3}$. The differential equations for this model can be derived in analogy to the one-tissue compartment model, but are more complex. For example the equations for the model shown in ***Figure 3C*** are given by

$$\frac{dC_{tiss,1}(t)}{dt} = K_1 C_{pl}(t) - (k_2 + k_3 + k_5) C_{tiss,1}(t) + k_4 C_{tiss,2}(t) + k_6 C_{tiss,3}(t) \quad (2)$$

$$\frac{dC_{tiss,2}(t)}{dt} = k_3 C_{tiss,1} - k_4 C_{tiss,2}(t) \quad (3)$$

$$\frac{dC_{tiss,3}(t)}{dt} = k_5 C_{tiss,1} - k_6 C_{tiss,3}(t) \quad (4)$$

After the determination of radioactivity time courses in tissue (C_{tiss}) and in arterial plasma (C_{pl}) the parameters of a model (K_1, k_2, …, k_n; with the number of rate constants depending on the number of compartments (see ***Figure 3***)) are fitted such that the calculated tissue time activity curve (TAC) fits the measured values as adequately as possible.

The amount of tracer delivered to tissue is affected by the blood flow. Once inside the capillary bed, some part of the tracer is extracted into the tissue. This fraction is called the first pass extraction fraction (EF). As mentioned above, for their delivery to the brain tissue (K_1) all tracers initially depend on cerebral blood flow (CBF) even though blood flow may not be the process of primary interest. The relation

$$K_1 = CBF \times EF \quad (5)$$

illustrates this dependence. Renkin (1959) and Crone (1963) calculated the extraction as

$$EF = 1 - e^{-PS/CBF} \quad (6)$$

where P denotes the capillary permeability and S the surface of the endothelium by which the capillary exchanges tracer with the tissue.

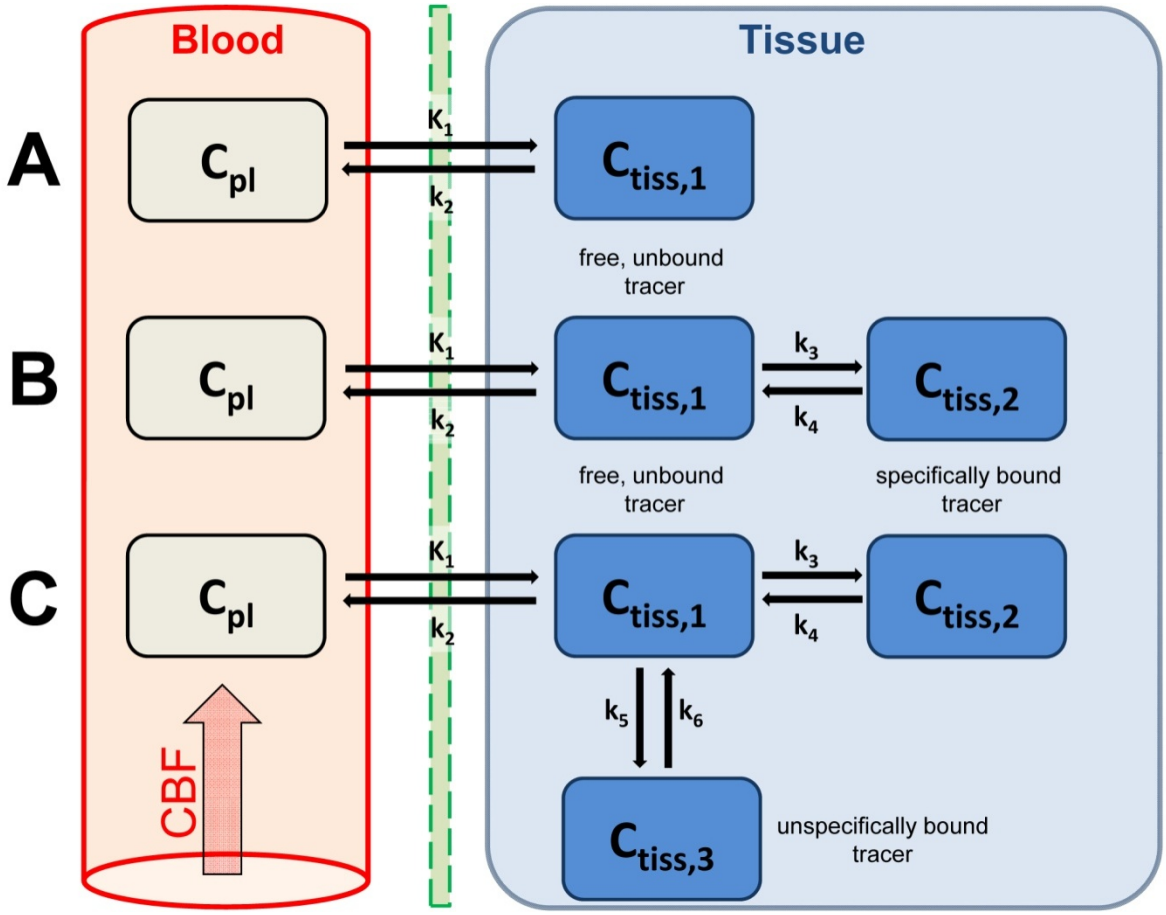

Figure 3. Examples for configurations of classic compartment models

Rectangles display various compartments, arrows represent mass transfer between the compartments. A: One-tissue compartment model. B: Two-tissue compartment model. C: Three-tissue compartment model. The Ctiss,x indicates the tracer concentration in the respective compartment, Cpl denotes plasma concentration and the k's the transfer coefficients of the tracer exchange between the compartments.

The relation demonstrates that the extraction fraction depends on the properties of the endothelium with respect to the tracer (PS) as well as the perfusion (CBF). The higher the perfusion (CBF) the smaller the extraction, because the average time spent close to the capillary wall decreases. However, the mass transfer in general still increases with flow, as the decrease of EF is more than compensated for by the higher abundance of tracer (CBF in the term CBF x EF in equation 5). For tracers with very high permeability (P), the extraction fraction is virtually independent of perfusion and approaches one. In this case, K_1 equals CBF according to equation (5). However, in accordance with the reasoning above, a way to reduce dependence of the delivery on CBF is to select tracers that have a low extraction fraction across the capillary wall, which depends on S and P.

Fitting of the model to measured data

The signal obtained by radiotracer measurements consists of contributions from the capillary bed and from the different tissue compartments and cannot be assigned to a single specific compartment. The plasma concentration is known from the measurement of the input curve as stated above. The task now consists of finding a set of rate constants (k values) such that the modeled tracer concentration optimally matches the measured tracer concentration. To this end, transfer coefficients are varied until the sum of squared residuals becomes minimal. Such analysis of measurements requires appropriate software (***Figure 4***).

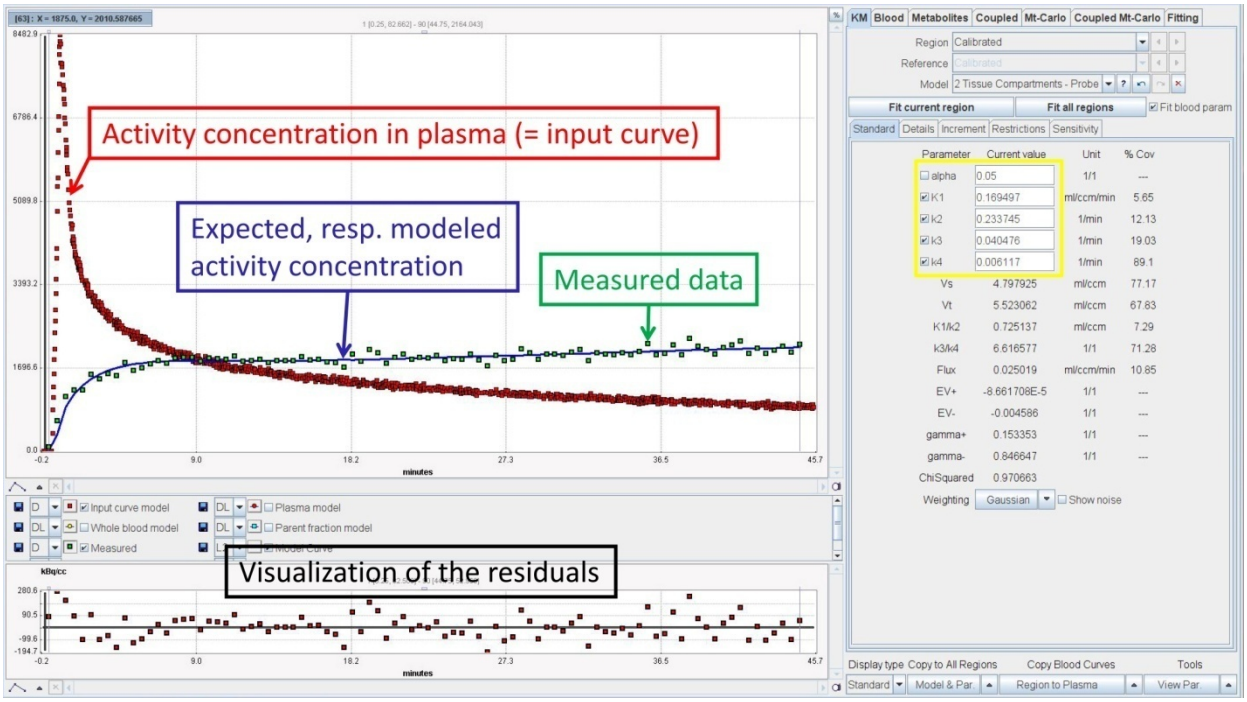

Figure 4. Kinetic modeling user interface of PMOD (Mikolajczyk et al. 1998) a dedicated software for compartmental modeling of kinetic data

Using an appropriate software, a model curve (blue line) is fitted till to optimally match the measured tissue time activity curve (green symbols). The measured time course of tracer activity in plasma is shown in red (input curve). The resulting transfer coefficients from this procedure are indicated on the right (yellow box; in this example for a two-tissue compartment model (K_1 – k_4)). The random distribution of the residuals (bottom window) indicates that the chosen model explains the kinetics of the tracer adequately.

It is common knowledge that more complex models better fit acquired data, but for compartment models this means that the number of transfer coefficients increases and may vary significantly without major changes in the resulting model curve. Under these circumstances, the transfer coefficients cannot be estimated reliably. A general rule in kinetic modeling states that models should be applied that predict the measurements with the least possible number of parameters.

Most often only simple models with one or two tissue compartments are applied and the question arises whether an additional tissue compartment improves the fit and should be considered.

Analogy of the radiotracer method with a pipe system

One of the goals of tracer methods is to evaluate mass fluxes in a biological system. Fluxes can mathematically be described as follows:

$$F_X = k_i \times C_X \quad (7)$$

Here, F_X denotes the mass flux of substance X through a biological system, C_X is the concentration of substance X in the originating compartment and k_i is a composite function of all factors determining the flux of the substance X through the system and is practically what we measure using radiotracer kinetics. The system can be compared to fluid flow in a pipe system with valves, where the flow is determined by the pressure at the entry (~ concentration of the substance C_X) and the position of the valves (corresponding to k_i). The aim of radiotracer methods is to determine factor k_i – the position of the valves in the system. If k_i is known and C_X can be measured, the flux can be calculated easily from equation (7).

In the next few sections, the most common radiotracer imaging methods will be introduced and detailed characteristics of every method are discussed.

Radiotracer methods for the measurement of brain metabolism

Autoradiography

This methodology was introduced more than fifty years ago and measures tissue concentrations of radiolabeled compounds in animals injected with the tracer. Concerning the work in the field of brain metabolism, particularly autoradiographic studies for the measurement of glucose utilization (Sokoloff et al. 1977) and cerebral blood flow (Landau et al. 1955; Sakurada et al. 1978) are widely used.

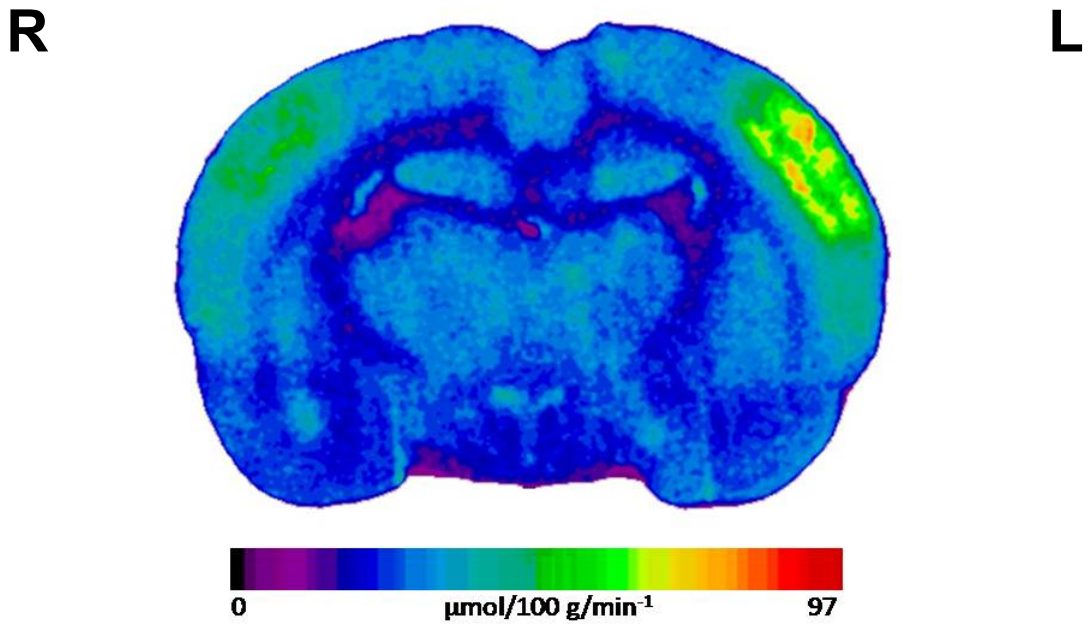

Figure 5. Example of an ^{18}F-fluorodeoxyglucose autoradiography of the rat's brain

The autoradiographic approach nicely shows the spatial distribution of radiotracers. In this example the elevated glucose utilization in the left somatosensory cortex during 2 Hz electrostimulation of the right infraorbital nerve is reflected by a clear increase of ^{18}F-fluorodeoxyglucose uptake (uptake time: 45 minutes). 10 µm thick brain slices were exposed to a phosphor imaging plate during 4 hours. The high spatial resolution provided by the autoradiographical method is evident if compared with Figure 8 (human brain PET study using ^{18}F-fluorodeoxyglucose).

In short, the procedure of an autoradiographic experiment can be described as follows: The radiochemical drug tracing the investigated biochemical process is injected intravenously. After an adequate uptake period, the animal is sacrificed and the brain is removed. The brain is cut in a

cryostat and the sections are exposed to X-ray films or phosphor imaging plates for the measurement of the radioactivity concentration in the tissue. The resulting autoradiographs provide a circumstantial representation of the relative radiotracer distribution in the tissue under study. Local tissue radioactivity concentrations are determined using a calibration curve obtained in previous calibration experiments with methylacrylate standards, which are exposed together with known tissue concentrations. The autoradiographical approach is the method of choice if a high spatial resolution is important as depicted in ***Figure 5***.

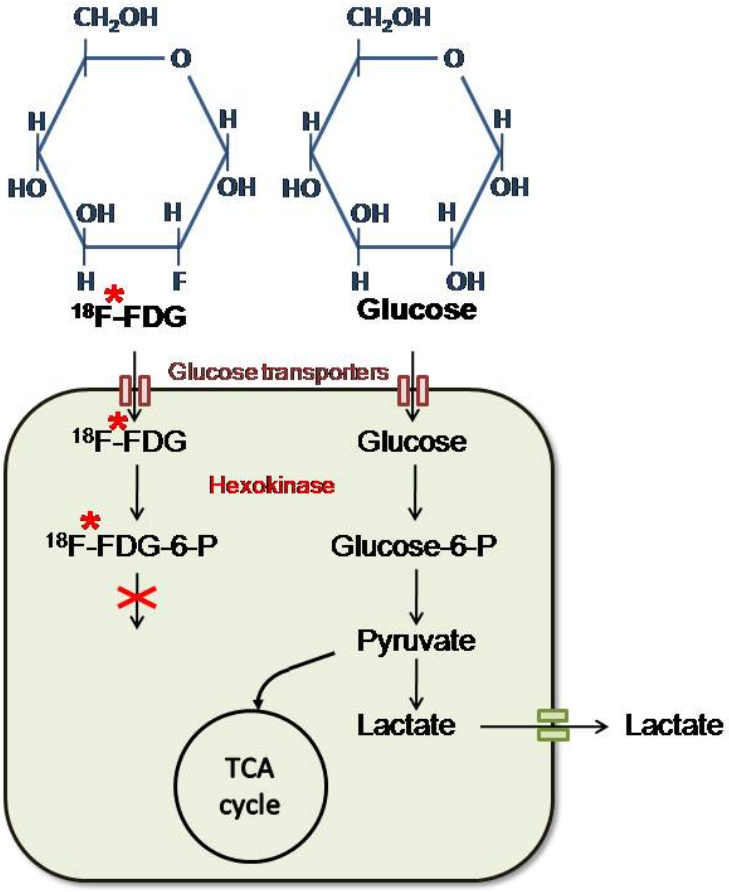

Figure 6. Metabolism of 2-deoxyglucose in comparison to native glucose

Radiolabeled deoxyglucose (e.g. ^{18}F-FDG, marked with an asterisk) is taken up into the cell via glucose transporters independent of blood flow and phosphorylated by the enzyme hexokinase similar to native glucose. But it is not further metabolized thereafter and trapped within cells. Intracellular accumulation of the radiolabeled deoxyglucose derivative is directly proportional to hexokinase activity or to the cellular glucose utilization.

The main disadvantages of this technique are its invasiveness and the fact that only one time point in the evolution of the tracer distribution can be measured per animal, which obviously limits the applicability for investigations of tracer kinetics. To obtain time courses of a tracer's enrichment in the tissue there is a need for sacrificing a large number of animals at different time points. For

accurate kinetic validation better real kinetic data is needed, which can be obtained by PET or beta probe studies (see below).

Furthermore, the capability of the autoradiographic method to derive quantitative values critically depends on the kinetic behavior of the tracer. Only if the tracer gets trapped within the tissue and the trapping is not dependent on blood flow, one autoradiograph is sufficient to derive quantitative measures such as the assessment of glucose metabolism using radiolabeled deoxyglucose/fluorodeoxyglucose. The cells process these glucose-analogues in a similar fashion as native glucose only up to the phosphorylation step catalyzed by the enzyme hexokinase (***Figure 6***). Then, no further metabolization takes place and these compounds are trapped within the tissue making them suitable tracers for autoradiographic studies.

In contrast, for tracers exhibiting strong washout kinetics single autoradiographs are not sufficient to obtain meaningful data. In ***Figure 7***, this is illustrated with the example of radiolabeled acetate, a tracer for the estimation of astrocytic oxidative metabolism (reported in chapter I). Increases of oxidative metabolism in astrocytes are reflected by an increase in the washout of the tracer. This leads to a decreased tracer accumulation in the tissue after about >20 minutes as shown in ***Figure 7***. Between 15 and 20 minutes tracer accumulation is similar to that at rest conditions. Only at times shorter than 15 minutes an increased tracer uptake can be detected using autoradiographic studies, however, this increased tracer uptake could be explained by increased blood flow alone as modeling studies demonstrated. This example illustrates that knowing only single time points of a tracer's tissue accumulation may not be sufficient to draw correct conclusions. Methods are needed that provide the possibility to measure the full time course of a tracer concentration.

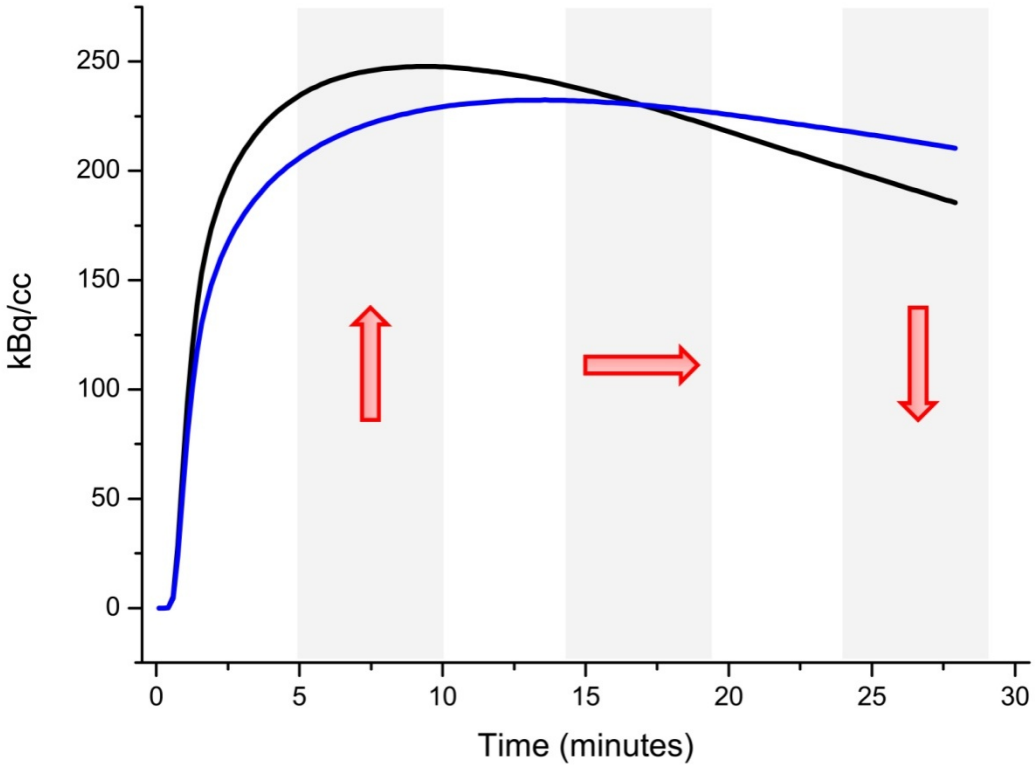

Figure 7. Illustration of the difficulties arising in autoradiographic studies that use tracers exhibiting washout kinetics

^{11}C-acetate – a tracer for the estimation of astrocytic oxidative metabolism – displays an increased washout during infraorbital nerve stimulation (black line) compared to baseline (blue line). Red arrows illustrate tracer uptake as determined in autoradiographic studies performed at corresponding time points (e.g. after 25 minutes a decrease in tracer uptake is observed despite the fact that oxidative metabolism increases in astrocytes. See main text for further details).

Positron Emission Tomography

The development of PET made it possible to extend the autoradiographic approach for measuring rates of biochemical processes non-invasively in humans (Phelps et al. 1975; Phelps et al. 1982; Phelps et al. 1986). Highly sensitive PET offers the possibility to assess regional brain function in a fully quantitative way and provides dynamic tomographic information (***Figure 8***). It allows the investigation of biochemical pathways or molecular targets with specific radiolabeled compounds. The continuing development of novel imaging probes labeled with a positron-emitting isotope (the most common used PET isotopes together with some of their physical characteristics are listed in ***Table 1***) will further expand the range of PET imaging in the future.

The principle of the method is based on the detection of the positron decay. The radiolabeled

compounds are introduced in the organism generally by intravenous injection. The radiotracer will distribute in the organism according to its delivery, uptake, metabolism and excretion characteristics. At any given time, some of the radioactive nuclides will decay by emission of a positron and a neutrino. The neutrino leaves the body without any further interaction. In contrast, the positron travels a short distance in the tissue while losing energy and finally annihilates with an electron leading to the conversion of the mass of the positron and the electron to electromagnetic energy. During this process two gamma rays are emitted at an angle of 180° with an energy of 511 keV each, which escape the body and can be detected by the PET detector crystals. The PET scanner acquires these coincidence events on opposite sides of the crystal ring. The line on which such an annihilation reaction occurs is called line of response. By combining millions of such lines of response of many different angles, the data can be reconstructed into cross-section images using standardized image reconstruction algorithms. The distribution of counts in the resulting images reflects the concentration of the positron-emitting radiotracer in the tissue. To attain a linear relationship between the counts measured by PET and the tracer concentration in the tissue several corrections are necessary.

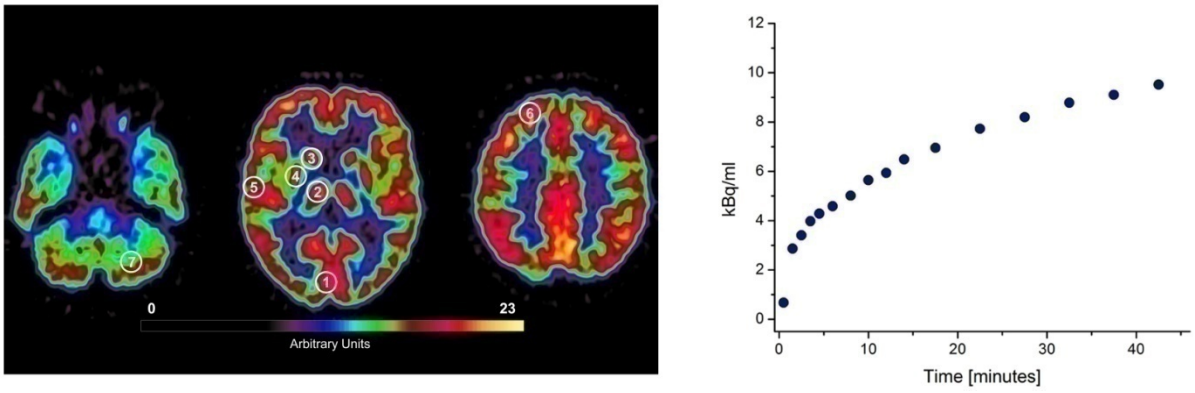

Figure 8. PET study of a human brain using ^{18}F-fluorodeoxyglucose

On the left human brain PET slices are shown of a ^{18}F-FDG study. The corresponding time activity curve of the cortex is plotted on the right. (1) visual cortex, (2) thalamus, (3) caudate nucleus; (4) putamen, (5) temporolateral cortex, (6) frontal cortex and (7) cerebellum.

Besides correction for gamma ray attenuation by the tissue, images have to be corrected for scattered and random events detected in order to obtain images reflecting real tracer concentration in the field of view. Spatiel resolution of clinical human PET scanners is physically limited to about 4 to 6 mm rendering its use in rodents nearly impossible. Recently dedicated small animal PET

scanners were introduced for experimental studies in the rodent which reach spatial resolutions down to 1 mm (Chatziioannou 2002; Hume and Myers 2002; Rowland and Cherry 2008; Weber and Bauer 2004). The advent of these high-resolution small animal PET systems may help to bridge the gap between animal and human studies. However, these systems suffer from various drawbacks as discussed below.

Beta probe system

The range of PET applications is continuously broadening by the current development of new radiotracers. However, new compounds require validation in laboratory animals before their use in humans. In earlier years, these validation experiments consisted in *ex vivo* measurements requiring the sacrifice of a large number of animals. The introduction of small animal PET systems facilitated the quantification of tracers over time in significantly less animals. However, these systems suffer from several drawbacks: 1.) they are expensive, 2.) have a low temporal resolution, 3.) animals have to be immobilized by anesthesia which restricts neurophysiological investigations and 4.) fully quantitative experiments with the need for parallel measurement of the arterial input curve are difficult due to the geometry of the scanners. Furthermore, quantitative *in vivo* evaluation of new PET tracers for brain studies often requires only the measurement of the radioactivity concentration in a few brain structures and a tomograph is unnecessary. Therefore, recently introduced beta probe systems offer an elegant way to measure time courses of radiotracer enrichment in single tissue regions in rodents with high temporal resolution (Ginovart et al. 2004; Pain et al. 2000; Pain et al. 2002b; Weber et al. 2003). Until now they were mostly used in brain studies but obviously they could also be used in other body organs. The potential applications of this method are widespread. Examples are blocking and displacing experiments with receptor ligands (Galineau et al. 2006; Wyss et al. 2007), measurement of glucose metabolism using ^{18}F-fluorodeoxyglucose during different conditions ((Millet et al. 2004; Pain et al. 2002a); for an example see ***Figure 9***) and blood flow measurements (Weber et al. 2003).

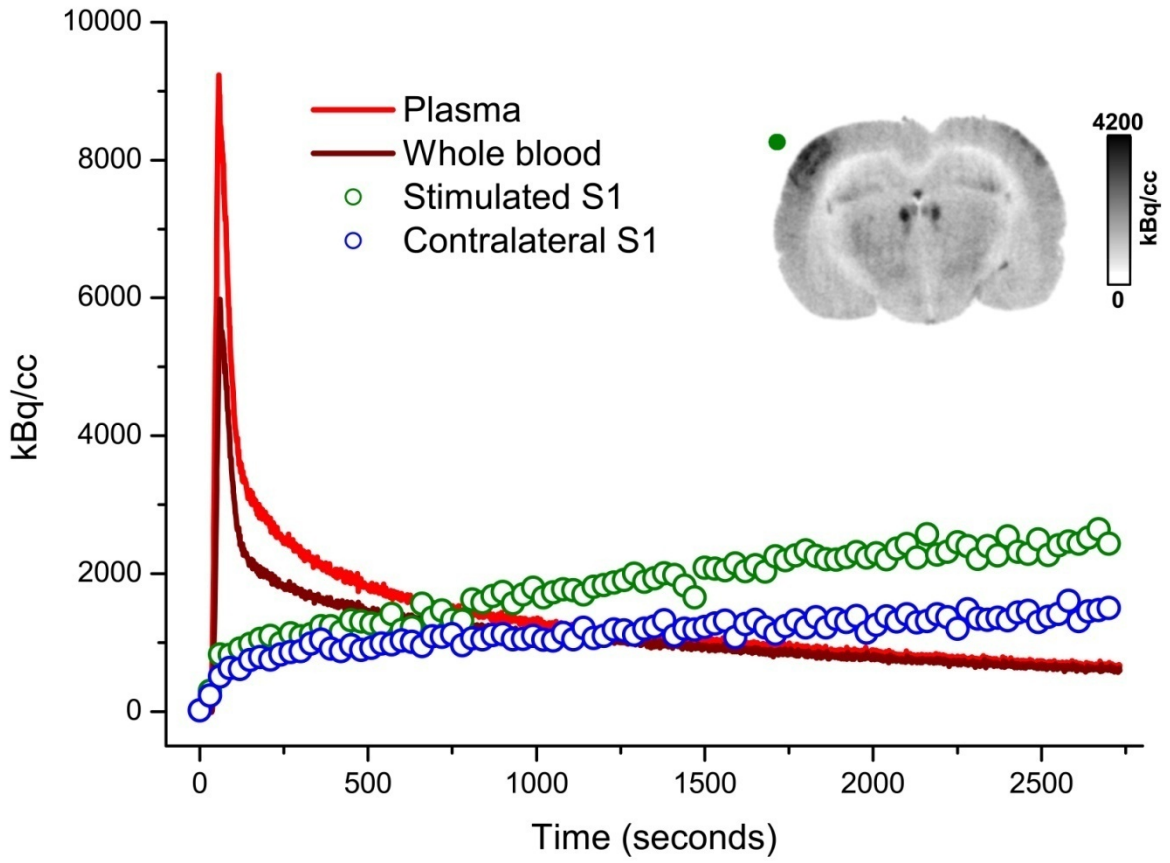

Figure 9. Beta probe study in the rodent brain

Decay corrected time activity curves of ^{18}F-FDG in tissue, whole blood, and plasma. Electrostimulation of the left infraorbital nerve led to an increased glucose utilization in the right primary somatosensory cortex as measured by beta probes placed in both hemispheres of a rat brain. The inset depicts the corresponding autoradiography of this animal performed at the end of the kinetic measurement (the green filled circle marks the stimulated S1). S1 = primary somatosensory cortex.

Compared to animal PET systems, beta probe systems are less expensive, demonstrate a higher temporal resolution and can potentially be performed in the awake animal (see Chapter III). Currently, available beta probes consist of a scintillating crystal (1 mm in length and 0.25 to 1 mm in diameter), which is attached to an optic fiber. Due to the limited range of β+ particles within tissue, only β+ particles from a defined sphere around the tip of the probe excite the crystal (Pain et al. 2002b). β+ particles originating from distances beyond the maximum range in biological tissues (see ***Table 1***) will be stopped in the tissue before they can interact with the crystal and will not be detected. The photons produced in the scintillating crystal are measured using photomultiplier tubes and counting electronics yielding a measure of the radioactivity concentration.

Table 1. Physical properties of the most commonly used PET isotopes

Radionuclide	Half-life (min)	Range in tissue (mm)	β^+ maximum energy (keV)	FWHM[b] (mm)
F-18	109.8	2.4	640	0.6
C-11	20.4	4.1	960	0.9
N-13	9.96	5.4	1720	1.0
O-15	2.07	8.2	1190	1.6

[b]Fundamental PET resolution limit calculated for a 20-cm-diameter scanner and infinitely thin detectors (Levin and Hoffmann, 1999)
FWHM = full width at half maximum

Comparison of radiotracer techniques with other *in vivo* methodologies common used for the study of brain metabolism

The following section highlights some aspects of two other *in vivo* methods that have been used in the field of brain metabolism research for several years to investigate the organisation of brain energy metabolism and its compartmentalization. Among other techniques, which are not discussed in this introduction, nuclear magnetic resonance spectroscopy and microdialysis studies have played a major role in advancing our understanding of human brain metabolism. Some general aspects are introduced and put into context with radiotracer methods.

Nuclear magnetic resonance spectroscopy

Nuclear magnetic resonance spectroscopy (MRS) has been introduced in the 1980s for the non-invasive study of human brain metabolism (Prichard and Shulman 1986). The most common MRS approach for brain metabolic studies relies on the infusion of stable ^{13}C- enriched substrates (e.g. ^{13}C-glucose, -acetate, -lactate, ketone bodies etc. (Escartin et al. 2006)). ^{13}C has a low natural abundance of ~1.1% which makes the measurement of the isotopic incorporation into brain metabolites possible by way of i.v. infusion of ^{13}C enriched substrates. The quantification of energy metabolism by MRS is mainly based on the detection of ^{13}C accumulation within metabolites of the two large cerebral pools (neuronal pool of glutamate / astrocytic pool of glutamine). MRS has the unique property that it can specifically identify different molecules and the atomic position of the ^{13}C label. In contrast to radiotracer techniques that measure a single time activity curve of all radiolabeled substrates in the region of interest, MRS provides several ^{13}C time courses, which is sufficient to derive metabolic fluxes from all major pathways labeled by the infused ^{13}C compound. The ^{13}C enrichment pattern of amino acids in the brain reflects the compartmentation of brain energy metabolism (Bouzier-Sore et al. 2003a).

The fine biochemical probing comes at the expense of a low intrinsic sensitivity. The detection of trace amounts of the label is not possible. Another consequence of the low intrinsic sensitivity is the need to perform MRS in large brain voxels at least one order of magnitude larger than in

radiotracer techniques (Escartin et al. 2006). Therefore, MRS is not yet really suitable for exploring focal brain activation. However, promising developments are under way that provide high resolution MRS. As is the case for presently available radiotracer techniques, MRS is currently unable to directly resolve the controversy about the existence of the proposed lactate shuttle between neurons and astrocytes (Magistretti et al. 1999) because a clear compartmentation of lactate in the brain does not exist.

Microdialysis

Microdialysis studies have been used to measure both levels of neurotransmitters and of energy substrates (Obrenovitch and Zilkha 2001). After the insertion of a specific probe into an area of interest of the living brain, the measurements allow monitoring changes in the composition of the extracellular fluid with enzyme-based dialysate analyses or the detection of CO_2 recovery after infusion of radiolabeled substrates. Especially the latter methodology has been used regularly for brain metabolism-related studies. Via microdialysis probes, radiolabeled compounds are infused to pulse label the respective endogeneous substrates. The resulting radiolabeled CO_2 formed by the oxidative metabolism is then measured in the eluate from the probe (Huang et al. 1993; Zielke et al. 1998; Zielke et al. 2007) yielding a direct measure of oxidative metabolism. However, absolute rates of oxidative metabolism cannot be determined by this methodology. Furthermore, resulting CO_2 levels are usually determined in several minute dialysate fractions largely limiting the temporal resolution. In addition to the low temporal resolution, the method is also hampered by limited spatial resolution due to simultaneous probing of a large number of brain cells. Microdialysis studies report only bulk changes in extracellular metabolites with severely limited temporal and spatial resolution. Rapid and localized events may be averaged out. The strength of the method is the possibility to be performed also in the freely-moving animal (Obrenovitch and Zilkha 2001).

Aims of the project

The concept of compartmentalization of cerebral metabolism has existed for about 40 years mainly based on experiments studying the occurrence of label in brain metabolites after the injection of various radiolabeled compounds (Cremer 1970; Minchin and Beart 1975a; Minchin and Beart 1975b; Van den Berg et al. 1969). In the following years there were several MRS-based studies that evaluated different aspects of the compartmentalization such as the glutamate-glutamine cycle (Aureli et al. 1997; Serres et al. 2008; Shen et al. 1999), distinct TCA cycle activities in neurons and astrocytes (Lebon et al. 2002; Tyson et al. 2003) and their close coupling to different states of brain activity (Sibson et al. 1998).

However, low temporal and spatial resolution, low sensitivity, and the inability of absolute quantification limit the abovementioned methodologies, giving rise to the development of complementary methods for the study of brain energy metabolism. Approaches that allow the *in vivo* estimation of specific process rates in distinct cerebral metabolic compartments can extend the knowledge about the compartmental interplay and the contribution of single metabolic compartments in the working brain.

In general, the main objectives of the present work were on the one hand to evaluate radiotracers for their use in brain studies, on the other hand to improve the applied methodology.

(I) In a first part 1-^{11}C-acetate, previously used for the measurement of oxygen consumption in the heart (Armbrecht et al. 1990; Buck et al. 1991; Lindner et al. 2006), was investigated with regard to its potential use in brain to study oxidative metabolism in astrocytes. Based on the hypothesis that label washout after injection of the radiolabeled astrocyte-specific substrate acetate reflects oxygen consumption in astrocytic cells, experiments using different interventions were performed. The results demonstrate the potential of the approach.

(II) A second part of the project focused on the neuronal compartment. The newly synthesized lactic acid enantiomer (Drandarov et al. 2006) 1-^{11}C-L-lactate was tested. Numerous studies

demonstrated that lactate constitutes an excellent oxidative substrate for neurons (for review see (Pellerin 2003)) and that lactate is preferentially consumed by neurons (Bouzier-Sore et al. 2006). The current study is motivated by these results and based on the hypothesis that changes in kinetics of the radiolabeled lactic acid may reflect changes in neuronal oxidative metabolism. The following specific issues were addressed:

1.) Characterization of 1-^{11}C-L-lactate kinetic properties in brain tissue, such as first pass extraction fraction.

2.) Investigation of possible changes in kinetic behavior during increased neuronal activity.

3.) Explanation of these potential changes according to the actual knowledge of brain metabolism.

(lll) Finally, the last objective of the work was to develop and evaluate a novel surface probe. The current intracortical probes suffer from several drawbacks: the need for insertion into the tissue leads to potential tissue damage, the probes exhibit limited detection sensitivity, and it is difficult to use the system in the non-anesthetized animal. A more sensitive surface probe that can be applied through the bone has the potential to be used in awake animals.

A better understanding of the kinetics of lactate and acetate utilization in the brain *in vivo* may increase our knowledge about the compartmentalization of brain energy metabolism. The possibility to study neuronal and astrocytic oxidative metabolism *in vivo* in an independent, quantitative, and separate manner is a promising approach to improve our understanding of the interplay between the two major cerebral cell types.

Chapter I

Stimulation-induced Increases of Astrocytic Oxidative Metabolism in Rats and Humans investigated with 1-^{11}C-Acetate

Matthias T. Wyss[1], MD, Bruno Weber[1,2], PhD, Valerie Treyer[1], PhD, Stefan Heer[1], MD, Luc Pellerin3, PhD, Pierre J. Magistretti[4], MD PhD, Alfred Buck[1], MD

[1]PET Center, Division of Nuclear Medicine, University Hospital, Zürich, Switzerland

[2]Institute of Pharmacology and Toxicology, University of Zürich, Zürich, Switzerland

[3]Physiology Department, University of Lausanne, Lausanne, Switzerland

[4]Brain Mind Institute, École Polytechnique Fédérale de Lausanne (EPFL), Lausanne, Switzerland

Running title: *In vivo* 1-^{11}C-Acetate Kinetics in the Brain

Published in the Journal of Cerebral Blood Flow and Metabolism (2009), 29; 44-56.

Abstract

The purpose of this study was to investigate astrocytic oxidative metabolism using 1-^{11}C-acetate. 1-^{11}C-acetate kinetics were evaluated in the rat somatosensory cortex using a beta scintillator during different manipulations (test-retest, infraorbital nerve stimulation and administration of acetazolamide or dichloroacetate). In humans a visual activation paradigm was used and kinetics were measured with positron emission tomography. Data were analyzed using a one-tissue compartment model. The following features supported the hypothesis that washout of radiolabel (k_2) is due to ^{11}C-CO_2 and therefore related to oxygen consumption ($CMRO_2$): 1) the onset of ^{11}C washout was delayed; 2) k_2 was not affected by acetazolamide-induced blood flow increase; 3) k_2 demonstrated a significant increase during stimulation in rats (from 0.014 ± 0.007 to 0.027 ± 0.006 min^{-1}) and humans (from 0.016 ± 0.010 to 0.026 ± 0.006min^{-1}) and 4) dichloroacetate led to a substantial decrease of k_2. In the test-retest experiments K_1 and k_2 were very stable.

In summary, 1-^{11}C-acetate seems a promising tracer to investigate astrocytic oxidative metabolism *in vivo*. If the washout rate is indeed representing the production of ^{11}C-CO_2, then its increase during stimulation would point to a substantially higher astrocytic oxidative metabolism during brain activation. However, the quantitative relationship between k_2 and $CMRO_2$ needs to be determined in future experiments.

Key words: 1-^{11}C-acetate, astrocytes, beta scintillator, oxidative metabolism, positron emission tomography, washout

Acknowledgments

The authors acknowledge the important laboratory and editorial help by Prateep Beed and John Mc Clacken respectively and thank Tibor Cservenyàk and Konstantin Drandarov for radiosynthesis of the tracer. We would also like to thank Rolf Grütter for valuable discussions. The study was

supported by the Swiss National Science Foundation (Grants 3100A0-105804/1 and PP00B-110751/1) and by the OPO-Stiftung Zürich.

Introduction

There is increasing evidence that astrocytes and neurons constitute a tightly coupled metabolic unit. Already early studies of brain metabolism using ^{14}C-labeled precursors such as glucose or acetate led to the concept of two distinct tricarboxylic acid (TCA) cycle compartments, i.e. two separate pools for glutamate and glutamine (Berl and Frigyesi 1969; Cremer 1970; Minchin and Beart 1975a; Van den Berg et al. 1969). Later histochemical work on the restricted localization of glutamine synthetase to glial cells (Martinez-Hernandez et al. 1977; Norenberg and Martinez-Hernandez 1979) further supported the idea on the glial and neuronal site of these distinct pools. Simplification of these data has sometimes led to the wrong assumption that the oxidative activity of astrocytes is negligible. However, studies using mainly NMR spectroscopy have suggested that astrocytic energy metabolism indeed contains a substantial oxidative component which may account for up to 30% of total oxidative metabolism in brain under resting conditions (for review see (Hertz and Kala 2007; Hertz et al. 2007; Hyder et al. 2006). Recent transcriptome analysis has revealed a pattern of gene expression in astrocytes consistent with a significant oxidative activity (Lovatt et al. 2007).

Another question is how astrocytic metabolism behaves during activation. A recent study using *ex vivo* autoradiography with ^{14}C labeled acetate at the carbon 2 position suggested that astrocytic oxidative metabolism increases with brain activity (Cruz et al. 2005). Labeled acetate is a promising candidate to investigate astrocytic oxidative metabolism *in vivo* because it is selectively taken up and metabolized by astrocytes (Hassel et al. 1992; Muir et al. 1986; Waniewski and Martin 1998). Earlier studies in the heart muscle have further revealed that quantitative measures for oxygen consumption can be derived from the washout rate of label after injection of radiolabeled acetate (Buck et al. 1991). Acetate can be labeled in the 1- or 2-carbon position. Whole body studies using ^{13}C labeled acetate demonstrated that labeled CO_2 is produced during the second or third turn in the TCA cycle, depending on whether 1-^{13}C-acetate or 2-^{13}C-acetate was used (Wolfe and Jahoor 1990). However, these results reflect whole body metabolism, brain-

specific reactions cannot be directly derived from them. In brain, with 1- and 2-labeled acetate there was substantial labeling of amino acids, such as glutamate, glutamine and aspartate and further TCA cycle intermediates as shown in older and more recent literature (Badar-Goffer et al. 1990; Berl and Frigyesi 1969; Lebon et al. 2002; Tyce et al. 1981; Tyson et al. 2003; Van den Berg et al. 1969; Van den Berg and Ronda 1976). However, the static measurement of metabolites at single time points yields only limited information on astrocytic oxidative metabolism.

In this study we applied 1-^{11}C-acetate and dynamic measurements to investigate astrocytic oxidative metabolism. Specific questions were: 1) what is the extraction fraction of the tracer, 2) what is the kinetic behavior at baseline and during stimulation and 3) how does dichloroacetate, an agent that increases the production of acetyl-CoA from pyruvate in the cell, change the kinetics of 1-^{11}C-acetate and 4) is the loss of radiolabel dependent on blood flow. Studies were performed in rats and humans. In rats data were acquired using a beta scintillator, in humans we applied positron emission tomography.

Material and Methods

Automated radiosynthesis of sodium 1-^{11}C-acetate

^{11}C-CO_2 was produced by the 14N(p,α)^{11}C nuclear reaction using a nitrogen gas (N_2/0.5%O_2) target. ^{11}C-CO_2 was bubbled at room temperature in a mixture of methylmagnesium bromide (3M solution in diethyl ether; Fluka, 70 µl, 0.21 mmol) and dry diethyl ether (3 ml) placed in the reactor, where the chemical trapping of the ^{11}C-CO_2 by C-carboxylation of the Grignard reagent takes place instantly. After delivery (10 min) the reaction was quenched by automated addition of nearly equimolar amount of acid (1 ml 0.2M aqueous HCl, 0.2 mmol HCl) and the diethyl ether from the bilayer mixture was removed by evaporation in a stream of nitrogen (100 ml/min) for about 10 min. The residual water solution of 1-^{11}C-acetic acid was automatically drawn into the loop of the preparative chromatograph (Merck-Hitachi chromatograph equipped with L-4000A UV detector at 254 nm, isocratic pump L-6000A, 5 ml loop, and radiation detector Radiation Monitor, Eberline Instrument Corporation, Santa Fe, New Mexico), injected into a semipreparative reversed phase column (Polymerx, 10 µm, 250 x 10 mm, Phenomenex) and eluted with a mixture of sterile salt physiologic solution as the mobile phase. The fraction corresponding to the 1-^{11}C-acetic acid (tR = 7 min) was collected to give up to 10 GBq activity of no-carrier-added sodium 1-^{11}C-acetate with over 99% radiochemical purity and specific activity of about 400 GBq/µmol at the end of the synthesis in 10 ml sterile isotonic, buffered at physiological pH solution. The radiolabeling was performed in a lead shielded cell using a computer assisted homemade automatic apparatus controlled by LabVIEW software (National Instruments) via Modulink and RS232 interfaces.

Radiotracer experiments

Experiments were performed in animals using the beta scintillator and in humans using positron emission tomography (PET). All animal experiments were approved by the local veterinary authorities and were carried out in accordance with their guidelines. The experiments were performed by licensed investigators. The animals were kept in cages in a ventilated cabinet with standardized conditions of light (night/day-cycle 12h/12h) and temperature and free access to food

and water. Before the experiment the animals were fasted overnight. 29 Sprague-Dawley rats (5 for the extraction fraction determination, 24 for the different experimental paradigms (for details see below) weighing 310 ± 41 g (mean ± standard deviation) were included in the study.

The human study population was composed of six healthy male volunteers aged between 24 and 36 yrs without any known neurological impairments. All subjects were studied at the University Hospital Zurich. Informed written consent was obtained from all subjects before the beginning of the experiment. The protocol was approved by the local Ethics committee.

MR scanning was performed on each subject (Twin Speed, GE Medical systems, Milwaukee, USA) to rule out any cerebral pathologies and for anatomical coregistration of the PET scan.

Animal preparation

Surgery was performed under isoflurane anesthesia and involved the placement of an arteriovenous (a-v) shunt from the right femoral artery to the right femoral vein, tracheotomy for mechanical ventilation and exposition of the skull with subsequent thinning of the bone above the primary somatosensory cortex using a dental drill. The actual experiment was then performed under urethane anesthesia (1400 mg/kg i.p.). The a-v shunt was used for the injection of the tracer, for collecting blood samples for metabolite analysis, for the monitoring of arterial blood pressure and for the continuous measurement of total arterial ^{11}C activity. For the latter purpose, the shunt was run through a coincidence counter (GE Medical Systems) that stored the whole blood radioactivity concentration at 1-second intervals. The online arterial sampling procedure is described in detail elsewhere (Weber et al. 2002a).

Beta scintillator

The beta scintillator (Swisstrace, Zurich, Switzerland) has been described in detail earlier (Weber et al. 2003; Wyss et al. 2007). In short, it consists of a scintillation tip (Bicron, BF12, Newbury, OH, USA) with a length of 1 mm and a diameter of 0.25 mm attached to a high numerical aperture glass fiber. The scintillator was made light-tight by applying a uniform coating of silver particles. The scintillations were measured using a photomultiplier tube and counting electronics (Perkin Elmer, Massachusetts, USA). The limited range of beta particles within biological tissues leads to a

limited detection volume centered around the scintillating tip of the probe. Monte Carlo simulations demonstrated that for C-11 the distance required to detect 90 % of the beta particles around the probe is 2.0 mm (Pain et al. 2002b). The sensitivity of the used beta scintillator was in the range of 0.036 to 0.047 cps/kBq/cc.

The scintillator was inserted into the cortex using a stereotactic frame (David Kopf Instruments, Tujunga, CA, USA). At the insertion point, which was about (according to Bregma) 1 mm posterior and 5 mm lateral, the thinned bone was removed and the dura was carefully incised. The scintillator tip was lowered 1.4 mm below the dura. In the stimulation experiments, the correct position was verified by Laser Doppler flowmetry (Periflux System 5000, Perimed AB, Järfälla, Sweden). This position was adjusted to avoid large superficial blood vessels. Only one scintillator penetration was performed per animal. The count rate was stored on a personal computer using a bin width of 1 second yielding tissue time activity curves.

Positron emission tomography

All subjects were scanned on a whole-body Positron emission tomography/ Computertomography-scanner (Discovery ST-RX; GE Medical Systems, Waukesha, USA). This is a scanner with an axial field of view of 14.6 cm and a reconstructed in-plane resolution of about 7 mm. Before the positioning of the subjects in the scanner, a radial artery was cannulated for timed arterial blood sampling. An additional catheter for administration of the radiotracers was placed in the contralateral antecubital vein. At the beginning of each study, a low dose computer tomogram for attenuation correction was performed.

Experimental protocols

a) Cerebral blood flow measurements using $H_2{}^{15}O$ - First pass extraction fraction

The first pass extraction fraction (EF) of 1-^{11}C-acetate at baseline was determined according to the relationship EF = K_1/CBF, where K_1 is the transport parameter of the one-tissue compartment model and CBF is cerebral blood flow. CBF was determined in 5 animals using ^{15}O labeled water injected prior to measurement of 1-^{11}C-acetate kinetics. In the human study CBF was measured in all subjects 10 minutes before the 1-^{11}C-acetate injections. The visual stimulation was interrupted

between CBF and acetate measurements. Approximately 300 MBq $H_2{}^{15}O$ were injected intravenously using an automatic injection device. Following the arrival of the bolus in the brain, the acquisition of a series of 18 frames (10 s each frame) was started.

b) Measurements of 1-^{11}C-acetate kinetics during different conditions

In the animal experiments two injections spaced 30 minutes apart were performed. Data were acquired for 20 minutes after the injection (slow injection over a period of 30 seconds) of 230-260 MBq (diluted in 0.5 ml) of radiotracer. This part of the study included 24 animals, which were distributed among the following experimental subgroups: I) in this group the baseline was followed by electrostimulation (bas-stim); II) the order was reversed (stim-bas). Groups I) and II) were examined with respect to a potential order effect. III) To evaluate the reproducibility two consecutive baseline measurements were performed (bas-bas). IV) In four animals the effect of acetazolamide (Diamox®, 66 mg/kg), a carbonic anhydrase inhibitor increasing CBF but not oxygen consumption ($CMRO_2$; (Okazawa et al. 2001)), on the kinetics of 1-^{11}C-acetate was examined. After 20 minutes of baseline acquisition, acetazolamide was intravenously injected over one minute. Ten minutes later the same amount of 1-^{11}C-acetate was injected for the second time. In a last group (V) the effect of dichloroacetate was investigated. Four hours after the injection of dichloroacetate (50 mg/kg, Sigma-Aldrich Prod. No. 347795) a baseline study was followed by electrostimulation (dichloroacetate challenge). Dichloroacetate was dissolved in physiological saline and was adjusted to pH 7.4.

To activate the whisker-to-barrel pathway the infraorbital branch of the trigeminal nerve was electrically stimulated with two stainless steel electrodes. The cathode was inserted through the infraorbital hiatus and the anode was positioned in the masticatory muscle on the ipsilateral side. The current was adjusted to 2 mA and 2 Hz stimulation frequency was chosen because previous measurements using ^{18}F-fluorodeoxyglucose-autoradiographies demonstrated this frequency to be optimal eliciting a maximal increase in glucose consumption of 70 to 80 % (unpublished data). The stimulation started 30 seconds before the tracer injections. To check the effectivity of the applied stimulation and the effect of acetazolamide in group IV) animals, a Laser Doppler flowmetry probe

was fixed just above the primary somatosensory cortex to follow regional cerebral blood flow (rCBF) changes.

In humans PET was performed under baseline conditions with eyes closed and during visual stimulation using different video clips presented on a screen (Charlie's angels & Rolling stones). In three subjects the baseline examinations were preceding the stimulation studies and in the other three subjects the order was reversed to rule out any order effect. The visual stimulation was started 20 seconds before scan start and continued during complete PET acquisition. After the intravenous injection of 250 MBq 1-^{11}C-acetate administered as a slow bolus over approximately 60 s data were recorded for 20 minutes (25 frames: 6 x 20 s, 3 x 40 s and 16 x 60 s).

Time activity curves were derived from volumes of interest defined on three consecutive slices on the anatomical MR scans and subsequently transferred to the PET data. Volumes of interest were drawn in the visual cortex as the target region and in the frontal cortex and cerebellum as references.

Statistics

The Wilcoxon Signed Rank test for dependent samples was used to evaluate differences between within-subject conditions and the Mann Whitney U test was used for group differences. The criterion for significance was set at $p < 0.05$. Values are expressed as mean ± sd.

Data acquisition and analysis

The details are described in the appendix.

Results

A. Animal studies

Metabolites of 1-^{11}C-acetate in the blood

HPLC identified ^{11}C-CO_2 as the only metabolite in blood. The time course of the fraction of authentic ^{11}C-acetate in arterial plasma is demonstrated in ***Figure 1***. The pH and arterial blood gases were all in the physiological range (pH = 7.35 – 7.45; pCO_2 = 35 – 45 mmHg; pO_2 = 70 – 100 mmHg).

Plasma lactate levels were also determined as lactate competes with acetate for the uptake into brain. They ranged between 1.4 and 2.1 mmol/l. However, no relationship between plasma lactate levels and changes in the kinetics of 1-^{11}C-acetate could be found. Only in group V (dichloroacetate challenge) there was a statistically significant difference in plasma levels between the two different modalities (see below).

First pass extraction fraction.

CBF was measured in 5 baseline experiments and was 56 ± 16 ml/min/100g. The first pass extraction fraction of 1-^{11}C-acetate calculated in these experiments was 18 ± 5 %.

Reproducibility of the 1-^{11}C-acetate measurements

The reproducibility of the time activity curves and of the parameters K_1 and k_2 is demonstrated in the top graphs of ***Figure 2 and 3***. In contrast to trigeminal nerve stimulation, the tissue time activity curves in the 2 sequential baseline experiments look identical. The difference of the mean K_1 ($K_{1experiment2}$ - $K_{1experiment1}$) was –0.001, and for k_2 the difference was 0.002 min^{-1}.

1-^{11}C-acetate kinetics during infraorbital nerve stimulation

The electrical infraorbital nerve stimulation increased the washout of 1-^{11}C-acetate as shown in the middle graph of ***Figure 2***. The order of the experiments (baseline-stimulation or stimulation-baseline) had no significant effect on the changes of the kinetic parameters (***Figure 3C and 3D***).

Therefore the two groups I) and II) (bas-stim and stim-bas) were pooled. During stimulation, k_2 increased by 93 % from 0.014 ± 0.007 to 0.027 ± 0.006 min^{-1} ($p < 0.01$) in the primary somatosensory cortex. In parallel, K_1 increased from 0.080 ± 0.015 at baseline to 0.095 ± 0.017 ml/min/ml tissue ($p < 0.01$). The efficacy of the stimulation was confirmed by the increase of the laser Doppler flowmetry signal by 20 – 25 % (data not shown).

To check for a delayed onset of the radioactivity washout, the first 5 minutes of data were refitted with only k_2 as a free parameter. In this data set k_2 decreased from 0.014.± 0.007 to 0.001 ± 0.002 min^{-1} in the baseline experiments and from 0.027 ± 0.006 to 0.003 ± 0.004 min^{-1} in the stimulation experiments. An example of a 5 minute fit is illustrated at the bottom of ***Figure 2***. The low k_2 of 0.001 fits the initial data well, then the washout is clearly increased.

Effect of acetazolamide on k_2

In the 4 experiments k_2 was 0.016 ± 0.002 min at baseline and 0.016 ± 0.002 min^{-1} 10 minutes following acetazolamide injection. Laser Doppler flowmetry showed a signal increase of 61.1 ± 8.1 %.

Effect of dichloroacetate on k_2 during baseline and stimulation

Dichloroacetate pretreatment lowered arterial plasma lactate from 1.5 ± 0.1 to 1.25 ± 0.2 mmol/l (mean ± sd; $p < 0.05$) but exerted no change of arterial blood gases which stayed in the physiological range. Four hours after intravenous dichloroacetate administration, k_2 was lower at baseline and during stimulation, compared to the experiments without dichloroacetate. At baseline the values were on average 36% lower (0.009 ± 0.002 compared to 0.014 ± 0.007 min^{-1}), however, this difference failed to reach significance ($n = 5$; $p = 0.15$). During stimulation k_2 was 26% lower ($n = 5$; $p < 0.05$) than in the experiments without administration of dichloroacetate (0.020 ± 0.004 compared to 0.027 ± 0.006 min^{-1}). There was still a significant 122 % increase of k_2 from baseline to electrostimulation (from 0.009 ± 0.002 to 0.020 ± 0.004; $n = 5$; $p < 0.05$; ***Figure 3E***)

Relationship of the tissue activity and changes of the washout rate k_2

This relationship is a measure of the parameter identifiability. A larger change of the tissue activity with a unit change of k_2 is associated with a better parameter identifiability. The sensitivity analysis demonstrated that at 20 minutes, a 10 percent change in k_2 led to a 2.1 percent change in tissue activity at baseline (k_2 = 0.014 min^{-1}) and to a 3.8 percent change during stimulation (k_2 = 0.027 min^{-1}). Furthermore, the activity change in tissue was linear in the investigated range 0 – 30 % k_2 change.

B. Human studies

1-^{11}C-acetate kinetics present the same characteristics as in animal studies

In all subjects the blood gas parameters were always in the physiological range (pH = 7.35 – 7.45; pCO_2 = 35 – 45 mmHg; pO_2 = 70 – 100 mmHg). An illustration of the effect of the visual activation on the kinetic of 1-^{11}C-acetate is demonstrated in ***Figure 4*** and the quantitative values are shown in ***Figure 5***. The calculated EF of 1-^{11}C-acetate in visual cortex was 19 ± 4 % at baseline and 13 ± 3 % during stimulation. The visual stimulation increased mean CBF in visual cortex by 64 % ($p < 0.05$). In the control regions 'cerebellum' and 'frontal cortex' no significant change of the CBF was noticed. In visual cortex mean K_1 and k_2 values of 1-^{11}C-acetate were 11 % and 62 % ($p < 0.05$ for both) higher during stimulation as shown in ***Figures 5F and 5I***. No significant changes of K_1 or k_2 were noted in frontal cortex and cerebellum. However, in frontal cortex K_1 and k_2 data are somewhat distorted by a single subject which showed a decrease of the values in this region in response to visual stimulation.

Discussion

It was previously suggested that the astrocyte-specific substrate acetate allows to measure metabolism in human brains in vivo (Hosoi et al. 2004; Muir et al. 1986). However, to our knowledge this is the first study using label clearance from brain after 1-^{11}C-acetate administration for the investigation of astrocytic oxidative metabolism *in vivo*. Labeled acetate was already used in various studies to illuminate certain aspects of astrocytic metabolism. Some groups used autoradiographical determination of ^{14}C-acetate uptake (Cruz et al. 2005; Muir et al. 1986), other groups measured the metabolic fate of acetate by measuring the appearance of labeled compounds as the label travelled through the TCA cycle (e,g, (Badar-Goffer et al. 1990; Berl and Frigyesi 1969; Lebon et al. 2002; Van den Berg and Ronda 1976)).

Our study demonstrates for the first time changes of 1-^{11}C-acetate kinetics during stimulation *in vivo* which are thought to be correlated with changes of astrocytic oxidative metabolism. While total cerebral $CMRO_2$ can be successfully measured *in vivo* using PET and inhaled $^{15}O_2$ (Mintun et al. 1984; Yee et al. 2006), a direct *in vivo* measurement of $CMRO_2$ in astrocytes alone is not available.

K_1 and extraction fraction

Compared to the heart where 1-^{11}C-acetate is almost 100% extracted, the cerebral extraction fraction is about 5-fold lower. Nevertheless, brain uptake is large enough to allow quantification. One consequence of the lower extraction fraction is the blunted increase of K_1 compared to CBF during stimulation. In the human study K_1 increased 11 % compared to a 64 % increase in CBF (visual cortex).

Quantitative relationship between k_2 and astrocytic $CMRO_2$

In the following discussion about the meaning of the rate constant k_2 we provide arguments that k_2 may be strongly related to $CMRO_2$. However, it is clear that a direct proof is not given and would be difficult to establish as there is actually no data available to prove this conclusion directly. One major reason is that a direct measurement of astrocytic $CMRO_2$ is yet impossible *in vivo*.

We hypothesize that k_2 is directly related to $CMRO_2$ in the astrocytes as has been demonstrated in the heart for the myocytes (Buck et al. 1991). Prerequisites for this hypothesis are a) the washout of radioactivity from the volume of interest is indeed due to the loss of $^{11}C\text{-}CO_2$ and b) the rate limiting step determining k_2 is the production of $^{11}C\text{-}CO_2$ and not its removal.

Prerequisite a)

There seems to be no doubt that at least part of the radioactivity loss is due to $^{11}C\text{-}CO_2$, since the production of labeled CO_2 from exogenous 1-^{14}C-acetate has been proven in astrocyte cultures (Waniewski and Martin 1998). However, a quantitative proof of prerequisite a) would be difficult. One theoretical possibility would be the measurement of the arterio-venous (a-v) difference of $^{11}C\text{-}CO_2$. However, a first order estimation of this difference demonstrates that it would be in the order of 4 % of the total blood counts. The conclusive demonstration of such a small difference would require a prohibitively large amount of animals.

Prerequisite b)

It is well known that CO_2 diffuses practically freely across the blood brain barrier (Paulson 2002). It could therefore theoretically be possible that the removal of CO_2 by the blood is a limiting factor for the washout of CO_2. However, the lack of a change of k_2 following the acetazolamide-induced blood flow increases demonstrates that the removal of the radioactivity from the volume of interest is not a limiting factor.

Other arguments which point at a strong relationship between k_2 and astrocytic $CMRO_2$ are: 1) the increase of k_2 during stimulation, 2) the delay of the onset of the label washout and the decrease of the K_1/k_2 ratio during stimulation 3) the behavior of k_2 under dichloroacetate and 4) reasonable values of astrocytic $CMRO_2$ can be obtained by applying the calibration established in the dog heart.

Changes of k_2 during increased brain activity

Parameter k_2 significantly increased during stimulation. In the animal study, k_2 almost doubled from baseline to infraorbital nerve stimulation, indicating a substantial increase in oxygen consumption.

In the human study the increase in the visual cortex was 63 %. Although not significant there also seemed to be a trend towards higher values in cerebellum and frontal cortex. In fact, omitting the subject with a lower value during stimulation, the increase became significant, not surprising considering the connectivity in the brain.

Delay of the washout onset and the decrease of the K_1/k_2 ratio during stimulation

Another result pointing at ^{11}C-CO_2 as the washout agent is the delay of the washout onset (bottom graph of ***Figure 2***). Such a delay for the appearance of labeled CO_2 was demonstrated by Waniewski and Martin in cultured astrocytes and is explained by the fact that labeled CO_2 is only produced in the second turn of the label in the TCA cycle (Waniewski and Martin 1998). If the loss of label was substantially due to backdiffusion of labeled acetate, one would not expect a delay. Furthermore, if backdiffusion of labeled acetate was the main factor determining k_2, one would expect the same effect of stimulation on K_1 and k_2, i.e. the ratio K_1/k_2 would remain constant. However, the data demonstrate a markedly lower ratio during stimulation. In the anesthetized rat studies, the mean ratio dropped 44 % ($p=0.08$), in the studies with dichloroacetate the decrease was 53 % ($p=0.001$) and in the human visual cortex the ratio dropped 44 % ($p=0.048$). This behavior suggests that the labeled compounds entering and leaving the brain tissue are different. The mentioned points are all consistent with the hypothesis that the washed out compound is indeed ^{11}C-CO_2. However, we cannot completely exclude that some label loss is due to release of other labeled substrates, particularly due to efflux of glutamine, which is quickly labeled after injection of radiolabeled acetate (Cremer 1970). Despite the fact that the blood brain barrier is closed for the passage of glutamate and glutamine from blood to brain the reverse direction seems possible. Glutamine is taken up by endothelial cells and intracellularly converted by the enzyme glutaminase to glutamate. When the glutamate concentration within endothelial exceeds the one in plasma net transport of glutamate takes place through facilitative transporters (Hawkins et al. 2006). The high number of steps involved in this process and the fact that normal plasma concentration of glutamate is about 10 times higher than glutamate concentration in the extracellular fluid of the brain (Hawkins et al. 2006) indicate that this process is slow and probably not of relevance during our acquisition period of 20 minutes.

Pharmacological interventions using dichloroacetate and acetazolamide.

Also the dichloroacetate experiments are consistent with the hypothesis that k_2 is related to $CMRO_2$. This compound activates pyruvate dehydrogenase (Abemayor et al. 1984) by inhibiting its phosphorylation by the PDH kinase (Whitehouse et al. 1974). As a consequence more pyruvate is converted to acetyl-CoA and less to lactate and the concentration of acetyl-CoA is expected to increase. If the rate constants in the following chain of acetyl-CoA oxidation, which are expected to be related to k_2, remained the same, the rate of the acetyl-CoA metabolism would increase and with it most likely $CMRO_2$. However, since the energetic demand is unchanged there is no reason why $CMRO_2$ should increase. Consequently one would expect a decrease in k_2 and this is exactly what was observed, at baseline as well as during stimulation. A good candidate for regulation at this stage is citrate synthase which condenses acetyl-CoA and oxaloacetate into citrate. It has been documented that this enzyme is inhibited by increased concentrations of acetyl-CoA (Bayer et al. 1981). This inhibition could be a major reason for the observed decrease of k_2 following dichloroacetate. Furthermore, the suggested increase of the cold acetyl-CoA concentration under dichloroacetate is itself indirect evidence for the ability of astrocytes to completely oxidize glucose, as is the work by Lovatt et al. which confirmed significantly higher relative expression of almost all TCA cycles enzymes in freshly isolated astrocytes than neurons and showed that the oxidative pathways were active in astrocytes (Lovatt et al. 2007).

Analogy with previous heart studies

The idea to use the washout rate k_2 of 1-^{11}C-acetate as a marker of $CMRO_2$ was inspired by earlier studies performed in the heart (Armbrecht et al. 1990; Buck et al. 1991; Lindner et al. 2006). In those studies it was clearly established that k_2 reflects myocardial oxygen consumption in a linear fashion. One rough indication that this approach may be also valid in the brain is derived from the following estimation. In the dog heart the relationship between $CMRO_2$ and k_2 was $CMRO_2$ [ml/min/100g] = 48.8 ml/100g x k_2 [min^{-1}]. Application of this relationship to this study yields an astrocytic $CMRO_2$ of 0.7 ml/min/100g in rats and humans at baseline. This amounts to approximately 20 % of whole brain oxygen consumption (3.4 ± 0.28 ml/min/100g in man (Kety and Schmidt 1948)).This value compares favorably to published values for the fraction of astrocytic

ATP generation by oxidative processes (Hertz and Kala 2007; Hertz et al. 2007; Oz et al. 2004) which are in the range of 14 to 30 %.

Is k_2 specific for astrocytic metabolism?

One important observation in this regard is that labeled acetate is only taken up by astrocytes and not neurons (Waniewski and Martin 1998). However, a fraction of the label will eventually end up in neurons as labeled glutamine/glutamate (via the glutamate/glutamine cycle), which was produced via the α-ketoglutarate-glutamate step in the astrocytes. Nevertheless, the transfer of labeled glutamine to neurons is slow relative to the 20 minute acquisition time of this study. Lebon et al investigated astrocytic energy metabolism using nuclear magnetic resonance spectroscopy and 2-^{13}C-acetate in humans (Lebon et al. 2002). They concluded that the labeled glutamine/glutamate observed during the first 20 minutes following the start of the 2-^{13}C-acetate infusion reflected astrocytic glutamate only. It therefore seems reasonable to assume that most of the ^{11}C activity measured in our study was originating from astrocytes. Even if a small fraction of labeled glutamine/glutamate had reached the neurons, the contribution of neuronal ^{11}C-CO_2 production could be expected to have been small. Hertz et al. (Hertz et al. 1988) demonstrated in cell cultures, that glutamate oxidation of neurons was at most 25 percent of the one in astrocytes. In addition, recent work found a 4.3-fold higher expression of the enzyme glutamate dehydrogenase Glud1 in astrocytes, also suggesting a substantially higher capacity for astrocytes to metabolize glutamate (Lovatt et al. 2007).

Comparison of the k_2 method with autoradiography

Cruz et al investigated the accumulation of 2-^{14}C-acetate during acoustic stimulation in rats (Cruz et al. 2005) using autoradiography performed 5 minutes following tracer injection. They reported a 15-18% increase of 2-^{14}C-acetate uptake in the stimulated compared to the contralateral structures. These results are in line with our experiments. At 5 minutes the uptake of 1-^{11}C-acetate was 14 % higher in the stimulation compared to the baseline experiments (***Figure S1***; supplementary data). This value was calculated by simulating tissue time activity curves with a mean input curve and the mean K_1 and k_2 values of the stimulation and baseline experiments.

Here, it is crucial to point to an important difference in the methodology. By evaluating just one time-point as in autoradiographic studies, it is not easy to determine to what degree the differential uptake is influenced by increased blood flow, although this influence seems to be low for acetate (Dienel et al. 2007), but probably not negligible as our demonstration of a small K_1 increase during stimulation suggests. To separate delivery and washout a kinetic approach as chosen in this study seems advantageous. On the other hand autoradiographic studies deliver images and, when using the long-lived ^{14}C, allow an easier determination of metabolites.

Using the short-lived isotope ^{11}C we simply concentrated on two aspects of the label kinetics, delivery and washout. We cannot deliver any data concerning the fate of the label between these steps which may be very complex. An indication of this complexity is demonstrated in the model of ***Figure 6***. Previous work by Berl et al. (Berl and Frigyesi 1969) demonstrated a) that 5 minutes following injection of 1-^{14}C-acetate most label is found in amino acids and b) that there is a decline of their concentration afterwards. This may indicate that most acetate oxidation happens indirect via amino acids. More extended information on the fate of the label is found elsewhere (Berl and Frigyesi 1969; Dienel et al. 2007). Nevertheless, still more studies are needed to identify the contribution of acetate and TCA cycle metabolites as direct substrates for oxidative metabolism.

General remarks

Due to the delay of the onset of the label washout k_2 is smaller during the first minutes following injection. This effect was not taken into account in the tracer kinetic modeling, e.g. k_2 was assumed constant. To estimate the resulting error we calculated simulated tissue time-activity curves with k_2 = 0 during the first 5 minutes and = 0.027 min^{-1} thereafter. The refit of these curves using a constant k_2 demonstrated only a 1.5 % change of k_2.

Another point concerns parameter identifiability. The sensitivity analysis demonstrated that the dependence of tissue activity on k_2 is more pronounced at the higher values, implying that the k_2 values during baseline are less reliable than during stimulation. This aspect and the fact that k_2 at baseline is relatively small may lead to a relatively large error margin in the ratio $k_{2simulation}/k_{2baseline}$. We also did not consider the effect of blood-borne ^{11}C-CO_2 on K_1 and k_2. Most of the CO_2 in blood is converted to HCO_3^- which does not cross the blood brain barrier. Approximately 5 percent of

total HCO_3^-/CO_2 is present as dissolved ^{11}C-CO_2 (Brooks et al. 1984) which freely penetrates the brain. We constructed simulated tissue time activity curves using the one-tissue compartment model and the blood-borne ^{11}C-CO_2 as a second input curve. K_1 and k_2 values for this fraction of CO_2 were taken from Brooks et al. (Brooks et al. 1984). These tissue time activity curves were then refitted using the standard one-tissue compartment model not considering blood borne ^{11}C-CO_2. The deviation of the K_1 and k_2 values was less than 1.5 percent, demonstrating that the effect of blood-borne ^{11}C-CO_2 on K_1 and k_2 is negligible.

Summary

1-^{11}C-acetate seems a promising tracer to investigate astrocytic oxidative metabolism in animals and humans. If the washout rate is indeed representing the production of ^{11}C-CO_2, then its increase during stimulation would point to a substantially higher astrocytic oxidative metabolism during brain activation. However, the quantitative relationship between k_2 and $CMRO_2$ needs to be determined in future experiments.

Appendix

Details of beta probe experiments and human PET measurements

Blood and tissue processing

a) Physiological blood parameters

Several blood gas variables (pH, pCO_2, pO_2) relevant to cerebral energy metabolism were measured with a pH/blood gas analyzer (AVL, Compact 3, Roche Diagnostics, Switzerland) before the start of tracer kinetic measurements. Plasma lactate levels were determined before the first tracer injection in 24 animals (Ektachem DT, Kodak, USA). In animals of group V (dichloroacetate challenge) lactate levels were determined twice, before and 4 hours after injection of dichloroacetate respectively. (Ektachem DT, Kodak, USA). In 5 animals there were technical problems with the analyzer rendering a measurement impossible.

b) Determination of the arterial plasma input curve

For the CBF measurements arterial blood was continuously drawn during scanning and the activity in the catheter was measured in a coincidence counter (GE Medical Systems) which was cross calibrated with the beta scintillator and the PET scanner respectively. During the 1-^{11}C-acetate scan arterial radioactivity was also measured online for the total scan time in the animal experiments (for an example of acquired time activity curves see ***Figure 1***). In the human study it was acquired online only for the first five minutes so as not to miss the peak of the arterial input curve, thereafter for the remaining 15 minutes four single samples were taken manually at different time points (around 3, 6, 15 and 25 minutes) and processed as described below. Whole blood activity was then corrected for a) a different tracer concentration in whole blood and plasma and b) the build-up of labeled metabolites. The ratio "$^{11}C_{plasma}/^{11}C_{whole\ blood}$" was determined in all animals at different time-points (3 blood samples per injection). The data of all animals were then pooled and the time course of the ratio was approximated by fitting a quadratic polynomial to the data. This function was then used to convert counts in whole blood to counts in plasma. In humans, the ^{11}C

concentration in whole blood (CB) was first converted to ^{11}C concentration in plasma (C_{PL}) using the same conversion function as determined in rats.

Secondly, plasma activity was corrected for the build-up of labeled metabolites using data from previous 1-^{11}C-acetate studies in the human heart (Buck et al. 1991).

c) Metabolite analysis in blood

Three blood samples (about 400 µl each) were collected at different time points during each 20 minutes acquisition for analysis of authentic tracer and metabolites. These samples were first centrifuged for 3 minutes at 2000 rpm. Proteins were then precipitated with 75 µl acetonitrile in 50 µl plasma. After a second centrifugation for 3 minutes at 2000 rpm, the composition of the ^{11}C-derived radioactivity in the supernatant (80 µl) was analyzed by high-pressure liquid chromatography (HPLC) on a polymeric column (PRP-1, 5-µm, 250 × 4.1 mm i.d., Hamilton, U.S.A.) with 3 mmol/l phosphoric acid in water (pH 2.67) as the mobile phase (1 ml/min). The amount of authentic tracer was expressed as a fraction of total plasma ^{11}C counts (f).

The fraction data of all animals was then pooled and the time-course of the fraction was approximated by a decaying exponential function of the form function $f = 1-\alpha(1-\exp(-\mu t))$. This function was subsequently employed to convert the total plasma activity to the time-course of authentic 1-^{11}C-acetate (= input curve).

Data analysis

In the animal and human studies the analytical and statistical methods were similar as described below. All calculations were performed using the software package PMOD ((Mikolajczyk et al. 1998); PMOD Technologies, Adliswil, Switzerland).

a) CBF measurements

The basis of the calculation for CBF measurements was the one-tissue compartment model including a partition coefficient for H_2O (see ***Figure 6A***). The change of the radioactivity concentration in tissue C_T is then defined by the following differential equation

$$dC_T/dt=CBF(C_A(t)-C_T(t)/p) \quad (1)$$

where C_A is the arterial tracer concentration and p is the tissue partition coefficient, e.g that fraction of tissue that is permeable for $H_2{}^{15}O$. In this configuration C_T is the concentration of $H_2{}^{15}O$ in 1 ml of brain and it is assumed that $H_2{}^{15}O$ immediately reaches a homogeneous concentration in permeable space and no division into a vascular and a tissue compartment is necessary. The analytical solution of (1) is

$$C_T=CBF \exp(-CBF/p\ t) \otimes C_A \quad (2)$$

where $\otimes$ means mathematical convolution.

Equation 2 was fitted to the data using least squares fitting (Marquardt algorithm) implemented in the software PMOD (Mikolajczyk et al. 1998). Prior to data analysis tissue TACs and arterial input curves were corrected for physical decay of ^{15}O.

With the human $H_2{}^{15}O$ PET data we calculated quantitative parametric maps representing regional cerebral blood flow (rCBF) using the integration method described by Alpert (Alpert et al. 1984). This method yielded maps of K_1 and k_2 which represent rCBF and rCBF/p respectively (p = partition coefficient). Before calculation of the parametric maps, the input curve was corrected for delay and dispersion.

b) 1-^{11}C-acetate experiments

The investigated method consisted of standard compartmental modeling using an arterial input function. Tracer kinetic modeling was performed using the one-tissue compartment model depicted in ***Figure 6B***.

K_1 : describes uptake of tracer across the blood brain barrier. K_1 is related to the first pass extraction fraction (EF) and CBF through the following equation: K_1= EF x CBF. This equation was used to determine EF in the animal and human experiments.

k_2 : represents back-diffusion of radioactivity from tissue to vascular space

Tracer exchange between the compartments is described by the following differential equation

$$\frac{dC_T}{dt} = K_1 C_p - k_2 C_T \qquad (3)$$

Since the total activity measured in a region is composed of counts from tissue and blood, all models contained a parameter (α) correcting for blood activity.

$$C_{voi} = (1-\alpha)C_T + \alpha C_B \qquad (4)$$

where

C_{VOI}: in the human PET study, C_{VOI} is the ^{11}C activity concentration in the defined volume of interest, in the animal study it is the ^{11}C activity measured by the tip of the beta scintillator.

α: percentage of intravascular space in tissue

C_T: Activity in the extra vascular compartment

C_B: total blood activity

C_T was calculated by numerical integration of the differential equations. The correction for the contribution of blood in the brain (α) was fixed at 0.05. This value considers that signals originating from large superficial pial vessels impact the beta scintillator measurements.

Delay of onset of radiolabel washout

To check whether the start of the radioactivity washout from tissue was delayed, the first 5 minutes of data following tracer injection were refitted with only k_2 as a free parameter and K_1 fixed to the full length fit.

Figures of Chapter I:

Stimulation-induced Increases of Astrocytic Oxidative Metabolism in Rats and Humans investigated with 1-^{11}C-Acetate

Figure I-1. Acquired time activity curves of 1-^{11}C-acetate and plasma fraction of true 1-^{11}C-acetate

In the upper panel the time course of ^{11}C radioactivity in whole blood (●), plasma (□) and brain tissue (▼) acquired over 20 minutes is shown. In addition the model fit is demonstrated (straight line, K_1 = 0.085 ml/min/ml tissue, k_2 = 0.015 min^{-1}). The goodness-of-fit is demonstrated by the random distribution of the residuals, demonstrated in the insert.

In the lower panel the fraction f of true 1-^{11}C-acetate in plasma in animal and human studies is plotted. The filled circles represent data points from animal studies (anesthetized rats) and the solid line is the corresponding fit of the function f = 100-α(1-exp(-μt)). Least squares fitting yielded α = 93 % and μ = 0.11 min^{-1}. In the human study (open circles; conscious humans), α and μ were taken from previous experiments which had yielded very similar values (α = 91%, μ = 0.13 min^{-1}) (Buck et al. 1991).

Figure I-1

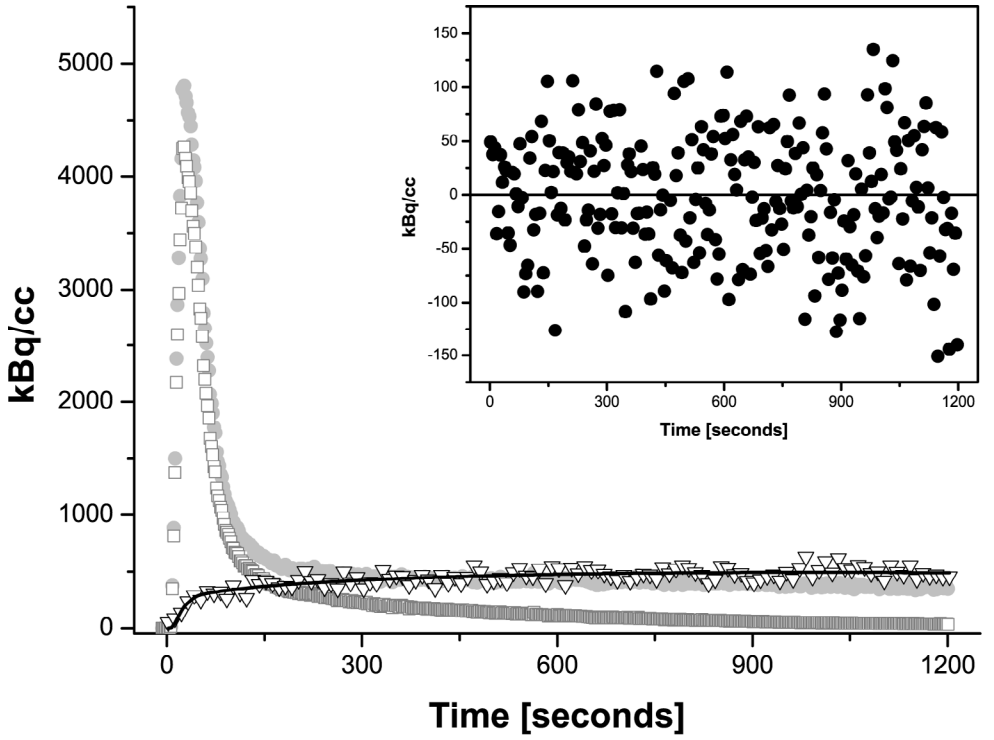
kBq/cc
Time [seconds]
kBq/cc
Time [seconds]

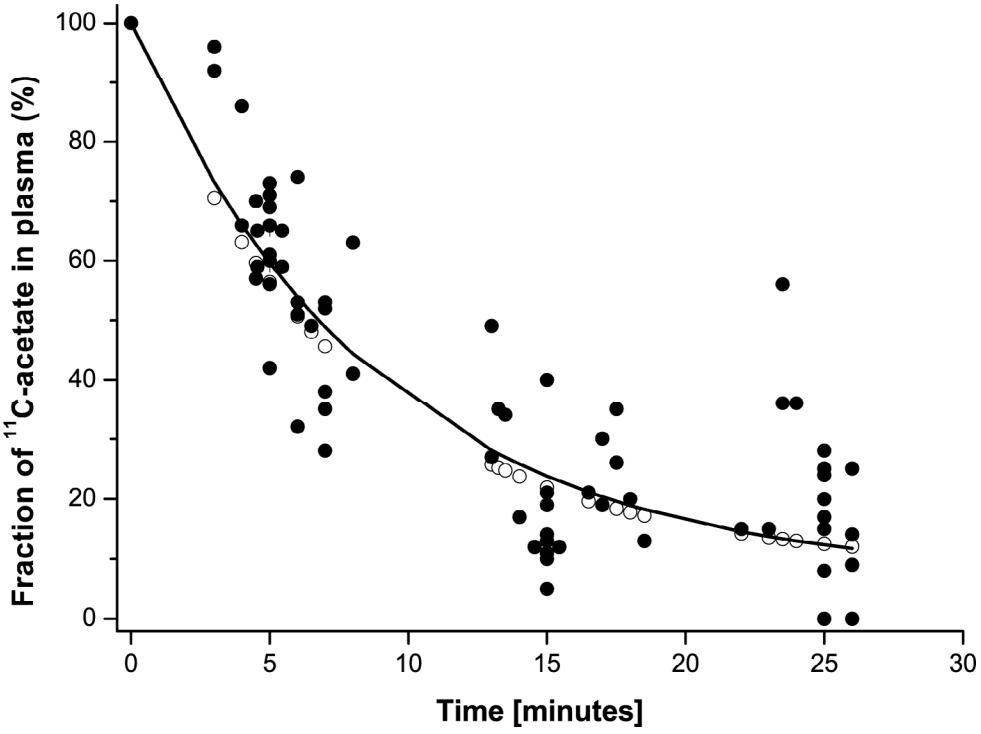
Fraction of ^{11}C-acetate in plasma (%)
Time [minutes]

Figure I-2. Label washout is increased during stimulation after a delay

The top and middle graph demonstrate time activity curves of ^{11}C activity in rat brain tissue normalized to injected activity per g bodyweight yielding standardized uptake values (SUV). The curves represent mean data from 5 experiments. In the baseline-baseline experiments (top panel) the curves appear identical. In contrast, the washout of ^{11}C activity is remarkably larger during stimulation (middle panel). The bottom panel illustrates the residuals between fit and data if only the first 5 minutes of data are fitted. Such a short fit yields substantially lower initial washout rates than a 20 minute fit, demonstrating that the onset of the washout of radiolabel from tissue is delayed.

Figure I-2

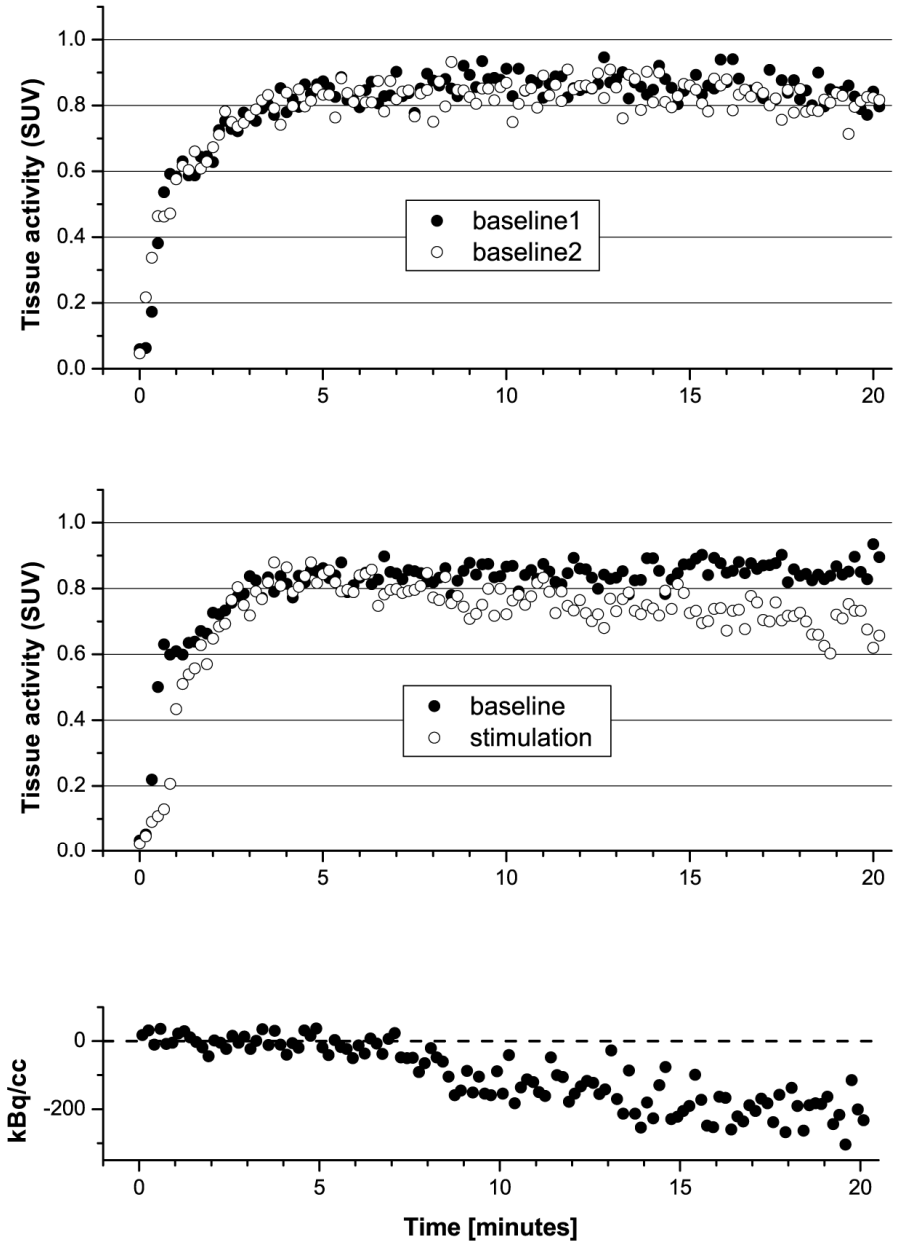
Tissue activity (SUV)
1.0
0.8
0.6
0.4
0.2
0.0
0
5
10
15
20
baseline1
baseline2
Tissue activity (SUV)
baseline
stimulation
kBq/cc
0
-200
Time [minutes]

Figure I-3. Summary of animal data

Panels A and B demonstrate the reproducibility of parameters K_1 and k_2. There was no significant change of K_1 and k_2 between sequential baseline experiments. Panels C and D show the increase of K_1 and k_2 during infraorbital nerve stimulation. The values of k_2 following the administration of dichloroacetate (DAC, 50 mg/kg) at baseline and during infraorbital nerve stimulation are demonstrated in panel E. The p values were calculated using the Wilcoxon Signed Rank test. Values are given as mean ± SD.

Figure I-3.

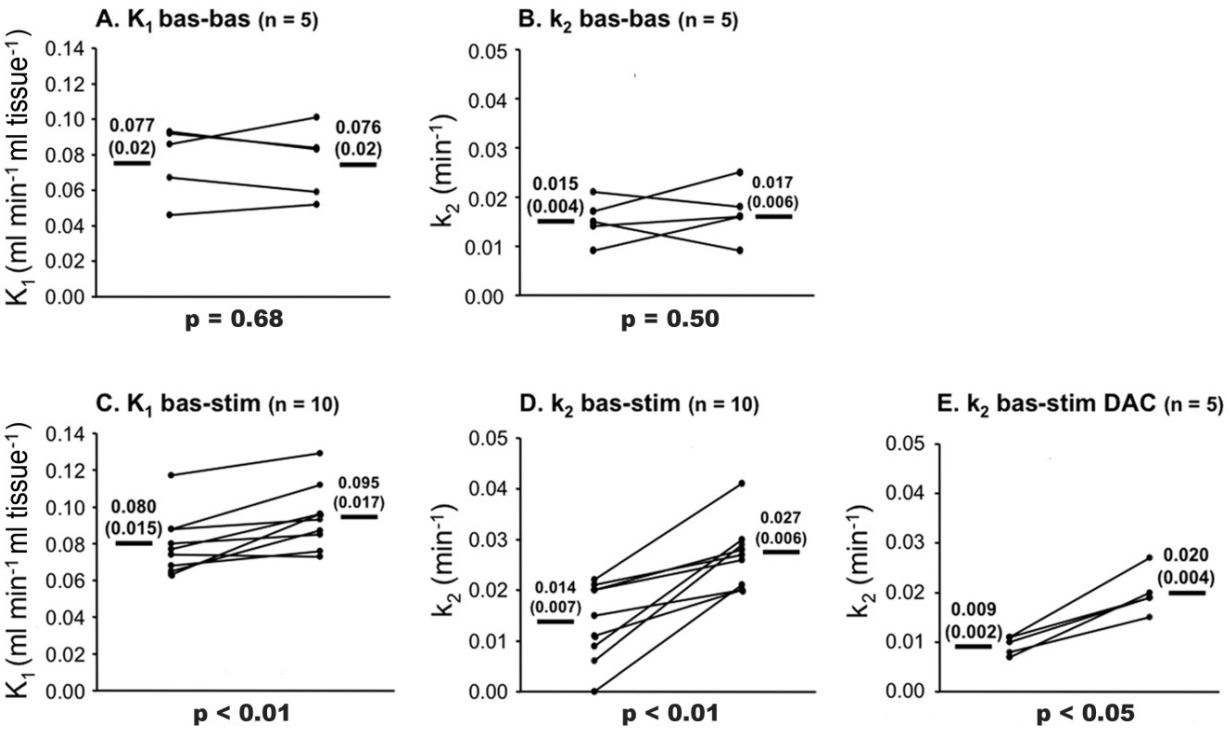
A. K1 bas-bas (n = 5)
K1 (ml min-1 ml tissue-1)
0.077 (0.02)
0.076 (0.02)
p = 0.68
B. k2 bas-bas (n = 5)
k2 (min-1)
0.015 (0.004)
0.017 (0.006)
p = 0.50
C. K1 bas-stim (n = 10)
K1 (ml min-1 ml tissue-1)
0.080 (0.015)
0.095 (0.017)
p < 0.01
D. k2 bas-stim (n = 10)
k2 (min-1)
0.014 (0.007)
0.027 (0.006)
p < 0.01
E. k2 bas-stim DAC (n = 5)
k2 (min-1)
0.009 (0.002)
0.020 (0.004)
p < 0.05

Figure I-4. Clearance of ^{11}C activity is also increased during stimulation in human visual cortex

Time-activity curves of 1-^{11}C-acetate uptake in the human visual cortex normalized to injected activity per kg bodyweight yielding standardized uptake values (SUV). The curves represent mean data from all 6 human experiments. During visual stimulation the clearance of ^{11}C activity is larger compared to baseline. Note also the modestly faster wash-in of radioactivity during stimulation.

Figure I-4

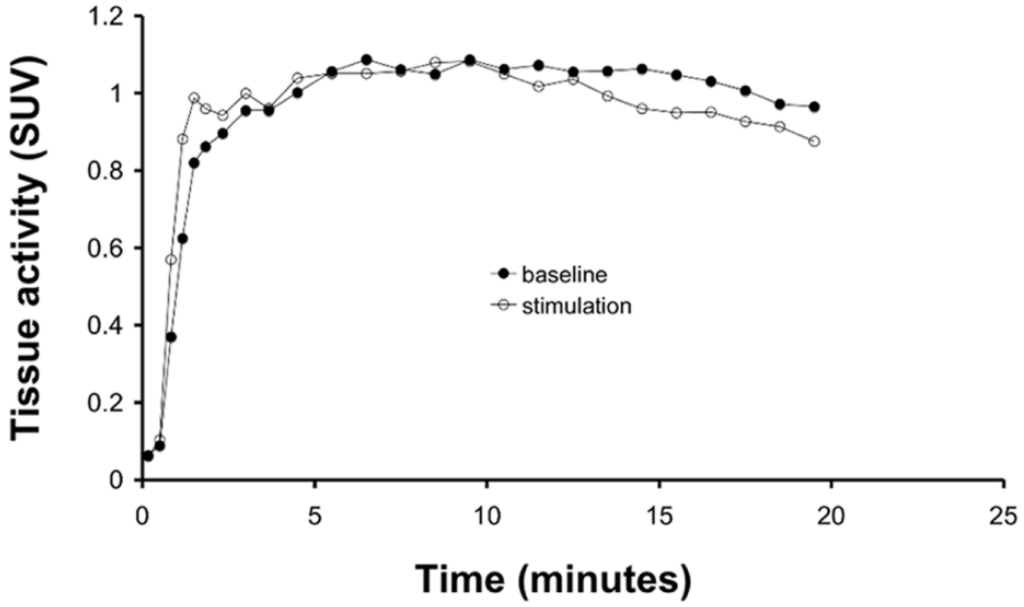
Tissue activity (SUV)
1.2
1
0.8
0.6
0.4
0.2
0
0
5
10
15
20
25
Time (minutes)
baseline
stimulation

Figure I-5. Summary of human data

Summary of human data. The change of CBF from baseline to visual stimulation in the 3 examined brain areas is demonstrated in the top panels, the one of K_1 and k_2 of 1-^{11}C-acetate in the middle and bottom panels respectively. The p values were calculated using Wilcoxon Signed Rank test. Values are given as mean ± SD.

Figure I-5

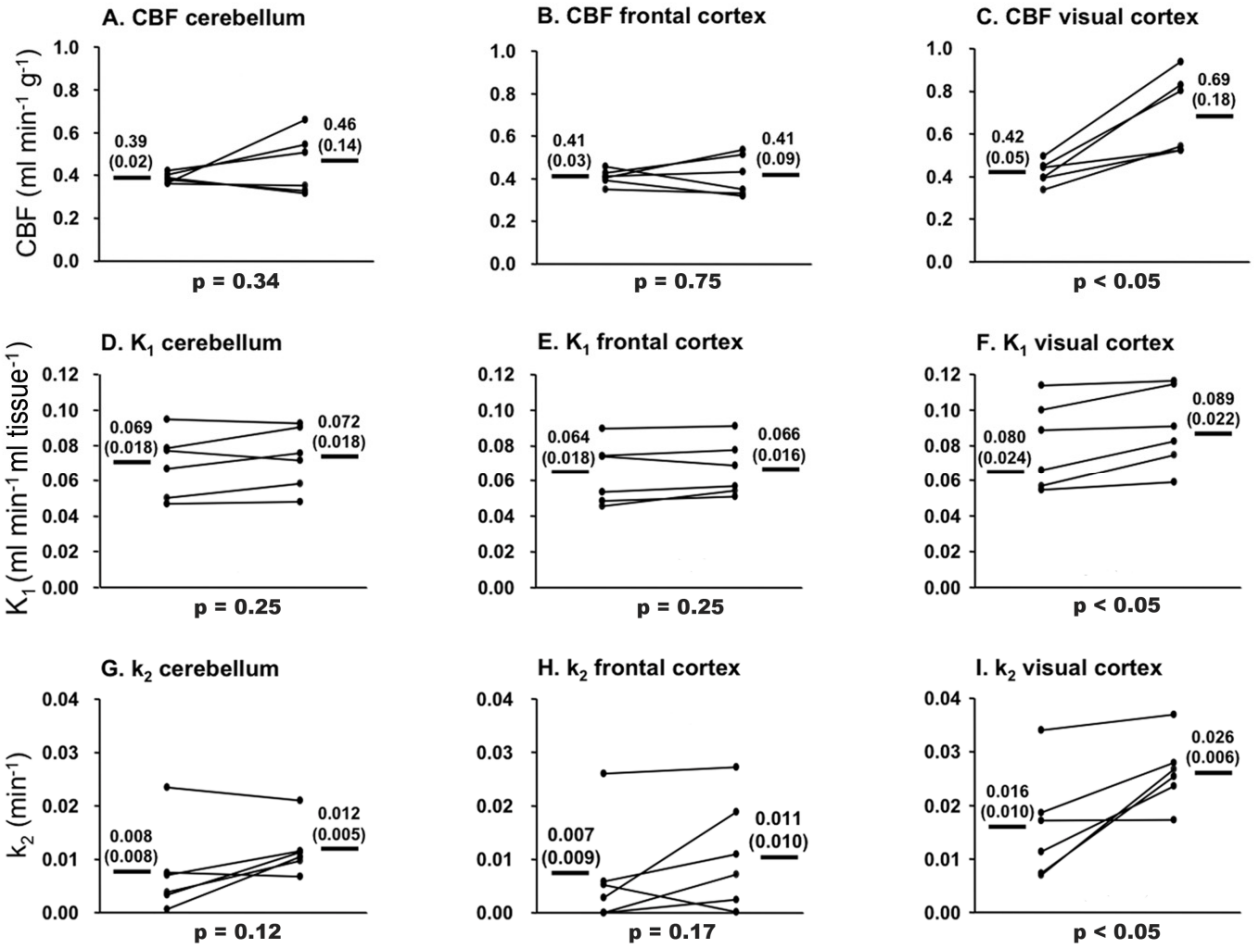
A. CBF cerebellum
CBF (ml min-1 g-1)
0.39 (0.02)
0.46 (0.14)
p = 0.34
B. CBF frontal cortex
0.41 (0.03)
0.41 (0.09)
p = 0.75
C. CBF visual cortex
0.42 (0.05)
0.69 (0.18)
p < 0.05
D. K1 cerebellum
K1 (ml min-1 ml tissue-1)
0.069 (0.018)
0.072 (0.018)
p = 0.25
E. K1 frontal cortex
0.064 (0.018)
0.066 (0.016)
p = 0.25
F. K1 visual cortex
0.080 (0.024)
0.089 (0.022)
p < 0.05
G. k2 cerebellum
k2 (min-1)
0.008 (0.008)
0.012 (0.005)
p = 0.12
H. k2 frontal cortex
0.007 (0.009)
0.011 (0.010)
p = 0.17
I. k2 visual cortex
0.016 (0.010)
0.026 (0.006)
p < 0.05

Figure I-6. Compartment models used for data analysis

One-tissue compartment models used in animal and human studies to analyze CBF using $H_2{}^{15}O$ (A) and the kinetics of 1-^{11}C-acetate respectively (B). K_1 describes the transfer of acetate from blood to tissue whereas k_2 corresponds to the flux of radiolabel from tissue to blood. Labeled acetate in tissue (Cac-tiss) is converted to acetyl-CoA, catalyzed by acetyl-CoA synthetase. Acetyl-CoA then enters the TCA cycle, where the label can either be transferred to CO_2 or metabolites (Cm-tiss) such as glutamine and glutamate which were produced via α-keto-glutarate. Some labeled metabolites will reenter the TCA cycle at the α-keto-glutarate level and in this way yield more labeled CO_2. In theory, k_2 denotes the backdiffusion of all labeled species from tissue. However, as discussed in the main text, we argue that the loss of label is mainly due to backdiffusion of ^{11}C-CO_2, and that the rate of this label loss, described by k_2, is reflecting the production of CO_2 and is therefore closely related to oxidative metabolism.

Figure I-6

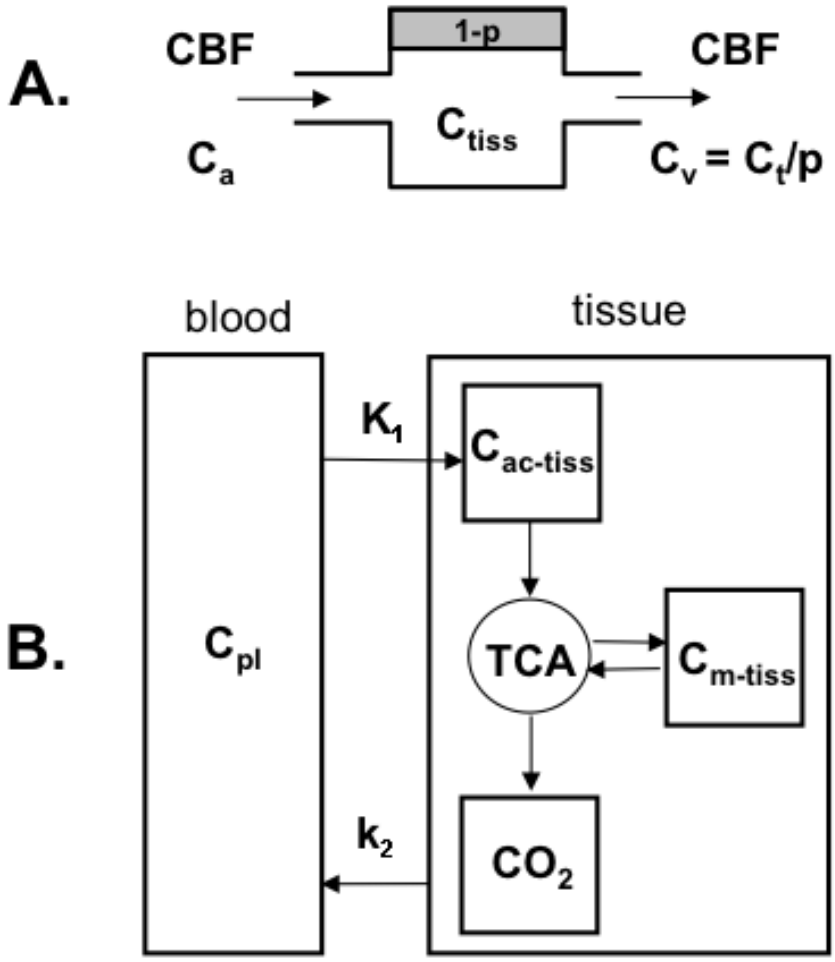
A.
CBF
1-p
CBF
C_{tiss}
C_a
$C_v = C_t/p$
B.
blood
tissue
K_1
$C_{ac\text{-}tiss}$
C_{pl}
TCA
$C_{m\text{-}tiss}$
k_2
CO_2

Supplementary Information

Supplementary Figure S1.

Tissue time activity curves are shown using a mean input curve and the mean K_1 and k_2 values of the stimulation and baseline experiments in anesthetized rats respectively. Note the higher uptake of 1-^{11}C-acetate (+ 14 %) after 5 minutes in the stimulation experiments.

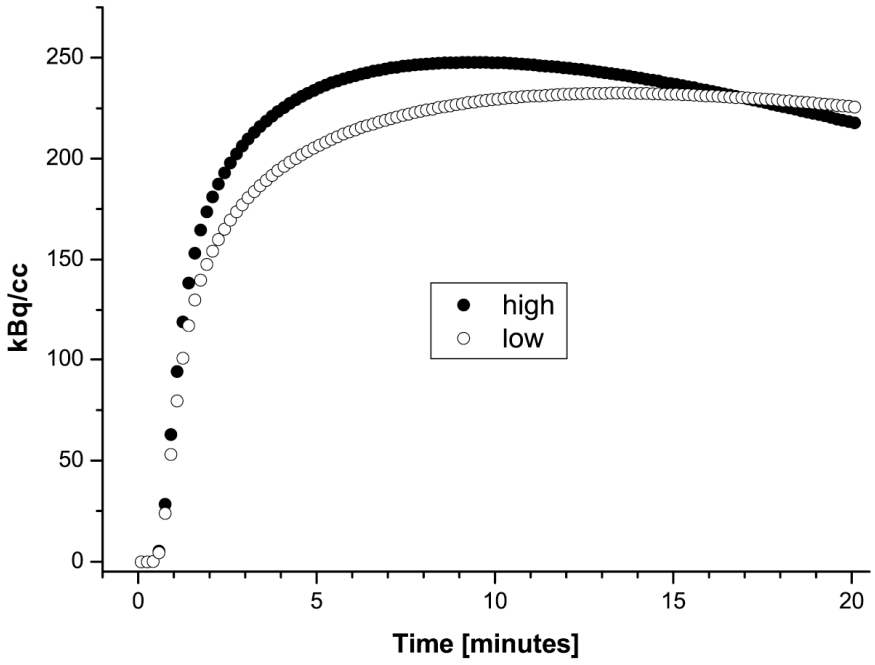

Chapter II

The Kinetic Behavior of radiolabeled L-lactate in the Rat Brain

M.T. Wyss[1], B. Weber[1,2], D. Wild[3], K. Drandarov[4], G. Westera[4], C. Burger[1], L. Pellerin[5], P.J. Magistretti[6] and A. Buck[1]

[1]PET Center, Division of Nuclear Medicine, University Hospital, Zürich, Switzerland
[2]Institute of Pharmacology and Toxicology, University of Zürich, Zürich, Switzerland
[3]Clinic and Institute of Nuclear Medicine, University Hospital Basel, Basel, Switzerland
[4]Center for Radiopharmaceutical Science of PSI, ETH and USZ, Villigen and Zurich, Switzerland
[5]Physiology Department, University of Lausanne, Lausanne, Switzerland
[6]Brain Mind Institute, École Polytechnique Fédérale de Lausanne (EPFL), Lausanne, Switzerland

Abbreviated title: Cerebral kinetics of radiolabeled L-lactate

Abstract

Introduction: There is considerable debate in the neuroscience community regarding cerebral lactate metabolism. The purpose of this study was to examine the kinetics of 1-^{11}C-L-lactate in the rat brain with the goal to use it for the investigation of neuronal lactate oxidation and neuronal oxidative metabolism in general. **Methods:** The study was performed in anesthetized adult Sprague Dawley rats. Following the injection of 200 – 300 MBq of 1-^{11}C-L-lactate, 20 minutes of data were recorded using a beta scintillator. The arterial input curve was determined by continuously monitoring the ^{11}C activity in a femoral a-v shunt and subsequent metabolite correction. Acquisitions were performed either during baseline or during electrical infraorbital nerve stimulation. In a second part of the study it was possible to use a novel high-sensitivity beta probe enabling two tracer injections in the same animal allowing intra-animal comparisons. Finally, lactate transport was pharmacologically blocked in two animals and the effect on the kinetics was investigated. Data were analyzed using a one-tissue compartment model containing the rate constants K_1 and k_2.

Results: In the inter-animal comparison no difference of the kinetics during the two different activity states could be observed. K_1 and k_2 during baseline were 0.105 ± 0.03 (mean ± sd) ml * min^{-1} * ml$_{tissue}^{-1}$, and 0.089 ± 0.03 min^{-1}, during stimulation 0.111 ± 0.04 ml * min^{-1} * ml$_{tissue}^{-1}$, and 0.086 ± 0.02 min^{-1}, respectively. In contrast, the intra-animal comparison showed an increased k_2 (on average +24% from baseline) during stimulation. Blockade of lactate transport largely reduced both lactate influx (K_1) and k_2.

Conclusion: 1-^{11}C-L-lactate is a feasible tracer for brain studies *in vivo*. Provided that lactate uptake is limited to neurons, the increase of the label washout rate during stimulation indicates that the tracer may be closely related to neuronal oxidative metabolism.

Key words: beta scintillator, kinetic modeling, neuronal lactate oxidation, radiolabeled L-lactate

Acknowledgements

Matthias Wyss and Bruno Weber were supported by the Swiss National Science Foundation (Grants 3100A0-105804/1 and PP00B-110751/1), by the OPO-Stiftung Zürich and the Novartis Research Foundation. Luc Pellerin is supported by the Swiss National Science Foundation Grant 3100A0-112119.

Introduction

The presence of lactate in the brain has been considered for a long time as a threat to proper brain function and as a sign of tissue suffering. Therefore, the finding that lactate is efficiently oxidized to CO_2 in different neuronal preparations, sometimes even preferred to glucose (Bouzier-Sore et al. 2003a; Larrabee 1995; Larrabee 1996; McKenna et al. 2001; Schurr et al. 1999; Tabernero et al. 1996), is surprising. Evidence that neurons oxidize lactate as a metabolic substrate to satisfy at least in part their energy needs was provided with different approaches also *in vivo*. Magnetic resonance spectroscopy studies showed that intravenously injected lactate was readily metabolized by the brain in a compartment lacking pyruvate carboxylase activity (Bouzier et al. 2000; Hassel and Brathe 2000). Because pyruvate carboxylase activity is found only in astrocytes (Hertz 2004), it was suggested that lactate oxidation occurs predominantly in neurons. Additionally, it was concluded from the labeling pattern of compounds such as glutamine, glutamate and γ-aminobutyric acid (GABA), that lactate must be used in large parts by glutamatergic neurons (Qu et al. 2000). An indirect *in vivo* confirmation of the preferred use of lactate over glucose by the brain was obtained in human subjects using positron emission tomography (PET) and ^{18}F-fluorodeoxyglucose. Smith and coworkers (2003) found that raising plasma lactate levels to values reached during moderate exercise substantially reduced brain glucose utilization, suggesting preferential lactate use by the brain. Despite of all this *in vivo* evidence, the insight in cerebral lactate oxidation is still weak and new approaches for the investigation of lactate use *in situ* are of interest.

Tracer kinetic measurements using radiotracer methods such as beta scintillators and PET provide powerful approaches for the *in vivo* determination of biochemical and physiological processes. If lactate is preferentially taken up and oxidized by neurons, then tracer studies with radiolabeled lactate may be a feasible method to gain more insight into neuronal energy metabolism. Furthermore, we hypothesize that the lactate tracer kinetics will not only probe the neuronal lactate metabolism but also total neuronal oxidative metabolism. Based on this hypothesis we evaluated the kinetics of 1-^{11}C-L-lactate in the rat brain at baseline and during various manipulations using a

beta scintillator. Topics of interest were the question if the tracer exhibits feasible kinetic characteristics enabling *in vivo* cerebral tracer studies and the evaluation of possible changes at increased activity of the brain.

Material and methods

Tracer production

1-[^{11}C]lactic acid enantiomers were produced as described elsewhere (Drandarov et al. 2006). In short, racemic 1-[^{11}C]lactic acid was made by [^{11}C]cyanohydrine synthesis starting from [^{11}C]HCN (trapped as [^{11}C]KCN) and acetaldehyde bisulfite adduct. The quantitatively formed 1-[^{11}C]-DL-lactonitrile was hydrolyzed by reflux in concentrated HCl and the reaction mixture was introduced directly into a semipreparative polymeric HPLC column (Phenomenex, Polymerx 10µ, 250x10 mm, 0.03% H_3PO_4 as the mobile phase) where the product was isolated from the aggressive reaction matrix. Then the collected racemic 1-[^{11}C]lactic acid was automatically introduced into a preparative chiral HPLC column coated with a penicillamine derived chiral selector and eluted with 1 mM $CuSO_4$ solution as the mobile phase where both enantiomers were separated by ligand exchange chromatography. The fractions corresponding to [^{11}C]-D- or [^{11}C]-L-lactic acid, were passed through anion exchanger Sep-Pak® cartridges (Accell™ Plus QMA, in CO_3^{2-} form) where the Cu^{2+} ions (as insoluble carbonate) and the [^{11}C]-lactate are retained. The latter was selectively washed out from the cartridges with 2 mmol/L sodium phosphate buffer pH 7.4 to obtain injectable solutions of pure Na-[^{11}C]-D- and L-lactate enantiomers. The quality control of the final product was done by chiral ligand exchange HPLC. The procedure lead to a product of >99 % chemical and enantiomeric purity. The specific activity at the end of synthesis was about 400 GBq/µmol.

Animals

The study included 22 male Sprague-Dawley rats weighing 245 to 327 g. Four animals were excluded from final analysis due to problems during surgery or during the experimental acquisitions. Finally 18 animals were included in the analysis. The experiments were carried out by licensed investigators and approved by the local veterinary authorities. The animals were kept in cages with standardized conditions of light (day/night-cycle 12h/12h) and temperature and free access to food and water. Before the experiments the animals were fasted overnight.

General animal preparation

Surgery was performed under isoflurane anesthesia (3.5% in air/oxygen 70%/30%) and involved the placement of an arteriovenous shunt (a-v shunt) from the right femoral artery to the right femoral vein and tracheotomy for mechanical ventilation. The actual experiment was performed under urethane anesthesia (1400 mg/kg i.p.). The a-v shunt was used for the injection of the tracer, for the collection of blood samples, for the continuous monitoring of arterial blood pressure and for the online acquisition of total arterial ^{11}C activity. For the latter purpose, the shunt was run through a coincidence scintillator (GE Medical Systems) that stored at 1-second intervals. The online arterial sampling procedure is described in detail elsewhere (Weber et al. 2002a).

Beta scintillator studies

Two different systems were used in this study. For a first series of experiments a single channel system with a intracortical probe was used. The beta scintillator (Swisstrace GmbH, Zurich, Switzerland) has been described in detail earlier (Weber et al. 2003; Wyss et al. 2007). In brief, it consists of a scintillation tip (Bicron, BF412, Newbury, OH, USA) with a length of 1 mm and a diameter of 0.25 mm attached to a high numerical aperture glass fiber. As described below in a second group of animals a recently developed two channel system with surface probes could be utilized. These devices consist of larger scintillator crystals with a thickness of 0.2 mm and a diameter of 3 mm leading to a higher sensitivity.

The scintillators were made light-tight by applying a uniform coating of silver particles. The scintillations were measured using a photomultiplier tube and counting electronics (Perkin Elmer, Massachusetts, USA). The limited range of beta particles within biological tissues leads to a limited detection volume centered around the scintillating tip of the probe. Monte Carlo simulations demonstrated that for C-11 the distance required to detect 90 % of the beta particles around the probe is 2.0 mm (Pain et al. 2002b). The sensitivities of the used beta scintillators were 0.036 to 0.047 cps/kBq/cc and 0.31 to 0.60 cps/kBq/cc for the intracortical and the surface probe device, respectively.

The intracortical scintillator was inserted into the primary somatosensory cortex using a stereotactic frame (David Kopf Instruments, Tujunga, CA, USA). The skull was exposed and a

craniotomy was performed using a dental drill. The dura was carefully incised at the insertion position, which was (according to Bregma) 2 mm posterior and 5 mm lateral. This position was adjusted to avoid large superficial blood vessels. The scintillator was carefully lowered to a depth of 1.4 mm. In experiments with the surface probe system the detector was adjusted just above the thinned skull at the same coordinates. The count rate was stored on a personal computer using a bin width of 1 second yielding tissue time activity curves (TACs). Following each experiment the beta scintillator was calibrated with known concentration of ^{11}C activity. For data analysis all data were background-corrected (range of background count rates: 0-2 cps for the intracortical system and 2-8 cps for the surface probe system), decay corrected to the time point of injection and converted to kBq/ml.

In the stimulation experiments, the efficiency of the stimulation and the correct positioning of the beta probe was verified by Laser Doppler flowmetry (Periflux System 5000, Perimed AB, Järfälla, Sweden).

Experimental protocols

a) Intracortical probe

In a first group of 6 animals the time-course of 1-^{11}C-L-lactate was measured at baseline. Twenty minutes of data were acquired after injection of 200-300 MBq (diluted in 0.5 mL) of tracer. In 4 of these animals baseline cerebral blood flow (CBF) was determined prior to 1-^{11}C-L-lactate injections using $H_2{}^{15}O$ and the methodology described previously (Weber et al. 2003). The first pass extraction fraction (EF) was calculated using the relationship $EF = K_1/CBF$ where K_1 is the transport parameter describing tracer transport from blood to tissue.

.

In a second group of 7 animals TACs were acquired during electrical infraorbital nerve stimulation to elicit increased brain activity. The current was adjusted to 2 mA and 2 Hz stimulation frequency was chosen because previous experiments using ^{18}F-fluorodeoxyglucose autoradiographies demonstrated this frequency to be optimal eliciting a maximal increase in glucose consumption of about 70 to 80 % (unpublished data). The stimulation started 30 seconds prior to tracer injections.

b) Surface probe

In total, in 5 animals 1-^{11}C-L-lactate experiments were performed with a novel surface probe, developed and evaluated in our lab. In this set of experiments two subsequent tracer injections were possible in the same animal due to the improved sensitivity of the system. In 3 animals one acquisition was performed during baseline conditions and the other during electrostimulation. The order was changed between single experiments to check for a potential order effect. Finally, in 2 animals the effect of blockade of the monocarboxylic acid transporters using α-cyano-4-hydroxy-cinnamate (4-CIN) on the kinetics of ^{11}C-L-lactate was tested. The MCT blocker was injected intraperitoneally in a concentration of 90 mg/kg 30 min prior to the tracer injection. The permeability of the blood brain barrier to 4-CIN has been shown previously (Schurr et al. 2001).

Data acquisition and analysis

a) CBF measurements

The basis of the calculation of the CBF measurements was the one-tissue compartment model including a partition coefficient for $H_2{}^{15}O$ (see ***Figure 1A***). The change of the radioactivity concentration in tissue C_{tiss} is then defined by the following differential equation

$$dC_{tiss}/dt = CBF(C_a(t)-C_{tiss}(t)/p) \qquad (1)$$

where C_a is the arterial tracer concentration and p is the tissue partition coefficient, e.g. that fraction of tissue that is permeable for $H_2{}^{15}O$. In this configuration C_{tiss} is the concentration of $H_2{}^{15}O$ in 1 ml of brain and it is assumed that $H_2{}^{15}O$ immediately reaches a homogeneous concentration in permeable space and no division into a vascular and a tissue compartment is necessary. The analytical solution of (1) is

$$C_{tiss} = CBF * \exp(-CBF/p\ t) \otimes C_a \qquad (2)$$

where $\otimes$ signifies mathematical convolution.

Equation 2 was fitted to the data using least squares fitting (Marquardt algorithm) implemented in the software PMOD ((Mikolajczyk et al. 1998); PMOD Technologies, Adliswil, Switzerland). Prior to data analysis tissue time activity curves and arterial input curves were corrected for physical decay of ^{15}O.

b) 1-^{11}C-L-lactate experiments

The investigated methods consisted of standard compartmental modeling using an arterial input function. Tracer kinetic modeling was performed using the one-tissue compartment model depicted in ***Figure 1B***.

K_1: describes uptake of tracer across the blood brain barrier and is related to blood flow (CBF) and the first pass extraction fraction EF (K_1= CBF * EF).

k_2: represents backdiffusion of label from tissue to vascular space.

Tracer exchange between the compartments is described by the following differential equations

$$dC_{tiss}/dt = K_1C_{plasma}(t) – k_2C_{tiss}(t) \quad (3)$$

Since the total activity measured in a region is composed of counts from tissue and blood, all models contained a parameter (α) correcting for blood activity.

$$C_{VOI} = (1 – \alpha)C_{tiss} + \alpha C_{blood} \quad (4)$$

where

C_{VOI}: ^{11}C activity measured by the tip of the beta scintillator

α: percentage of intravascular space in tissue

C_{tiss}: Activity in the extravascular compartment

C_{blood}: total blood activity

C_{tiss} was calculated by numerical integration of the differential equations. The vascular fraction α was included as a fit parameter which improved the least square fit as compared to a fixed value of α = 5%.

Model adjustments for the dual-injection paradigm

The kinetic model was adjusted in two ways for the analysis of the dual-injection data of the study part using the surface probe: (1) Two sets of rate constants (K_1, k_2) were used in the calculation of the operational equation. The first set for the time until the second injection, and the second set thereafter. The least-squares fit procedure resulted in estimates for all 4 rate constants and the vascular fraction. (2) The correction function to derive plasma activity from whole blood activity was adjusted to distinguish between the contributions from to the two injections. To this end, blood activity from the first injection was extrapolated using an exponential function which was fitted to the blood activity 10 minutes before the second injection.

Blood and tissue processing

a) Physiological blood parameters

Several blood gas variables (pH, pCO_2, pO_2; AVL, Compact 3, Roche Diagnostics, Switzerland) and metabolic measures such as plasma glucose and lactate levels (Ektachem DT, Kodak, USA) which are relevant parameters influencing lactate uptake in the brain were measured in all animals before the start of tracer kinetic measurements. Ventilation was adjusted according the blood gas values to reach physiological blood gas values.

b) Determination of the arterial plasma input curve

The total radioactivity in arterial blood was continuously recorded over 40 minutes using the coincindence counter (GE Medical systems). Whole blood activity was then corrected for a) a different tracer concentration in whole blood and plasma and b) the build-up of labeled metabolites. The ratio „$^{11}C_{plasma}/^{11}C_{whole\ blood}$“ was determined in all animals at different time-points (3 to 4 blood samples per animal). The data of all animals were then pooled and the time-course of the ratio was

approximated by fitting a quadratic polynomial to the data. This function was then used to convert counts in whole blood to counts in plasma.

c) Metabolite analysis in blood

Samples (about 400 µL) were collected at different time points after tracer injection, with a maximum of 4 blood samples per animal, to determine the time-course of the ratio of the ^{11}C activity in plasma to whole blood and for analysis of authentic tracer and metabolites. These samples were first centrifuged for 3 minutes at 2000 rpm. Proteins were then precipitated with 75 µL acetonitrile in 50 µL plasma. After centrifugation for 3 minutes at 2000 rpm, the composition of the ^{11}C-derived radioactivity in the supernatant (80 µL) was analyzed by high-performance liquid chromatography (HPLC) on a polymeric column (PRP-1, 5-µm, 250 × 4.1 mm i.d., Hamilton, U.S.A.) with 3 mmol/L phosphoric acid in water (pH 2.67) as the mobile phase (1 mL/min).The retention times of ^{11}C-HCO_3^- (3.3 min) and lactic acid (5.1 min) were determined by using aqueous solution of $NaHCO_3$ and DL-lactic acid as reference compounds, detected by UV absorption at 220 nm. The amount of authentic tracer was expressed as a fraction of total plasma ^{11}C counts (***Figure 2***).

The fraction data of all animals was then pooled and the time-course of the fraction was approximated by a decaying biexponential function. This function was subsequently employed to convert the total plasma activity to the time-course of authentic ^{11}C-lactate (= input curve).

d) Metabolite analysis in brain

At the end of the experiment the rats were perfused with PBS and brains were prepared for measurements with the HPLC system.

Each brain was first homogenized before adding acetonitrile (150%). The subsequent procedure was the same as with the blood samples described above, except that the amount of supernatant injected into the HPLC system was 200 µL.

Results

The pH and the arterial blood gases were all within physiological ranges (pH = 7.35 – 7.45; pCO2 = 35 – 45 mmHg; pO2 = 70 – 100 mmHg). Arterial plasma glucose (9.2 ± 2.5) and lactate (2.0 ± 0.6) levels were in physiological ranges in all animals and no differences between the groups were evident. In the two experiments with blockade of MCT transporters using 4-CIN an increase of the blood lactate levels was evident from 2.0 to 2.9 (mean of two animals).

Baseline kinetic properties

First pass extraction fraction and baseline kinetics in brain

CBF was measured in 4 baseline experiments and was 41 ± 15 ml/min/100g. The first pass extraction fraction calculated from EF = K_1 / CBF was 29.99 ± 10.4 % in these experiments.

Metabolite accumulation in arterial blood

^{11}C-CO_2 turned out to be the only identified metabolite in blood measured by HPLC. The time course of the fraction of authentic tracer in arterial plasma is demonstrated in ***Figure 2***. Metabolite build-up is fast for 1-^{11}C-L-lactate. At 20 minutes the fraction of true tracer in plasma dropped to about 40 % and furthermore to about 20 % at 40 minutes. The ratio of total ^{11}C activity in plasma and whole blood (plasma/whole blood) was stable. It was 1.38 ± 0.07 at 4 minutes and 1.40 ± 0.1 at 40 minutes.

Metabolite analysis of perfused brain tissue at the end of the experiment revealed 58 ± 8 % lactate and 42 ± 8 % CO_2. No difference was manifest between baseline and stimulation condition.

Tissue kinetics during baseline

Delivery to the brain (K_1) was 0.106 ± 0.025 ml*min^{-1}*ml tissue (mean ± sd). The time activity curves of 1-^{11}C-L-lactate at rest demonstrate a considerable washout after a peak at 4 minutes. The rate constant describing washout was k_2 = 0.089 ± 0.03 min^{-1}. At 20 minutes the tissue activity

dropped to 65 percent of the peak value. The one-tissue compartment model was adequate to fit the 1-^{11}C-L-lactate data as indicated by the random distribution of the residuals in ***Figure 3***.

Lactate kinetics during electrical infraorbital nerve stimulation

The efficacy of the stimulation was confirmed by an increase of the LDF signal by 20-25% (data not shown).

Intracortical probe – inter-animal comparison

The inter-animal comparison did not yield any significant difference in the k values of baseline and stimulation. A likely reason is the large inter-animal variation as demonstrated in ***Figure 4***.

Surface probe – intra-animal comparison

Our two channel probe system made the simultaneous measurement of radiotracer kinetic time courses at two different locations possible. Furthermore, the higher sensitivity of this system enabled us to perform two subsequent injections from one tracer production in the same animal. In the intra-animal comparison (n = 3) we observed a clear increase of the washout constant k_2 from baseline to stimulation (mean increase of k_2: +24 %; ***Figure 5A***). In contrast, the difference between the two hemispheres at rest was only 3 % (***Figure 5B***). On the ipsilateral side (***Figure 5C***) the mean increase of k_2 from baseline to stimulation was 6 %.

MCT blockade using α-cyano-4-hydroxy-cinnamate (4-CIN)

Blockade of the cerebral MCT transporters using 4-CIN led to a large reduction of lactate uptake (K_1, -62%) and label washout (k_2, -53%) as shown in ***Figure 6***.

Discussion

In this study we present for the first time the use of 1-^{11}C-L-lactate for *in vivo* experiments in the brain. This work was motivated by the perspective of developing a tracer to examine neuronal metabolism in the living brain. Lactate use by neurons as an energy substrate *in vivo* has been a highly debated issue for decades. It is well established that neurons can oxidize lactate. As elaborated in the introduction, neuronal lactate oxidation has been demonstrated in several neuronal preparations. In addition, it has been shown that synaptic activity can be maintained in slices by lactate in the absence of glucose (McIlwain 1953; Schurr et al. 1988). The situation is less clear in the intact brain. The debate focuses particularly on the amount of lactate oxidized by neurons *in vivo (Bonvento et al. 2005; Chih and Roberts Jr 2003; Korf 2006; Pellerin and Magistretti 2003)*. The astrocyte neuron lactate shuttle hypothesis (Magistretti 1999; Pellerin and Magistretti 1994) states, that a major fraction of the neuronal energy expenditure is covered by the oxidation of lactate which is produced in the astrocytes and shuttled to the neurons (for an update see (Pellerin et al. 2007)). In the past, magnetic resonance spectroscopy (MRS) has been the exclusive method for the investigation of ^{13}C-labeled lactate in the intact brain (Bouzier et al. 2000; Hassel and Brathe 2000; Qu et al. 2000; Serres et al. 2004; Serres et al. 2005; Serres et al. 2003). By analyzing the evolution of label in brain extracts after the injection of ^{13}C labeled lactate these authors could show that cerebral lactate metabolism contributed up to 50 % of that of glucose (Bouzier et al. 2000; Hassel and Brathe 2000). More specifically, it was suggested that more pyruvate coming from lactate than from glucose was metabolized in neurons (Qu et al. 2000). Furthermore, the contribution of lactate to cerebral metabolism seems to be activity dependent (Serres et al. 2004; Serres et al. 2005; Serres et al. 2003). However, present MRS systems suffer from a relatively low intrinsic sensitivity necessitating the constant infusion of considerably high concentrations of the labeled substrate. Until this date no methodology has been able to accurately measure neuronal lactate oxidation *in vivo* with high sensitivity. The recently synthesized 1-^{11}C-L-lactate (Drandarov et al. 2006) allowing the measurement of the tracer's kinetics with high temporal resolution might be a promising candidate for the direct investigation of neuronal lactate metabolism *in vivo.*

The rationale for using radiolabeled lactate

a) Preferential uptake of lactate in neurons

In the mammalian brain, transport of the short chain monocarboxylate lactate is mediated by a diffusional, saturable cotransport with protons via specific monocarboxylate transporters (MCTs) (Halestrap and Price 1999). Expression of different isoforms of MCTs on astrocytes (low affinity transporters MCT1, MCT4 (Dimmer et al. 2000)), endothelial cells (MCT1) and neurons (high affinity transporter MCT2 (Broer et al. 1999) have been found (Pierre and Pellerin 2005). The distribution of the MCTs with their respective kinetic properties such as substrate affinity and transport capacity is favoring a flux of lactate from astrocytes to neurons. In addition, different isoforms of lactate dehydrogenase (LDH) which is the responsible enzyme for the interconversion of lactate and pyruvate have been located in astrocytes and neurons (Bittar et al. 1996). The LDH-1 subunit (heart-type LDH), preferentially driving the reaction from lactate towards pyruvate, is the predominant LDH subunit found in neurons. Taken together, these findings support the hypothesis that lactate is preferentially used by neurons.

b) Feasibility for the use of radiolabeled L-lactate in brain studies

Uptake of lactate from blood into brain was already examined earlier. L-lactate, which is the predominant enantiomer of lactic acid in mammals, passes the blood-brain barrier at a rate of 25 % to 50 % of that of glucose uptake (Hassel and Brathe 2000; Knudsen et al. 1991). In line with these reports we calculated an EF of 30 % for 1-^{11}C-L-lactate. This brain uptake is large enough to allow quantitative tracer kinetic studies.

Interpretation of the 1-^{11}C-L-lactate kinetics

One obvious possibility is to calculate the cerebral uptake of blood-borne lactate as the product of K_1 and blood lactate concentration (in the present study plasma lactate levels were in the range between 1.5 and 2.4 mmol/l). Based on the baseline data the calculated cerebral uptake of lactate was in the order of 0.2 µmol/min/g. This value is somewhat higher than other published values but in the same range (LaManna et al. 1993; Lear and Kasliwal 1991). However, anesthetic protocols influencing plasma lactate levels and measurement methodologies were not the same in the

different studies. Assuming complete oxidation the aerobic degradation of all this lactate (0.2 µmol/min/g) would require 0.6 µmol/min/g O_2, which is about 40 % of total $CMRO_2$. This demonstrates that blood-borne lactate can be a major substrate in the anesthetized rat.

More intriguing is the interpretation of the label washout rate k_2. As demonstrated in ***Figure 7*** the label is lost with CO_2 cleaved from pyruvate by pyruvate dehydrogenase (PDH). Since the diffusion of CO_2 into the blood stream is fast (Hawkins et al. 2006; Paulson 2002) it is likely that k_2 represents the production of CO_2 and not its removal. In this case k_2 would be tracing the flux through PDH, e.g. the production rate of acetyl CoA. Since most of the latter is oxidized in the TCA cycle, k_2 is likely a close indicator of oxidative metabolism, and if lactate uptake is predominantly into neurons, of neuronal oxidative metabolism.

In our previous study (Wyss et al. 2009), we used ^{11}C labeled acetate to measure astrocytic metabolism. With the same stimulation paradigm we found a doubling of the washout rate during stimulation. In the present study the increase of k_2 was 25 %. Since lactate enters the metabolic chain only one step above acetate, one would expect a similar increase of k_2 for labeled acetate and lactate, if both were mainly taken up by astrocytes. The substantial difference in the k_2 increase of acetate and lactate therefore indicates that the 2 substrates are metabolized in different cell types, which leaves the neuron as the most likely candidate for lactate.

One could also argue that most of the labeled lactate does not enter the cells at all but just enters and leaves interstitial space. However, this possibility is rendered very unlikely by the blockade experiment. After the application of 4-CIN we observed a marked decline of K_1, indicating that the labeled lactate indeed enters cellular compartments without blockade. That parameter k_2 is reduced to similar values as K_1 suggests that under blockade it represents the backdiffusion of labeled lactate, and not the production of CO_2 anymore.

One could also claim that already under non-blocking conditions k_2 represents backdiffusion of lactate. However, if this were the case one would not expect such an increase of k_2 during stimulation.

General remarks

On the methodological side the study demonstrates the advantage of the highly sensitive surface probe as compared to the less sensitive intracortical scintillator. Only with the high sensitivity system was it possible to perform 2 injections into the same animal, and only the resulting intra-subject comparison yielded the predictedl results.

We think that k_2 is closely related to neuronal oxidative metabolism. It is clear that this refers to total metabolism. The study does not elucidate which substrates are oxidized, any substrate with pyruvate as an indermediate is possible. With regard to the astrocyte neuron lactate shuttle hypothesis, the study can therefore not address the open question of the neuronal fuel composition (glucose vs. lactate).

Summary

In this study we examined the kinetic behavior of radiolabeled L- lactate *in vivo* using beta probe instrumentation (Weber et al. 2003; Wyss et al. 2007). The kinetic properties of 1-^{11}C-L-lactate make brain studies *in vivo* possible. We demonstrate that radiolabeled L-lactate may be used for the measurement of oxidative metabolism, and if lactate uptake is preferentially taken up into neurons, of neuronal oxidative metabolism. Future experiments should now be designed to further verify the specificity of 1-^{11}C-L-lactate to investigate neuronal oxidative metabolism. The labeling with ^{11}C would also allow human studies using positron emission tomography, further enlarging the application field.

Figures of Chapter II:

The Kinetic Behavior of radiolabeled L-lactate in the Rat Brain

Figure II-1. One-tissue compartment model

One-tissue compartment model used to analyze CBF using $H_2{}^{15}O$ (A) and the kinetics of ^{11}C- L-lactate respectively (B).

Figure II-1

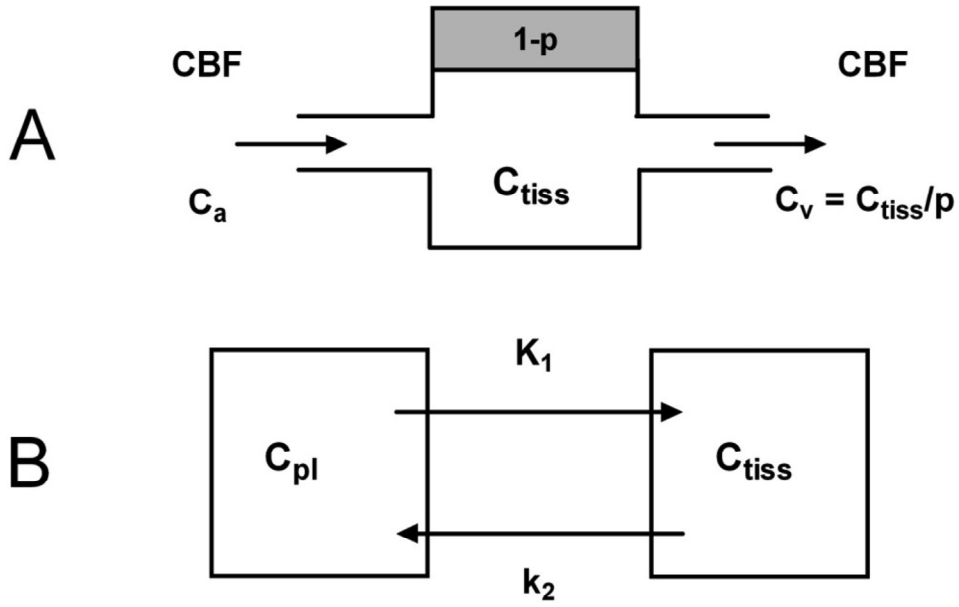

Figure II-2. Build-up of metabolites over 40 minutes after intravenous injection of 1-^{11}C-L-lactate in blood.

The y-axis represents the fraction of true 1-^{11}C-lactate in plasma. The filled circles represent pooled data points from all the baseline experiments (n = 6) and the solid line is the corresponding fit of a biexponential curve.

Figure II-2

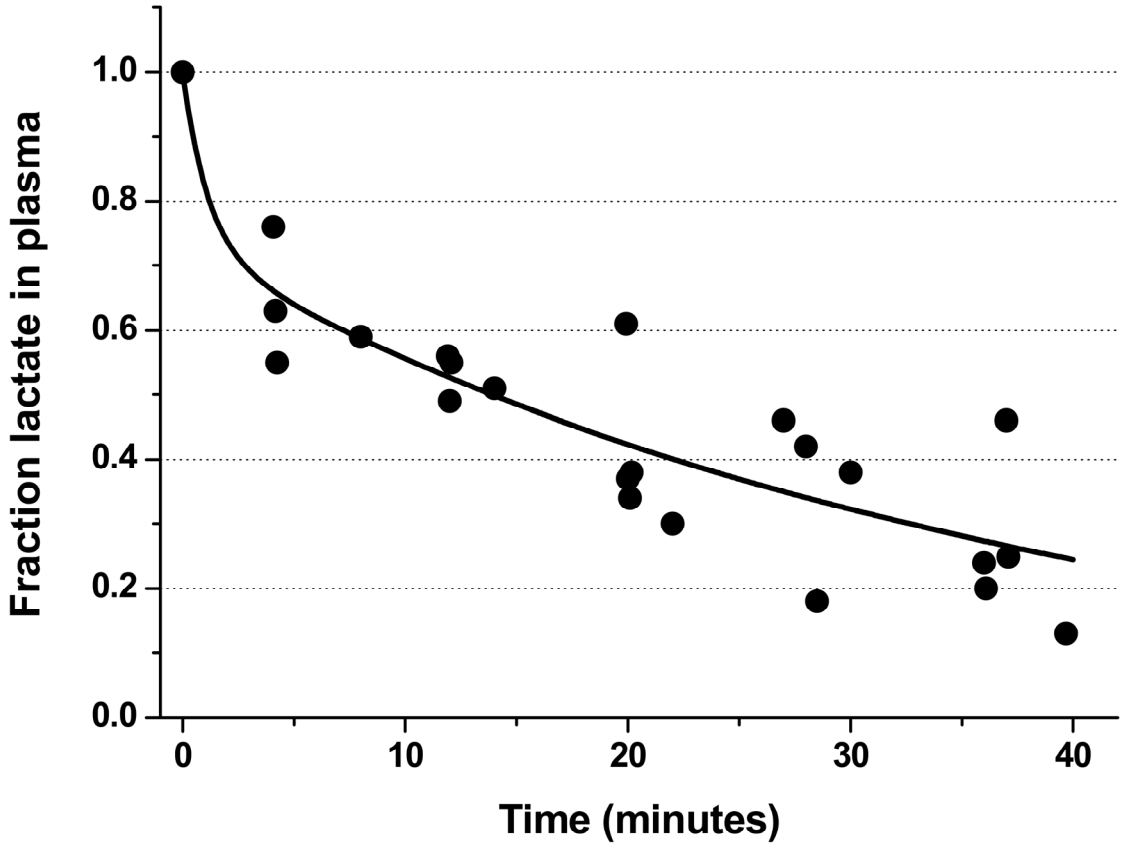
Fraction lactate in plasma
1.0
0.8
0.6
0.4
0.2
0.0
0
10
20
30
40
Time (minutes)

Figure II-3. Kinetic modeling of 1-^{11}C-L-lactate

The measured radioactivity concentration in the brain (open circles), the model fit (black line) and the arterial input curve (gray line) are shown. In the inset the residuals of the fitting to the one-tissue compartment model are shown. The absence of any bias in the distribution demonstrates the adequacy of the applied one-tissue compartment model.

Figure II-3

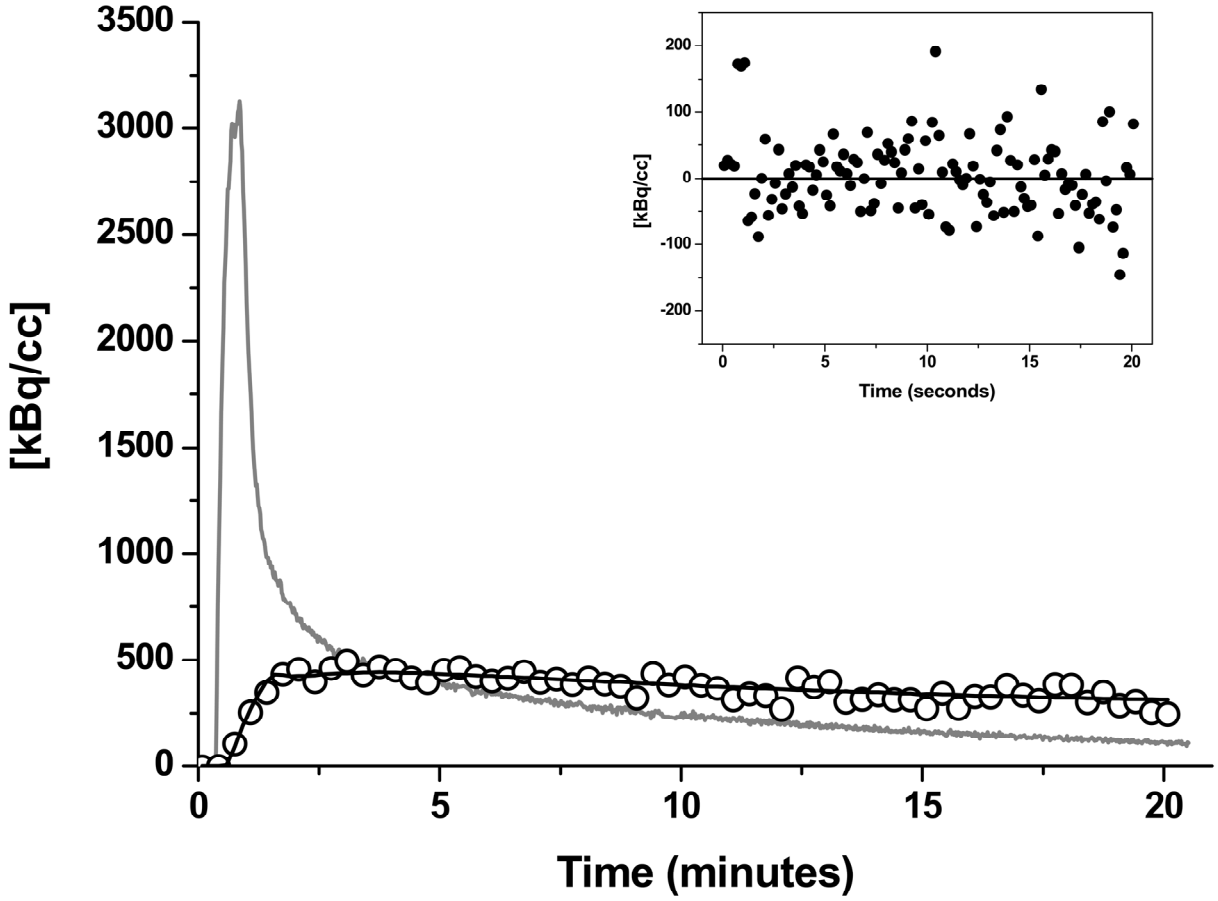
[kBq/cc]
3500
3000
2500
2000
1500
1000
500
0
0
5
10
15
20
Time (minutes)
[kBq/cc]
200
100
0
-100
-200
0
5
10
15
20
Time (seconds)

Figure II-4. Summary of experiments using the intracortical beta probe

Inter-animal comparison in experiments with the intracortical beta probe. K_1 and k_2 values are compared between the two different groups (baseline (n = 6), stimulation (n = 7)). Boxes denote mean ± sd. Base = baseline; Stim = electrical infraorbital nerve stimulation.

Figure II-5

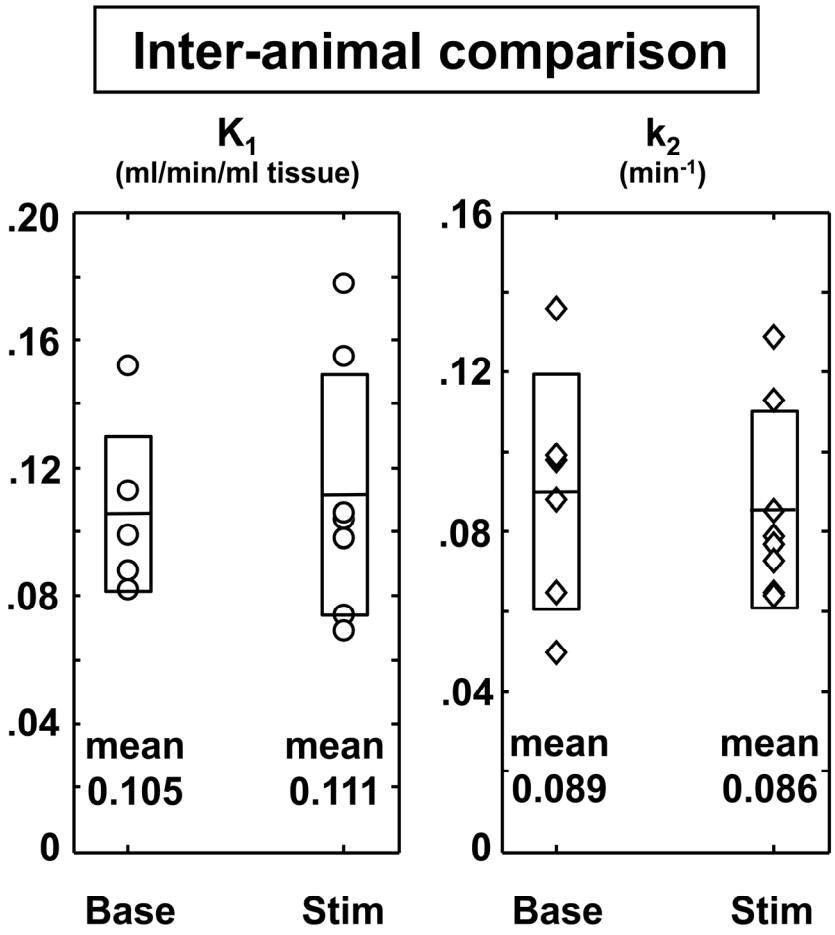
Inter-animal comparison
K1
(ml/min/ml tissue)
k2
(min-1)
.20
.16
.12
.08
.04
0
.16
.12
.08
.04
0
mean
0.105
mean
0.111
mean
0.089
mean
0.086
Base
Stim
Base
Stim

Figure II-5. Summary of ION stimulation experiments using the surface probe

In the three panels different comparisons of the rate constants (K_1, k_2) between the primary somatosensory (S1) cortex on the stimulated side during baseline and activation (A), of S1 on the stimulated and on the non-stimulated side (S1n; B) and of S1n during baseline and stimulation. Base = baseline; Stim = electrical infraorbital nerve stimulation.

Figure II-5

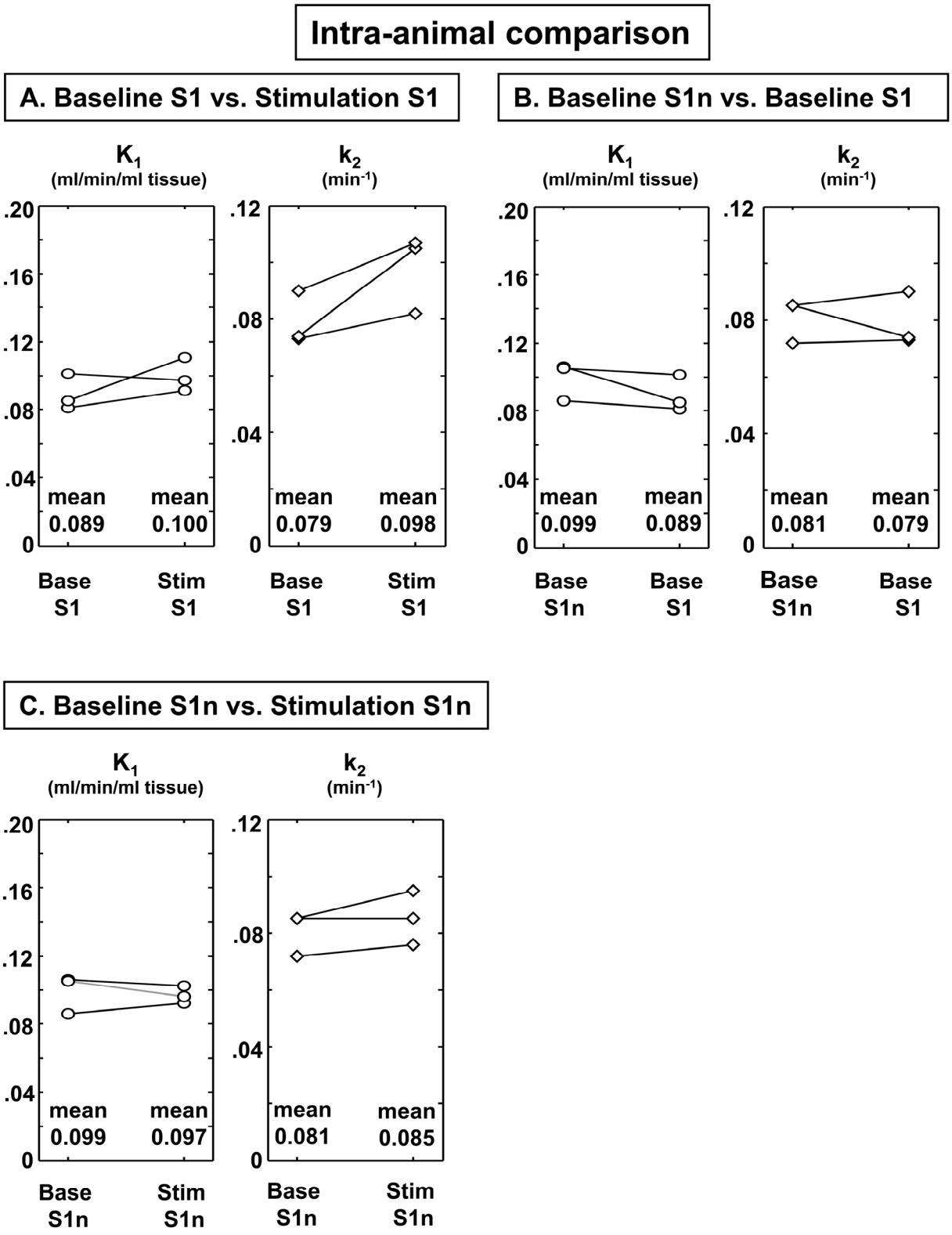
Intra-animal comparison
A. Baseline S1 vs. Stimulation S1
B. Baseline S1n vs. Baseline S1
C. Baseline S1n vs. Stimulation S1n
K1 (ml/min/ml tissue)
k2 (min-1)
.20
.16
.12
.08
.04
0
mean 0.089
mean 0.100
mean 0.079
mean 0.098
mean 0.099
mean 0.089
mean 0.081
mean 0.079
mean 0.099
mean 0.097
mean 0.081
mean 0.085
Base S1
Stim S1
Base S1n
Base S1

Figure II-6. MCT blockade using 4-CIN

Shown are the changes of K_1 and k_2 during inhibition of MCT transporters.

Figure II-6

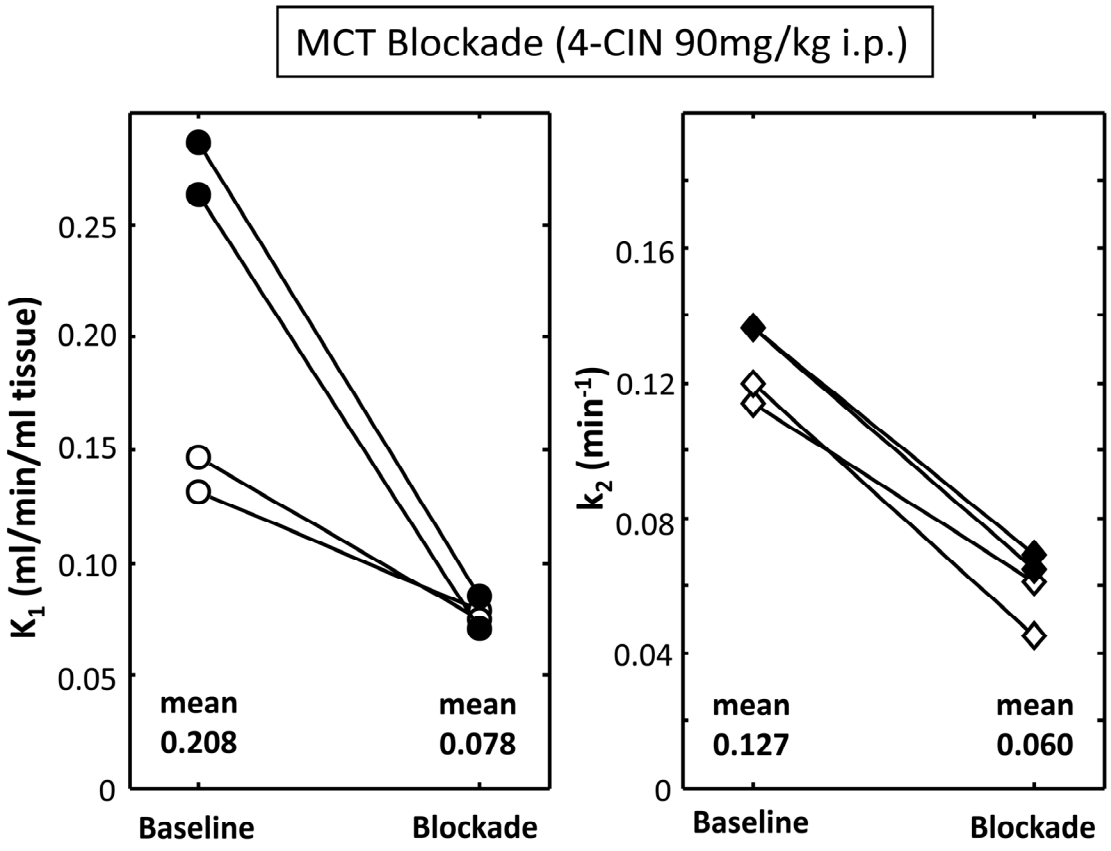
MCT Blockade (4-CIN 90mg/kg i.p.)
K1 (ml/min/ml tissue)
0.25
0.20
0.15
0.10
0.05
0
mean
0.208
mean
0.078
Baseline
Blockade
k2 (min-1)
0.16
0.12
0.08
0.04
0
mean
0.127
mean
0.060
Baseline
Blockade

Figure II-7. Scheme of the probable chain of events in the degradation of radiolabeled lactate in neurons

1-^{11}C-L-lactate (^{11}C-Lac) is taken up via monocarboxylic acid transporters (MCT2) into the cell. Within the cell lactate is converted to 1-^{11}C-pyruvate (^{11}C-Pyr) and further oxidized to acety CoA (Ac CoA) by releasing radiolabeled CO_2 (^{11}C-CO_2). This leads to removal of radiolabel before the entry of lactate into the tricarboxylic acid (TCA) cycle.

Figure II-7

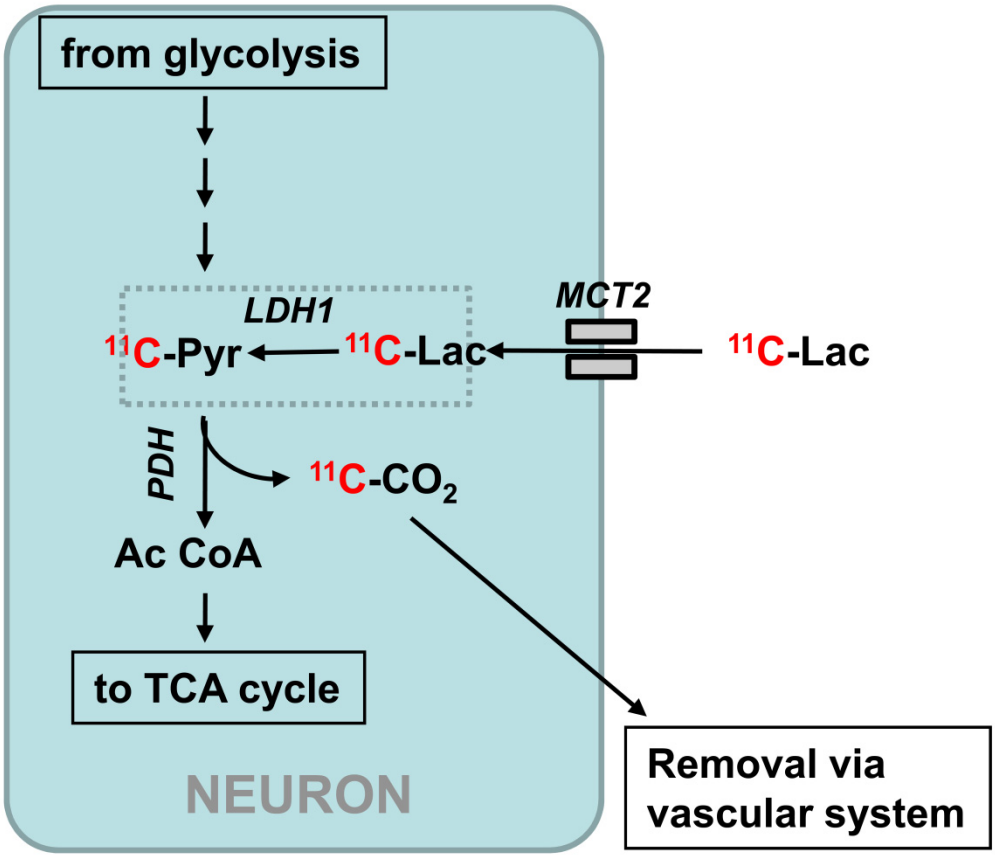
from glycolysis
LDH1
^{11}C-Pyr
^{11}C-Lac
MCT2
^{11}C-Lac
PDH
^{11}C-CO$_2$
Ac CoA
to TCA cycle
NEURON
Removal via vascular system

Chapter III

Novel high sensitivity Beta Scintillator for Cortical Measurements of Radiotracer Kinetics in the Rodent Brain

Matthias T. Wyss[1,2*], Nicolas M. Obrist[1*], F. Haiss[2], Rolf Eckert[3], Ross Stanley[3], Cyrill Burger[1], Alfred Buck[1] and Bruno Weber[2]

* these authors contributed equally to this work

[1]PET Center, Department of Nuclear Medicine, University Hospital Zürich, Switzerland

[2]Institute of Pharmacology and Toxicology, University of Zürich, Switzerland

[3]Swiss Center for Electronics and Microtechnology, Inc., Neuchâtel, Switzerland

Running title: *In vivo* evaluation of a novel surface beta probe

Submitted to Journal of Nuclear Medicine

Abstract

β^+-sensitive probes are useful tools for the measurement of radiotracer kinetics in small animals. They allow the cost-effective development of new PET tracers and offer the possibility to investigate a variety of cerebral processes. The study's main aim was the *in vivo* evaluation of a novel system for cerebral surface acquisitions. Methods: The detector system is a 0.2-mm thick scintillating disk of 3-mm diameter, positioned close to the cerebral surface. The study consists of 4 subparts: (1) simulation of the detection volume, (2) direct comparison with the classic intracortical beta probe regarding its capability to acquire kinetic data, (3) test of the ability to detect local tracer accumulations during infraorbital nerve (ION) electrostimulation and (4) demonstration of the feasibility to measure tracer kinetics in awake animals. Kinetic data were fitted with a standard ^{18}F-fluorodeoxyglucose two-tissue compartment model and a one-tissue compartment model for blood flow measurements using ^{15}O-H_2O. Results: The surface probe measurements were in good agreement with those obtained using the intracortical scintillator. ION electrostimulation induced a marked increase in tracer accumulation adequately detected by the surface probe. In the head-fixed animal, a marked change in FDG kinetics was detected between the awake and anesthetized state. Conclusions: The novel surface probe system proved to be a valuable instrument for *in vivo* radiotracer studies of the cerebral cortex. Its main advantages are an excellent counting sensitivity and the absence of any tissue damage. In addition, serial acquisitions of tracer kinetics in the awake animal turned out to be feasible.

Key words: Awake animal, radiotracer experiments, surface beta probe,

Acknowledgements

The authors want to thank the Center for radiopharmaceutical science of the ETH, PSI and USZ for tracer production. The study was supported by the Swiss National Science Foundation (Grants 3100A0-105804/1 and PP00B-110751/1), by the OPO-Stiftung Zürich and the Novartis Research Foundation.

Introduction

Despite the rapid development of new functional neuroimaging tools, radiotracer experiments are still considered the gold standard if absolute quantification is needed. Radiotracer methods are widely used for the investigation of physiological and biochemical processes in the brain, such as receptor binding, hemodynamics, substrate use and transport processes as well as for studies in early drug development. The progress of research in these fields during the last few years is in part due to the advance of methods applicable in small animals. At present, positron emission tomography (PET) and beta probe measurements are the two available methods for the acquisition of tracer kinetics in small animals (Chatziioannou 2002; Hume and Myers 2002; Pain et al. 2000; Pain et al. 2002b; Rowland and Cherry 2008; Weber et al. 2003; Weber and Bauer 2004; Wyss et al. 2007; Wyss et al. 2009). The cost of PET is substantial and it needs high counting statistics for image reconstruction largely reducing temporal resolution. This makes PET often insufficient for kinetic modeling. The recently introduced beta probes demonstrate a valuable and cost-effective alternative for the detection of positrons with high temporal and reasonable spatial resolution. This allows the precise evaluation of radiotracer kinetics *in vivo* labeled with a variety of PET nuclides (e.g. O-15, C-11, F-18). By using the appropriate model for this radiotracer, kinetic rate constants of transport processes and biochemical reactions may then be estimated. However, presently available beta detectors suffer from various limitations. These systems, which consist of a scintillating crystal of 0.25 to 1 mm in diameter, are designed for acquisitions within tissue and often lead to tissue damage. Secondly, their relatively poor sensitivity requires the injection of high doses of radioactivity. This may be a problem for receptor occupancy studies because the mass of injected compound may lead to a marked receptor occupancy.

In this study, we present a novel detection system designed for high sensitivity cerebral surface acquisitions *in vivo*. The probe is positioned close to the cerebral surface and thus does not cause any tissue damage. This new system broadens the field of application of beta probes. The aims of the present study were: (1) to estimate the detection volume of the surface probe using simulation, (2) to directly compare the novel system with the classic intracortical beta probe regarding its capability to acquire kinetic data, (3) to test the ability to detect local tracer accumulations during

infraorbital nerve (ION) electrostimulation and (4) to demonstrate the feasibility to measure tracer kinetics in awake animals.

Material and Methods

Design/specifications of the system

We used a twin probe system (Swisstrace GmbH, Zurich, Switzerland) with two photomultiplier tubes (Perkin Elmer, Massachusetts, USA) allowing simultaneous acquisitions of the radioactivity concentration in two separate brain regions. The detectors were connected with the PMTs via two high numerical aperture glass fibers. The detector of the surface probe consisted of organic scintillating crystal disks (Bicron, BF12, Newbury, OH, USA) with a thickness of 0.2 mm and a diameter of 3 mm embedded in a brass collimator (***Figure 1A***). The intracortical system consisted of a scintillation tip (Bicron, BF412, Newbury, OH, USA) with a length of 1 mm and a diameter of 0.25 mm. The probes were made light-tight by applying a uniform black polymer coating. The limited range of beta particles within biological tissues limits detection volume to a small sphere centered on the scintillating tip of the probe. Monte Carlo simulations demonstrated that for F-18 the distance required to detect 90% of the beta particles around the probe is ~1.0 mm (Pain et al. 2002b). The apparent sensitivity of the probes under real experimental conditions was measured after each experiment using a standardized calibration procedure as described below. The theoretical sensitivity (in cps/kBq/ml) was measured after complete immersion (> 5 mm) of the probes in a homogenous solution with a known radioactivity concentration. Measuring the decay of a radioactive phantom containing F-18 over the course of several hours allowed us to measure the linearity of our system. Kinetic data was stored on a personal computer using a bin width of 1 second. In the *in vivo* experiments acquisitions of radioactivity count rates began 10 - 30 seconds before tracer injection to evaluate dark counts. Thereafter, mean background counts were subtracted from raw data before data analysis.

Calibration procedure

Calibration measurements were performed after each experiment. A homogeneous solution with a known radioactivity concentration (range: 5.7 MBq/ml to 6.8 MBq/ml for F-18 and 7.1 MBq/ml to 8.0 MBq/ml for O-15) was prepared. For the intracortical probe the calibration was performed by

lowering the scintillating tip 1.5 mm into the solution. To calibrate the surface probe the solution was covered with an ultra-thin plastic foil to prevent adhesion of solution to the detector surface. For the actual calibration measurement the radioactivity of the test source was measured with the surface probe in close contact. The factors obtained by this procedure were used to convert the raw data reflecting counts per second (cps) to the apparent radioactivity concentration (kBq/cc) measured in the experiments. Furthermore, for the surface probe, the fraction of recorded events attributable to gamma radiation was estimated by counting the test source additionally with the interposition of a 4 mm thick brass disk sufficient to absorb the ^{18}F positrons but not attenuating 511 keV gamma photons.

Simulation of the detection volume

Since the calibration procedure demonstrated a relatively small contribution of (gamma) photons to the measured signal (≤15 %), only positrons were considered. We also assumed that positrons only enter the scintillator through the end surface and not through the side (metal shielding). For the simulation the space below the scintillator was sparsed into a 3D grid (P_{xyz}) and the scintillator surface was divided into discrete squares (SQ_{x1y1}). For each point in space P_{xyz}, the probability that a positron emitted at location P would enter square SQ_{x1y1} on the detector was calculated, yielding Q_{x1y1} (xyz). This probability depends on the spatial angle of SQ_{x1y1} as seen from P_{xyz} and the probability that the positron reaches SQ_{x1y1}. This probability, which depends on the distance, the material and the emission energy of the positrons was taken from recently published data derived from a Monte Carlo simulation (Le Loirec and Champion 2007). The total signal recorded from location P_{xyz} is then the sum of all Q_{x1y1}. We simulated the situation, in which the scintillator is placed 0.2 mm from the surface of water containing O-15, C-11 and F-18 (0.2 mm distance was chosen to match the thickness of the thinned skull). The sum of Q_{x1y1} (xyz) in the simulated volume was normalized to 100.

Animals and radiotracer production

All animal experiments were approved by the local veterinary authorities and were performed by licensed investigators. 16 female Sprague-Dawley rats (^{18}F-fluorodeoxyglucose experiments: n =

14; ^{15}O-H_2O: experiments n = 2) (weighing between 220 g to 280 g) were used for this study. The animals were kept in cages in a ventilated cabinet with standardized conditions of light (night/day-cycle 12h/12h) and temperature and free access to food and water. Animals used for the FDG experiments were fasted overnight.

^{18}F-fluorodeoxyglucose (FDG) was obtained from the daily in-house production by the Radiochemistry Department of the University Hospital Zurich. For the administration of the short-living ^{15}O-H_2O (half-life, 122.2 seconds) in high concentrations, O-15 was produced continuously in the cyclotron and transferred to the synthesis device (More information on this device can be found at http://www.swisstrace.com). The synthesis device delivered ^{15}O-H_2O at a concentration of about 1 GBq/ml into a glass vial from where 0.5 ml were drawn into a syringe for injection.

Animal Preparation

Surgery was performed under 2.5 – 3.5% isoflurane anesthesia and involved for experiments of paradigm 1 and 2 the placement of an arterio-venous shunt from the right femoral artery to the right femoral vein and tracheotomy for mechanical ventilation. In experiments where the intracortical probe was used, a craniotomy and small incision of the dura was performed for the placement of the beta scintillator. This was not needed for the surface probe measurements, where the cranial bone was merely thinned to translucency. The actual experiments were performed under α-chloralose anesthesia (44 mg/kg bodyweight s.c.) according to the protocol of Bonvento et al. (Bonvento et al. 1994). The shunt was used for the continuous monitoring of arterial blood pressure, the injection of the radiotracers, the continuous measurement of the total arterial blood radioactivity, the collection of blood samples and the administration of a lethal dose of pentobarbital at the end of the experiment. For the recording of the total blood radioactivity the shunt ran through a coincidence counter (GE Medical Systems). The online arterial sampling procedure was established earlier and is described in detail elsewhere (Weber et al. 2002a). During the experiments arterial blood gases were determined regularly (AVL, Compact 3, Roche Diagnostics, Switzerland) and ventilation was adjusted as necessary to keep the animals within physiological ranges. Blood glucose levels were determined before and after each 45 minute

acquisition (Ektachem DT, Kodak, USA) and the mean value of the two measurements was taken for the quantitative glucose utilization determinations.

For the experiment with the head-fixed animal (paradigm 3), after surgery and one week of recovery, the animal was trained to accept head fixation (Haiss and Schwarz 2005). Implantation of a head post for later head fixation was undertaken under 3% isoflurane anesthesia. After fixation of micro skull screws (Medartis, Basel, Switzerland) a base was built with dental cement for the final fixation of a standard M5 screw.

No dental cement was applied above the right primary somatosensory cortex and the cranial bone was thinned at this location using a dental drill. To prevent bacterial infections after surgery the chronically implanted animal received oral antibiotic treatment added to the drinking water for one week, starting one day before surgery (Baytril® 10% oral solution, Bayer, Germany, 1 ml/1 l).

Experimental protocols

The experiments were divided into three groups:

Paradigm 1) Comparison of surface probe with intracortical probe to measure cortical radioactivity time courses

In a total of 8 animals the novel probe system was directly compared to the classic intracortical system. For this purpose the surface probe was positioned over the primary somatosensory cortex on one side (S1; 2 mm posterior and 6 mm lateral according to Bregma (Paxinos and Watson 1998)). The intracortical probe was stereotactically positioned in the corresponding contralateral S1 and lowered 1.5 mm below the dura avoiding large blood vessels. For this paradigm two different radiotracers were used. In 6 animals local cerebral metabolic rates of glucose ($LCMR_{glu}$) were determined using ^{18}F-fluorodeoxyglucose. Only one radiotracer injection per animal was performed in this group (injected activity: 90 – 145 MBq). Kinetic data was acquired for a period of 45 minutes. Directly afterwards, autoradiographic studies were performed to measure relative contributions of the investigated brain structure (in the present study the somatosensory cortex) and the surrounding tissue. To this end the last 5 minutes of the calibrated probe time activity

curves (calibrated as described above) were compared with the autoradiographically measured activity in the cortex of corresponding experiments. This yielded factors regarding the current underestimation of the measured tracer accumulation in the region of interest by the whole detection volume of the probe, an effect similar to partial volume effects observed in PET imaging.

In 2 more animals the quantitative capability of the novel system was compared to the classical intracortical device performing cerebral blood flow (CBF) measurements. 180 seconds of data were recorded after each ^{15}O-H_2O injection. In each animal a total of 4 injections were performed 15 minutes apart to allow for sufficient activity decay to background level. After two acquisitions under baseline conditions the carbonic anhydrase inhibitor acetazolamide (Diamox®; 66 mg/kg i.v.) was injected. Acetazolamide leads to vasodilation and thus induces a global increase in cerebral blood flow. Ten minutes after drug application the last two measurements were started.

Paradigm 2) Quantification of localized increases of $LCMR_{glu}$ using the surface probe

In a second group (n = 5) the ability of the novel system to detect local metabolic activations was evaluated. For this purpose a surface probe was positioned over S1 of each hemisphere. Two subsequent radiotracer injections were performed in these experiments (injection 1: 25 - 35 MBq in 0.5 ml saline; injection 2: 80 - 100 MBq in 0.5 ml saline). Each data acquisition took 45 minutes. One of the two acquisitions of ^{18}F time-course served as the baseline, whereas the other FDG injection was performed immediately after initiation of electrical infraorbital nerve stimulation (2 Hz, 2 mA, pulse length 1 ms, continuous stimulation over 45 minutes). The order of baseline/activation conditions was balanced across the animals. An autoradiography was performed after the second tracer injection as a control for the effectiveness of the applied stimulation (only in animals with electrostimulation performed during the second injection; n = 3). In two additional animals both injections were performed during baseline conditions to control for possible drift during the experiment.

Paradigm 3) Surface probe measurement in an awake head-fixed animal.

The aim of this experiment was to demonstrate the feasibility of the system for measurements in

head-fixed non-anesthetized animals. First, the animal was carefully trained to tolerate head fixation. The training started one week after surgery and involved handling during the first week and habituation to the head holding device in the second week. In the third week, fixation of the animal in the head holding device started. Over the following two weeks, the duration of fixation was gradually increased up to 30 minutes. Finally, the tracer experiment was performed during head fixation. The acquisition started at the time of intraperitoneal tracer injection. After 20 minutes, anesthesia was induced with sevoflurane 3% in a mixture of oxygen and air (30%/70%) and data acquisition was continued until 45 minutes after tracer injection. Two days later the measurement was repeated in the same animal.

Autoradiographic studies

Autoradiographies were performed as described in detail earlier (Weber et al. 2002b). In brief, brains were removed directly after the probe measurements, frozen in chilled isopentane and cut in 10 µm slices. Brain slices were subsequently placed on a phosphor imaging screen (Fuji TR2025) together with C-14 standards (calibrated in a previous calibration experiment) for 240 min. After scanning the screens using a phosphor imager (Fuji BAS 1800 II, pixel size 50 µm) the data were converted to kBq/cc and analyzed as described below.

Determination of the arterial plasma input curve in FDG experiments

Total radioactivity in arterial blood was continuously recorded using the coincidence counter. The time course of the FDG concentration in arterial plasma (input curve) was then obtained by multiplying the whole blood values with a conversion function which had been established previously (Weber et al. 2002a).

Data analysis

Calculations were performed using the software PMOD (Mikolajczyk et al. 1998); PMOD Technologies, Adliswil, Switzerland) and Matlab (Mathworks, Natick MA, USA).

Calculation of the Local cerebral metabolic rate of glucose ($LCMR_{glu}$)

In the autoradiographic studies, the cerebral glucose metabolism was quantified using an operational equation which takes into account changing plasma glucose levels during the experiment (Savaki et al. 1980). The following kinetic rate constants were applied in the autoradiographic equation: $K_1 = 0.30$, $k_2 = 0.40$ and $k_3 = 0.68$ for gray matter (Ackermann and Lear 1989; Weber et al. 2002b). A lumped constant (LC) of 0.58 was chosen. The calculation yielded values for glucose consumption ($\mu mol*min^{-1}*g^{-1}$) in each image pixel. Regions of interest (ROIs) were defined over the stimulated and the contralateral cortex in ten consecutive slices. The mean glucose consumption in each ROI was calculated.

The procedure for the quantification of the probe studies follows the [^{14}C]-deoxyglucose method described by Sokoloff et al. (Sokoloff et al. 1977). It employs a compartmental model with two tissue compartments and three kinetic rate constants (K_1 to k_3, $k_4 = 0$). The operational equation, which was fitted to the probe time activity curve additionally included a vascular fraction α as a fit parameter. This improved the least square fit as compared to a fixed value of α = 5% (data not shown). $LCMR_{glu}$ values were calculated from the fitted rate constants by: $LCMR_{glu} = (K_1 * k_3/(k_2 + k_3))/(LC/C_{plasma})$, where C_{plasma} represents the plasma glucose concentration..

Model adjustments for the dual-injection paradigm

The kinetic model was adjusted in two ways for the analysis of the dual-injection data: (1) two sets of rate constants (K_1, k_2, k_3) were used in the calculation of the operational equation. The first set for the time until the second injection, and the second set thereafter. The least-squares fit procedure resulted in estimates for all 6 rate constants and the vascular fraction. (2) The correction function to derive plasma activity from whole blood activity was adjusted to distinguish between the contributions from the two injections. To this end, blood activity from the first injection was extrapolated using an exponential function, which was fitted to the blood activity 10 minutes before the second injection.

Calculation of cerebral blood flow measurements (CBF)

The basis of the calculation using the one-tissue compartment model included a partition

coefficient for ^{15}O-H_2O. Before data analysis, tissue time activity curves and arterial input curves were corrected for radioactive decay. Further details of the analysis procedure were described previously (Weber et al. 2003).

Statistics

Bland-Altman tests were used to assess the agreement of $LCMR_{glu}$ values obtained by kinetic beta probe measurements using the two different systems and by the static autoradiographic method (Bland and Altman 1986). Values are given as mean ± sd.

Results

Performance characteristics of the new probe system

The agreement of the decay of F-18 monitored with the beta probe and a monoexponential function as shown in ***Figure 1B*** demonstrates the linearity of the detector response. The mean sensitivity of the novel surface probe system was 0.83 ± 0.04 cps/kBq/ml using the calibration procedure described above. The theoretical sensitivity of the surface probe system is about 40 times higher than the one of the intracortical system used in this study. The background (dark counts) ranged from 2-8 cps. Stopping the positrons using the brass disk between the ^{18}F source and the detector tip reduced the count rate to 14.7 ± 4.4% of the initial value. Accordingly, the contribution of gamma radiation (originating from positron annihilation) to the total acquired count rate was about 15% for the new probe system.

Simulation of detection volume

The simulation yielded the detection volumes depicted in ***Figures 2A – 2C***. For F-18, 95% of the signal was detected from within an isosurface with maximum depth of about 1 mm. As expected, this range is considerably larger for C-11 and O-15. As can be seen in ***Figures 2A – 2D***, the sensitivity rapidly decays with depth.

Animal experiments

All time activity curves (TACs) presented are corrected for physical decay and multiplied by the calibration factor taking into account the respective experimental configuration for each probe (scintillating crystal above cortical surface or scintillating tip inside cerebral cortex).

Paradigm 1) Direct comparison of the two probe systems

Local cerebral metabolic rates of glucose consumption ($LCMR_{glu}$) based on measurements with the two probe systems are shown in ***Table 1*** (n = 6). The data of both probes were adequately fitted by the standard two-tissue compartment FDG model, as the lack of bias in the residuals indicates (***Figures 3A and 3B***). However, the higher sensitivity of the novel surface probe system led to a

marked decrease in the relative residual size. The Bland Altman plot in ***Figure 4*** shows that all differences in $LCMR_{glu}$ are in the range defined by the mean ± 2 SD. Nevertheless, the values measured with the surface probe were on average 22% lower than the ones determined with the intracortical probe.

A typical example of FDG time-activity curves recorded simultaneously with the 2 probe systems is demonstrated in ***Figure 5***. In order to illustrate the similarity of the shape, the curves were normalized to the integral of the tissue activity between 0 and 45 minutes.

For the CBF measurements (n = 2) a typical example of tissue time activity curves acquired with the two probe systems is shown in ***Figure 3*** (panel C and D). Again the surface probe yielded a considerably improved signal-to-noise ratio. CBF data are shown in ***Table 2***. The acetazolamide induced CBF increase was 51% with the surface probe and 48% with the intracortical probe. As with FDG, the absolute CBF values were somewhat smaller with the surface probe.

Paradigm 2) ION electrostimulation

To assess whether the surface probe is able to detect local increases in metabolic activity in the brain, electrical stimulation of the right infraorbital branch of the trigeminal nerve (ION) was applied. The stimulation of the ION caused the expected circumscribed increase of tracer uptake in the contralateral primary somatosensory cortex (S1) as shown by the autoradiographic slice in ***Figure 6***. Only a weak increase in tracer uptake is noticed on the ipsilateral side. The increase was correctly recorded by the surface probe in all 5 experiments and was on average 60.7% at 40 minutes. The subsequent autoradiographic evaluation showed a mean increase of 64.9%. A typical example of a probe acquisition during ION stimulation is presented in ***Figure 6***. In the 2 animals with two FDG injections during baseline conditions stable radiotracer accumulation was observed. The difference in $LCMR_{glu}$ between the first and the second injection was 8.7% and -14.9% in the two animals, verifying the stability of the double-injection protocol.

Paradigm 3) Determination of FDG kinetics in the awake head-fixed rat

The animal was successfully trained for 5 weeks to tolerate the head fixation for up to 30 minutes. ***Figure 7*** shows the constant increase of cerebral FDG uptake during the first 20 minutes in the

awake animal. After induction of sevoflurane anesthesia the slope of the tissue time-activity curve is markedly reduced. The repetition of the acquisition two days later produced similar results (data not shown).

Discussion

An increasing number of molecular imaging studies are performed with PET scanners. These devices allow imaging of the whole animal, if necessary several times in a longitudinal design. However, these PET scanners suffer from drawbacks, such as a high price and limited temporal resolution. The latter makes it difficult to use in a dynamic imaging design coupled with kinetic modeling. Another drawback of small animal PET is the requirement for anesthesia, which inevitably alters normal physiology. The recently introduced small beta probes for intracortical measurements in small animals overcame some of these problems (Ginovart et al. 2004; Pain et al. 2000; Pain et al. 2002b; Weber et al. 2003). They offer a cost-effective alternative whenever the measurement at a few locations in the brain is sufficient. They already found application in blood flow studies (Weber et al. 2003), metabolic studies (Millet et al. 2004; Pain et al. 2002a), receptor occupancy studies (Ginovart et al. 2004) and the evaluation of new radiotracers (Galineau et al. 2006; Wyss et al. 2007; Wyss et al. 2009). All these studies were performed using thin probes designed for direct acquisition within the structure of interest. However, a disadvantage of these intracerebral probes is the potential tissue disturbance caused by their insertion.

The present study demonstrates the suitability of the surface probe for accurate measurements of tracer kinetics in the rodent cerebral cortex through the thinned skull. The fact that there is no need for craniotomy facilitates and shortens the surgery and does not cause any tissue disturbance. The dura and brain remain untouched, leaving the cortex in a physiological state.

This novel probe system was able to reliably measure kinetic data using radiotracers labeled with nuclides of different energies. However, values for $LCMR_{glu}$ and CBF were both lower in the surface probe measurements. Several factors could contribute to these differences which include probe calibration procedures, differences in the geometry and size of the detection volume. In addition, tissues between the surface probe and cortical surface, such as blood vessels in the dura and thinned bone may affect the signal measured. As previously mentioned gamma radiation may be yet another source for error albeit small (Pain et al. 2000; Pain et al. 2002b; Weber et al. 2003).

Absolute values of measurements are prone to vary according to the technology used. Probably more important than absolute values is the reproducibility of a method and its ability to detect

changes associated with different activity states. Both are clearly demonstrated in this study. The increases in $LCMR_{glu}$ during ION and in CBF following acetazolamide were both detected by the surface probe and the percent increase was similar to that measured using autoradiography.

The reason we used F-18 and O-15 was the different emission energy of the positrons and that FDG and ^{15}O-H_2O display a very different kinetic behavior. The higher emission energy of O-15 leads to a different geometry and size of the volume of the detected positrons, as is demonstrated in ***Figure 2C***. Furthermore, the kinetics of ^{15}O-H_2O are much faster than those of FDG. It was therefore relevant to demonstrate the suitability of the surface probe for both tracers. One of the most critical issues with regard to absolute quantification is the precise calibration of instruments. The calibration procedure should also adequately mimic the *in vivo* situation. It can be assumed, that this is somewhat more difficult in the case of the surface detector as compared to the intracortical probe, mainly because the position of the surface detector cannot be perfectly reproduced from experiment to experiment (e.g., due to the thinning of the bone, angle and distance of the probe relative to brain surface).

A major advantage of the surface probe is its high sensitivity. In spite of acquiring the signal through several layers covering the brain, kinetic data can be acquired with low noise (***Figure 3***). This allows the injection of lower doses of radioactivity, while still yielding adequate counting statistics. This is especially important in receptor studies, where the mass of injected compound should be low in comparison to the number of receptors (Hume et al. 1998).

Finally, another valuable feature of the surface system is its use in awake animals. This clearly broadens the applicability of the device given the fact that an increasing number of studies are performed on awake animals to avoid the disturbing effect of anesthetics on brain function (Austin et al. 2005; Lindauer et al. 1993; Martin et al. 2006a; Nakao et al. 2001). Our preliminary data acquired in one animal at two different days demonstrates the marked effect of sevoflurane inhalation on brain metabolism.

Summary

In this work, we demonstrated the feasibility of a high sensitivity surface probe system for the measurement of radiotracer kinetics from the cerebral cortex of the rat. The system yielded reproducible results in the anesthetized rat. Its potential use in awake animal was demonstrated in a preliminary experiment. Due to its high sensitivity and low invasiveness compared to the original intracortical beta probe, this new device considerably widens the scope of applications of beta probes.

Table 1. Rate constants determined using a two-tissue compartment model during baseline

	Animal number	K_1 ml min^{-1} ml $tissue^{-1}$	k_2 min^{-1}	k_3 min^{-1}	LCMRglu µmol $100g^{-1}$ min^{-1}
Right somatosensory cortex surface probe	1	0.080	0.196	0.075	43.21
	2	0.107	0.256	0.070	45.37
	3	0.122	0.304	0.098	55.88
	4	0.111	0.264	0.060	35.67
	5	0.106	0.304	0.108	61.90
	6	0.128	0.269	0.058	45.89
	mean ± sd	0.109 ± 0.02	0.266 ± 0.04	0.078 ± 0.02	47.99 ± 9.4
Left somatosensory cortex intracortical probe	1	0.081	0.165	0.094	57.56
	2	0.103	0.204	0.069	51.6
	3	0.131	0.266	0.067	49.26
	4	0.089	0.156	0.063	45.63
	5	0.116	0.270	0.149	92.13
	6	0.173	0.224	0.060	72.06
	mean ± sd	0.116 ± 0.03	0.214 ± 0.05	0.084 ± 0.03	61.37 ± 17.69

Table 2. Rate constants determined using a two-tissue compartment model during baseline

	condition	animal number	CBF ml min^{-1} 100 ml $tissue^{-1}$	
Right somatosensory cortex surface probe	baseline	1	35.14	
		1	34.58	
		2	34.04	
		2	34.21	34.49 ± 0.5
	acetazolamide	1	50.82	
		1	50.4	
		2	53.87	
		2	54.07	52.29 ± 1.9
Left somatosensory cortex intracortical probe	baseline	1	37.38	
		1	38.92	
		2	39.53	
		2	39.20	38.76 ± 0.9
	acetazolamide	1	55.02	
		1	56.14	
		2	59.94	
		2	58.97	57.52 ± 2.3

Figures of Chapter III:

Novel high sensitivity Beta Scintillator for Cortical Measurements of Radiotracer Kinetics in the Rodent Brain

Figure III-1. The novel surface probe: Design and linearity

(A) Schematic of the novel probe. Dimensions are given in mm. The scintillation crystal and the optical fiber are covered by a tungsten shell. (B) Semi-logarithmic plot of the physical decay of F-18 detected by the novel surface probe. Linearity of the device is evident from the high agreement of the measured data (open circles) with the theoretical decay (black line).

Figure III-1

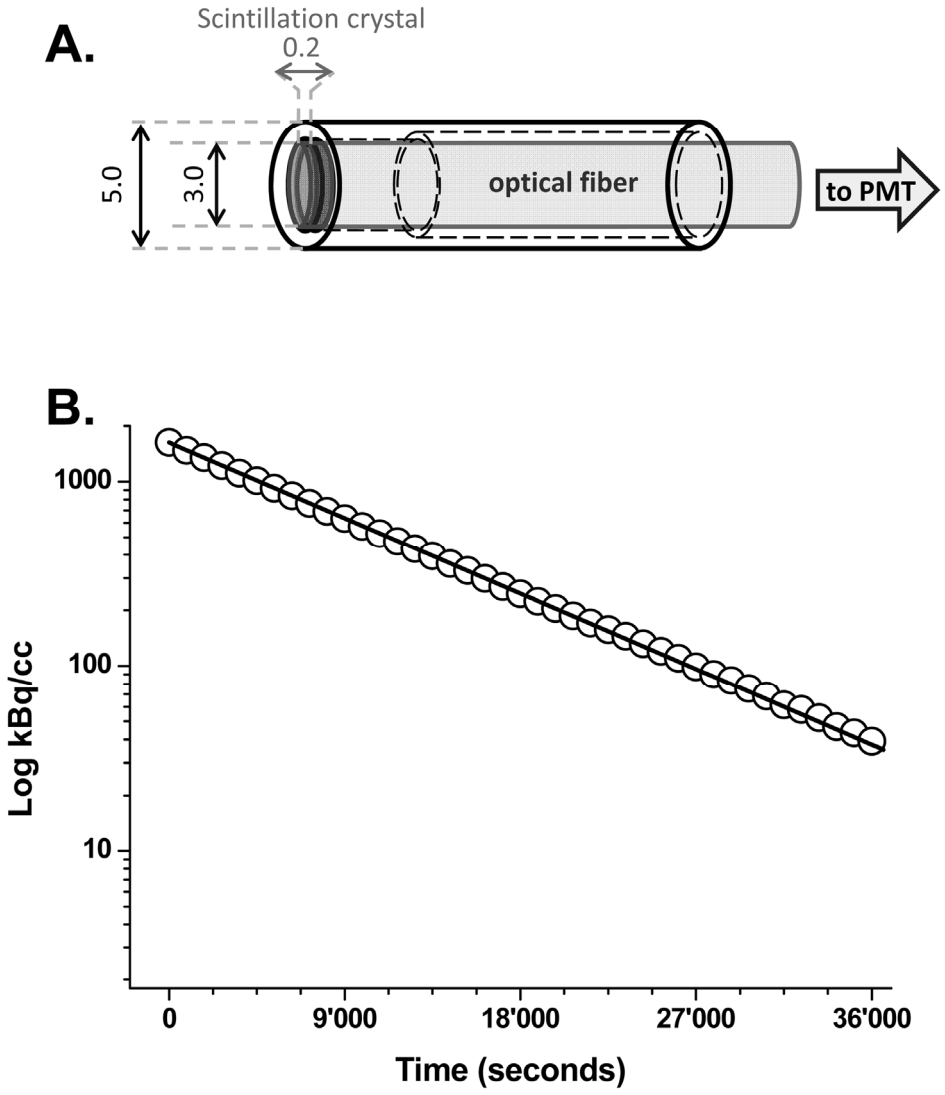
A.
Scintillation crystal
0.2
5.0
3.0
optical fiber
to PMT
B.
1000
100
10
Log kBq/cc
0
9'000
18'000
27'000
36'000
Time (seconds)

Figure III-2. Calculated detection volumes

Results from the detection volume simulations. (A) – (C): Detection fraction from a plane representing the sum projection along the Y-direction for F-18 (A), C-11 (B) and O-15 (C). The thin black lines represent the 95% isolines. The sum of all values in the simulated volume was set to 100. (D) The curves depict the normalized detection fraction for sums in planes along the depth (Z-direction) for the simulated isotopes. The vertical straight lines represent the 95% thresholds.

Figure III-2

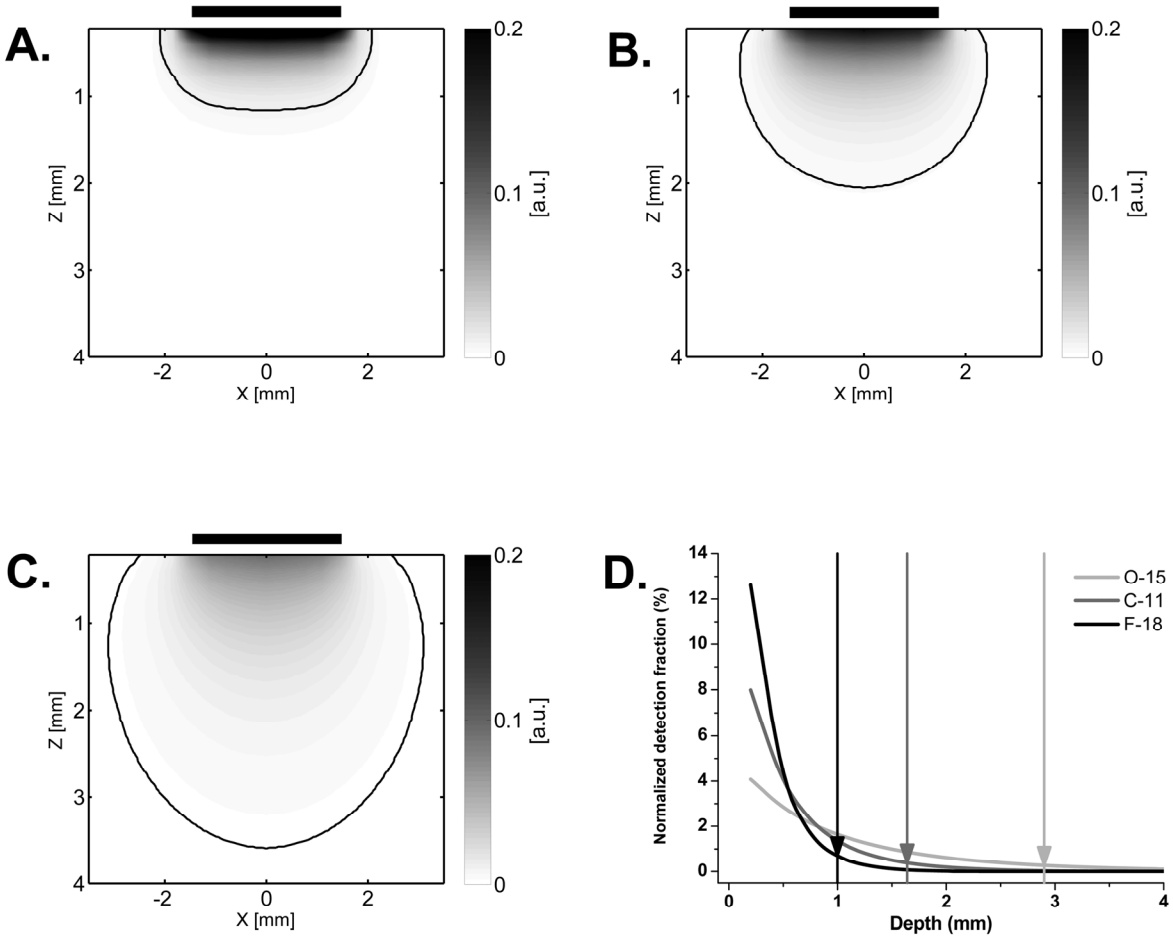
A.
B.
C.
D.
Z [mm]
X [mm]
[a.u.]
0.2
0.1
0
1
2
3
4
-2
0
2
Normalized detection fraction (%)
Depth (mm)
O-15
C-11
F-18
14
12
10
8
6
4
2
0

Figure III-3. Examples of acquired radiotracer data

Typical examples of tissue time activity curves acquired by the original intracortical probe (A, C) and the surface probe (B, D) using two different radiotracers, ^{18}F-FDG (A, B) and ^{15}O-H_2O (C, D). The radioactivity concentration in plasma (light gray line) in whole blood (dark gray line) and the model fit (black line) are also shown. The goodness-of-fit is demonstrated by the random distribution of the residuals (inset). Due to the increased sensitivity of the new system, signal-to-noise ratio is increased leading to an improved model fit illustrated by the narrower range of variability of the residuals.

Figure III-3

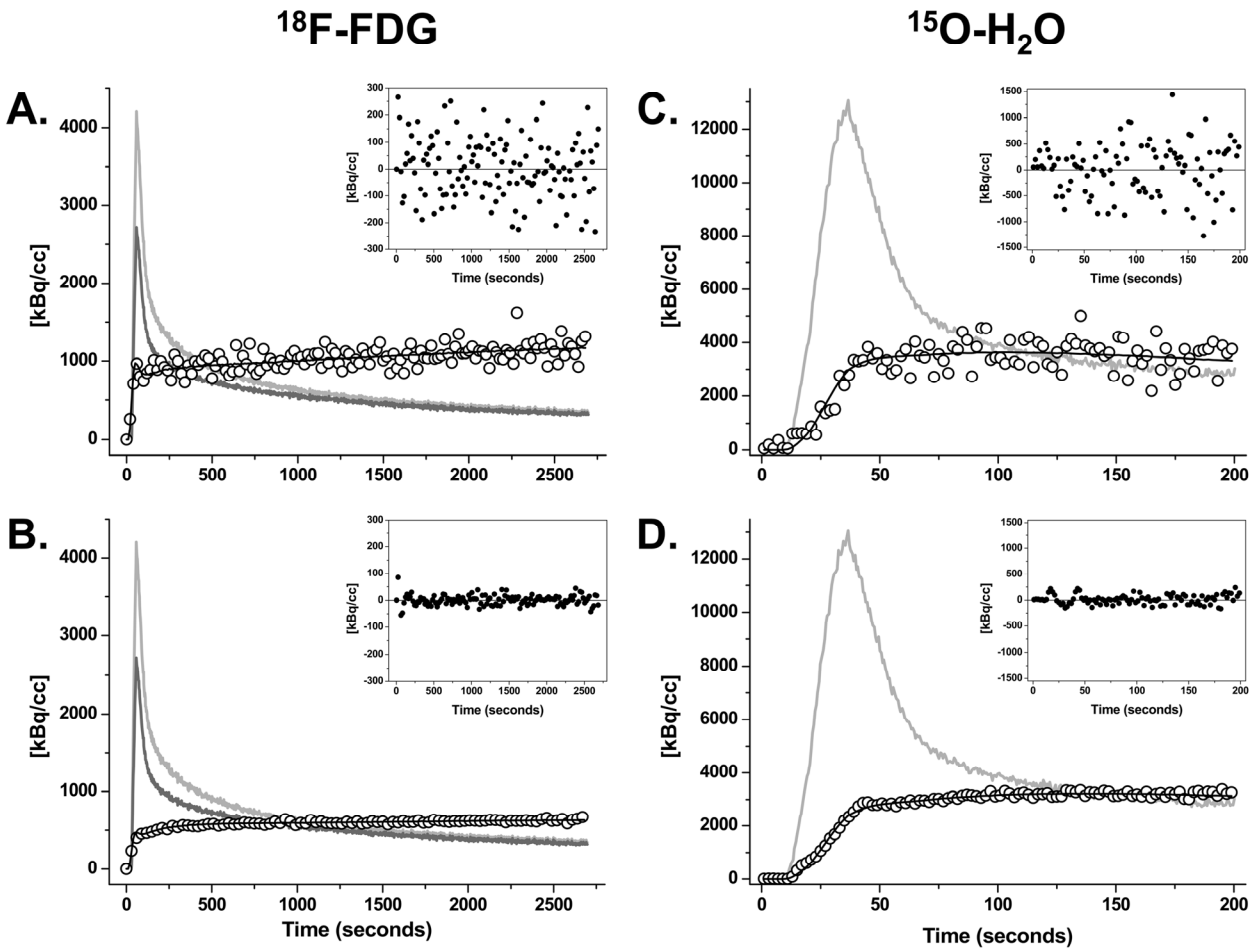

Figure III-4. Comparison of intracortical and surface probe measurements

Bland Altman plot to evaluate the agreement of the probe measurements in 6 animals using ^{18}F-FDG. The middle line represents the mean of two measurements in the same animal using the two different probe systems, the border dashed lines the mean +/- 2 sd, respectively.

Figure III-4.

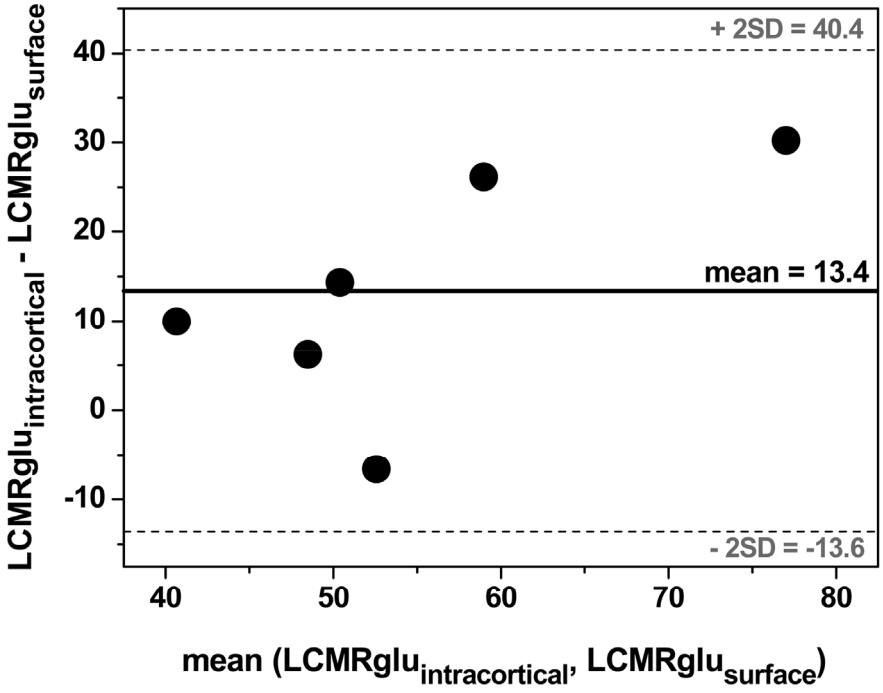
+ 2SD = 40.4
mean = 13.4
- 2SD = -13.6
40
30
20
10
0
-10
40
50
60
70
80
LCMRglu intracortical - LCMRglu surface
mean (LCMRglu intracortical, LCMRglu surface)

Figure III-5. Normalized ^{18}F-FDG accumulation measured by the two probe systems

Time activity curves of ^{18}F-FDG accumulation in the rat‘s somatosensory cortex normalized to the integral of tissue activity between 0 and 45 minutes. Shown is the measurement in a single animal acquired on one side with the intracortical system (open circles) and homotopically on the contralateral hemisphere with the surface probe system (filled gray circles).

Figure III-5

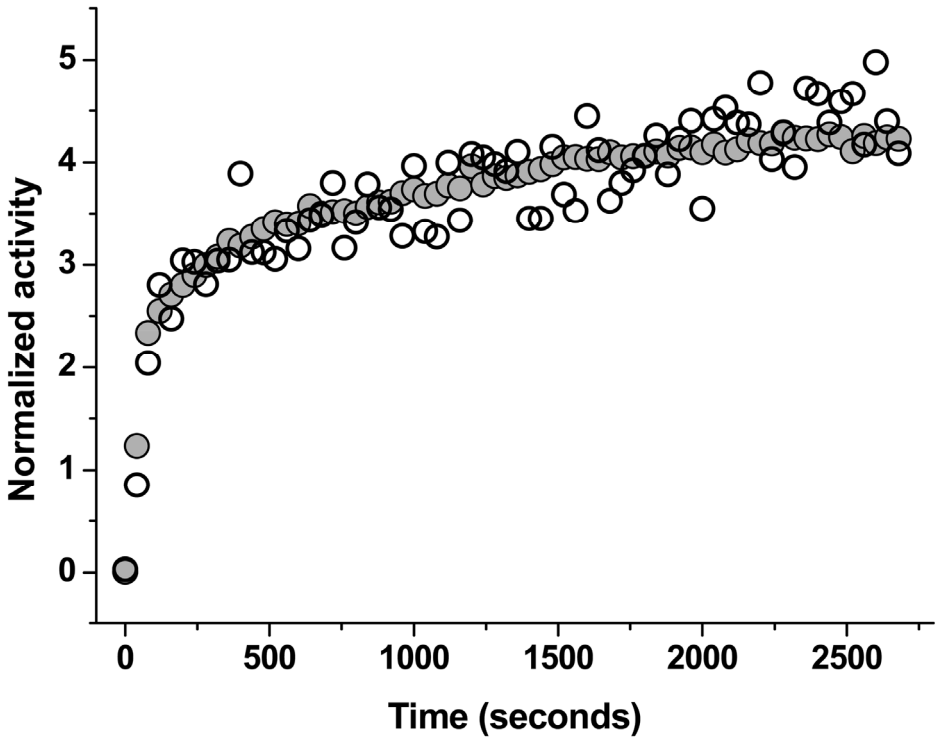
Normalized activity
0
1
2
3
4
5
0
500
1000
1500
2000
2500
Time (seconds)

Figure III-6. Glucose utilization during ION stimulation

Decay-corrected tissue time activity curves acquired by the surface probe system during electrical infraorbital nerve stimulation in one animal are demosntrated. As shown in the autoradiogram, contralateral to the stimulation site (arrow, gray squares in the graph) accumulation of ^{18}F-FDG was increased compared to the ipsilateral hemisphere (open circles in the graph). The radioactivity concentration in plasma (gray line) and in whole blood (black line) is also shown.

Figure III-6

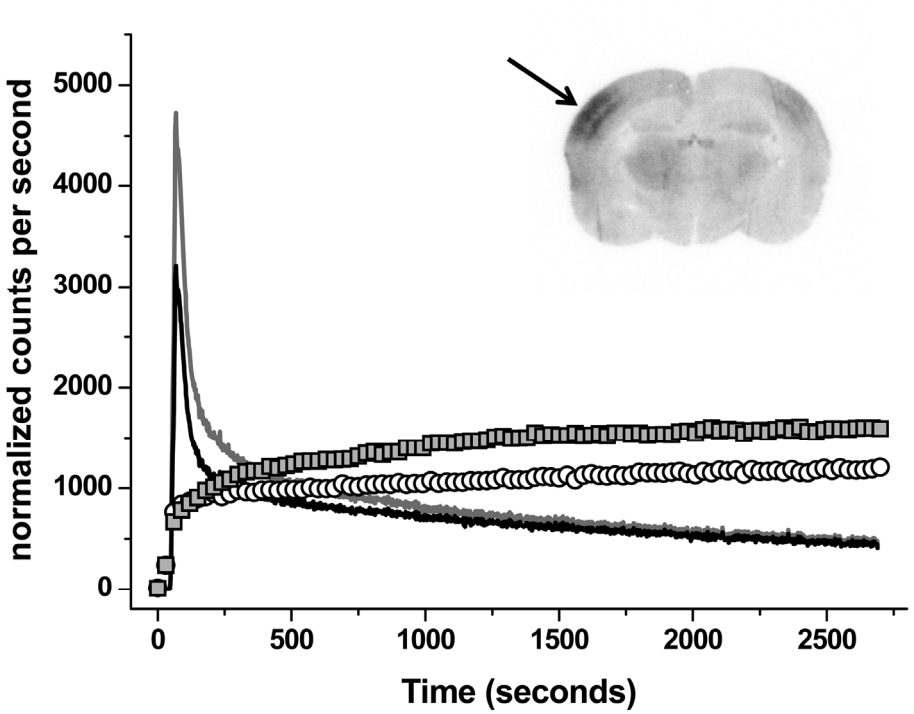
normalized counts per second
5000
4000
3000
2000
1000
0
0
500
1000
1500
2000
2500
Time (seconds)

Figure III-7. Acquisition in the awake, head-fixed animal

The decay-corrected time activity curve shows a steep slope in the awake state which considerably flattens after the induction of anesthesia with the fast-acting volatile anesthetic sevoflurane at time point 20 minutes.

Figure III-7

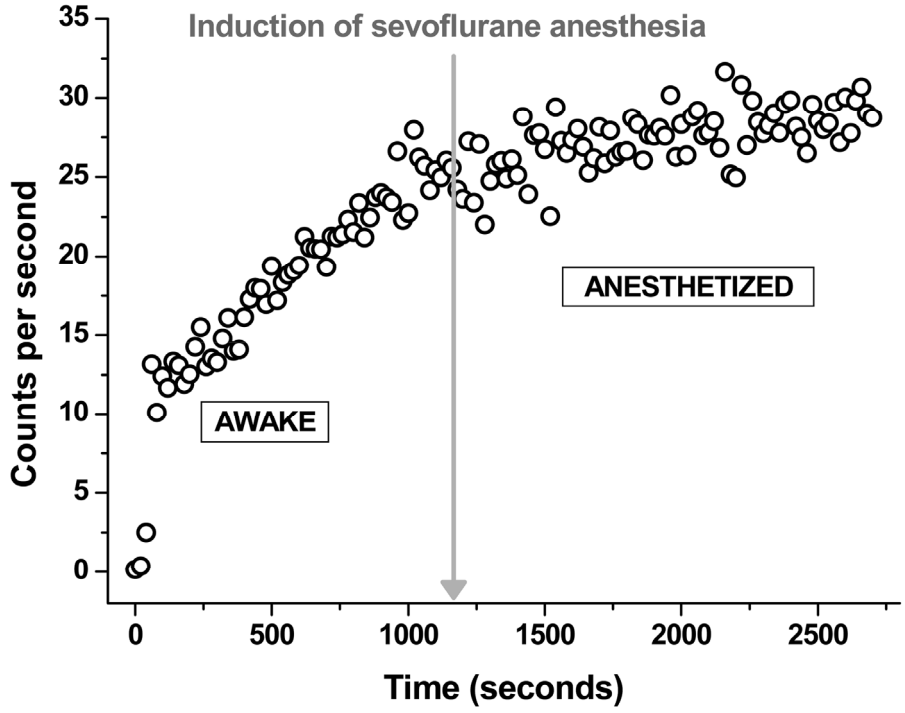
Induction of sevoflurane anesthesia
ANESTHETIZED
AWAKE
Counts per second
Time (seconds)
0
5
10
15
20
25
30
35
0
500
1000
1500
2000
2500

Implications and Future directions

The original intent of the project was to address the following specific questions:

What is the first pass extraction fraction of the different tracers?

What compartment model describes the cerebral kinetics of the tracers?

How does tracer kinetics change during electrical and pharmacological interventions?

How do these changes reflect neuronal lactate metabolism and astrocytic oxidative metabolism?

All these general questions were answered and discussed in detail by the individual studies in their respective sections. Overall, the project led to a better understanding of the characteristics of the applied radiotracers, rendering their application and indication easier. Furthermore, our research may provide a novel approach to the compartmentalized brain energy metabolism using radiotracer kinetics. In addition, the project went a step further and introduced a novel beta probe refining the methodology used to measure tracer kinetics with high temporal resolution. The individual studies were already discussed in detail in their respective sections. Here, I would like to stress some final points concerning selected aspects of the project. More specifically, I would like to highlight the work's significance regarding neurometabolic research development, the potential implications for a better understanding of metabolism-related neuroimaging using FDG, and its clinical relevance.

Beta probe studies in neurometabolic research

In general, the project aimed to pave the way for the beta probe methodology in the field of neurometabolic research. It is the first study that uses radiotracer kinetic measurements to collect information from separate metabolic compartments in the living brain. Indeed, beta probe acquisitions have already been employed for brain metabolism-related work, beside their use in receptor studies (Galineau et al. 2006; Ginovart et al. 2004; Wyss et al. 2007) and measurements of cerebral blood flow (Weber et al. 2003). However, studies about brain metabolism were highly

limited and the only tracer used so far together with kinetic beta probe measurements was ^{18}F-fluorodeoxyglucose (Millet et al. 2004; Pain et al. 2002a). As stated in the introduction, cerebral glucose utilization measurements using ^{18}F-fluorodeoxyglucose are integrating all separate metabolic compartments without offering site-specific information. However, site-specific information is crucial for a better understanding of a highly compartmentalized system such as brain metabolism. Supported by the experimental results, we could show for the first time compartmental information of brain metabolism (for summary see ***Figure 10***) using kinetic measurements. In previous years, radiotracer experiments were performed using the *ex vivo* autoradiographic approach that measures the distribution of nuclides and metabolites produced within brain tissue after injection of the labeled compounds (Berl and Frigyesi 1968; Berl and Frigyesi 1969; Cremer 1970). Although these studies increased our knowledge about the compartmentalization of brain metabolism (for a review see (Hertz 2004)), this approach, in contrast to kinetic approaches, did not offer the possibility to deduce transport and binding rates of the tracer under study. A significant advantage of beta probe experiments is that the characteristics of the dynamic process can be inferred. Analysis of such data acquired with high temporal resolution results in robust rate constants of the processes involved in the biological system under study. Kinetic data can theoretically also be obtained by the analysis of serial tomographic images from PET studies, but they may not provide accurate information about tracer uptake of different brain regions, especially in rodents (Chatziioannou 2002). Furthermore, the use of this sophisticated imaging technique is not as cost-effective as beta probe measurements. Robust kinetic data, such as those delivered by probe measurements, help to calculate quantitative results from kinetic modeling. A high temporal resolution is also mandatory for multiple-injection protocols, which can be carried out easily using beta probes. In addition, they can be combined with other modalities, such as laser Doppler flowmetry, magnetic resonance imaging, and nuclear magnetic resonance (Desbree et al. 2004; Desbree et al. 2007). In the future, especially the combination with MRS may result in valuable new insights into compartmentalized brain metabolism. The most common MRS approach relies on the infusion of ^{13}C-enriched substrates (e.g. glucose, acetate) and the measurement of label incorporation into brain metabolites (Escartin et al. 2006). It has the unique property to specifically identify the molecule

and the atomic position at which the ^{13}C label accumulates. These properties enabled MRS to contribute significantly to the knowledge about the neuron/astrocyte dialogue. The advantage of this very fine biochemical probing also has some drawbacks. On the one hand, the intrinsic sensitivity of the method is low making the detection of trace amounts of the label impossible, on the other hand, the spatial resolution is limited rendering the exploration of focal neural activation difficult.

Finally, the recent demonstration of the use of radiosensitive intracortical probes in the mouse is worth mentioning (Desbree et al. 2008). The increasing number of murine disease models and genetically altered mice will further enlarge the field of application for beta probe studies.

Compartmentation of brain metabolism

There still exists remarkable controversy regarding proportional contributions of the single compartments to the overall cerebral metabolism. Especially the percentage of oxidative and glycolytic energy metabolism is ambiguous (for review see (Hertz 2004)). The main difficulty is the fact that the proportions are not fixed during different states of activity. This is in agreement with previous observations made using different methods and stimuli, which consistently showed that oxygen consumption increases less than glucose utilization and CBF (Fox and Raichle 1986; Fox et al. 1988) during activation compared to baseline state. In the present work I disclosed the potential of radiotracer methodology to capture oxidative metabolism in segregated cellular populations, i.e. neurons and astrocytes. By using lactate and acetate radiolabeled with a positron-emitter, it was possible to investigate, for the first time, aspects of specific metabolic compartments of the brain in vivo in a dynamic manner. In future studies these methods will offer the possibility to further investigate the respective size of these compartments at varying neuronal activity and pharmacological manipulations of the involved energetic pathways. This can help to better understand some mechanisms of regulation.

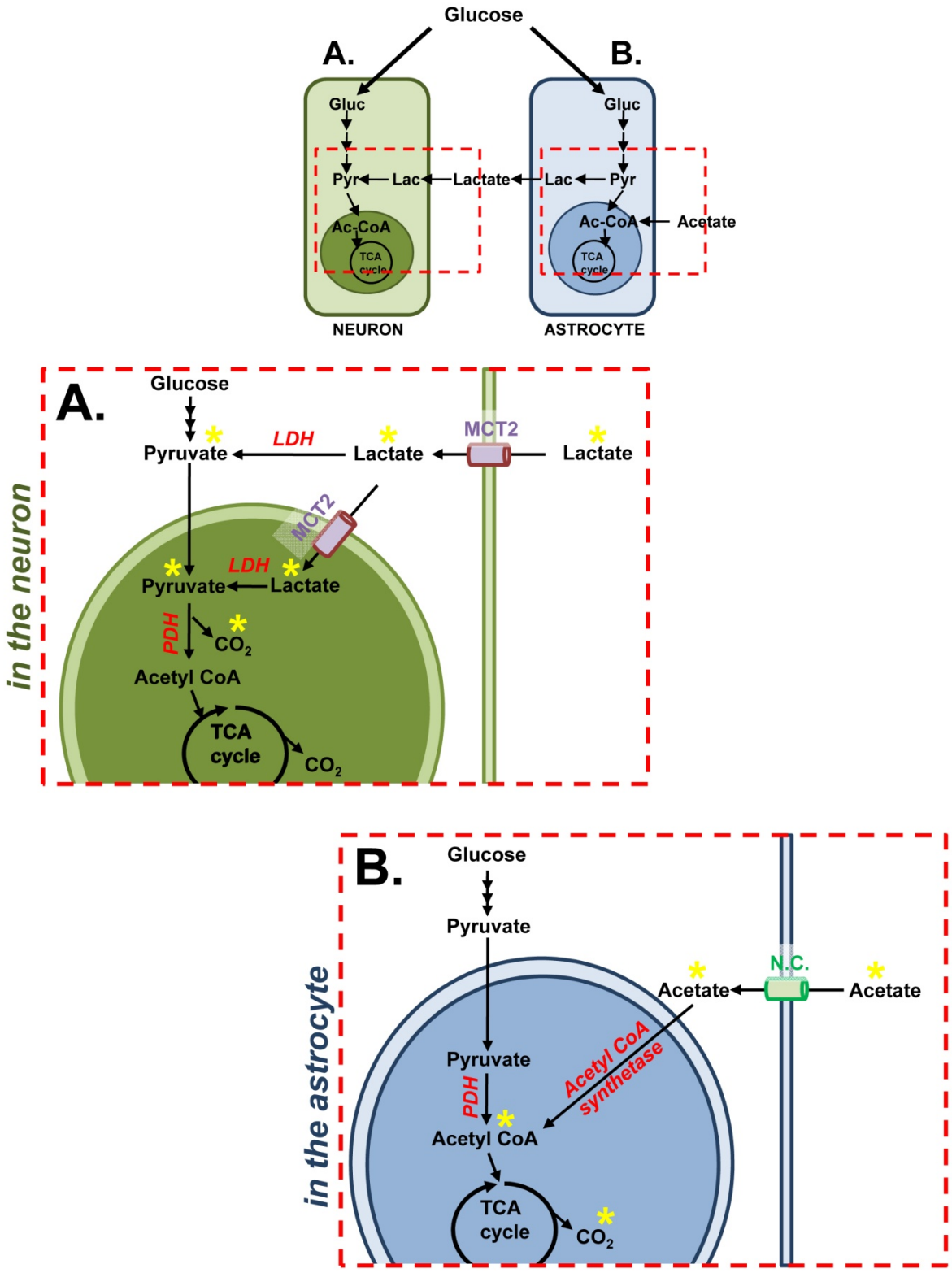

Figure 10. Schematic summary of the compartmental investigation of brain metabolism using ^{11}C-acetate and ^{11}C-L-lactate

The two tracers used in the present project allow the examination of specific metabolic steps within the two main oxidative compartments of brain metabolism. A.) ^{11}C-L-lactate, which is preferred by neurons, traces particularly neuronal uptake of lactate via the monocarboxylic acid transporter (MCT2) and its decarboxylation via pyruvate to acetyl CoA. B.) The astrocyte-specific compound ^{11}C-acetate traces the degradation to CO_2 via the TCA cycle and with it specifically astrocytic oxidative metabolism. Yellow asterisks indicate the path of the label (C-11). Formed CO_2 will then leave brain tissue by diffusion across the BBB and removal by the blood system (not shown in the diagram).

Neuroimaging using ^{18}F-fluorodeoxyglucose

Beside cerebral blood flow also energy metabolism is functionally coupled to brain activity which forms the fundament of modern neuroimaging methods (for review see (Raichle 2003; Raichle and Mintun 2006)). Neuroscience without this variety of brain imaging modalities is not conceivable anymore. As stated above, ^{18}F-FDG is the main radiotracer used in functional metabolism-related neuroimaging with positron emission tomography so far. The determination of glucose utilization using ^{18}F-FDG is an unspecific measure integrating all the spatially separated compartments and does not offer any site-specific information. Recently it was shown that glial cells take up 2DG only to a slightly lower extent than neurons (Nehlig et al. 2004) although glial energy need was calculated to be in a range of 5 to 20% (Attwell and Laughlin 2001; Gjedde et al. 2002). This obvious discrepancy was explained by the notion that the major part of glucose is processed via anaerobic glycolysis only in astrocytes. However, our study shows that also astrocytes exhibit significant aerobic metabolism at baseline (in the range of 20% of total cerebral oxygen consumption). Further studies about size and share of different metabolic compartments will help for a better understanding of the nature and meaning of findings obtained in the past using deoxyglucose methodology. Site-specific quantities are crucial for a significant improvement in our understanding of a highly compartmentalized system, such as brain metabolism. Also the debate about the existence of the ANLS can profit from the development and application of new approaches for the compartmental investigation of brain energy metabolism.

Energy metabolism and neurological diseases

For a variety of neurological and non-neurological diseases severe metabolic deficits in the brain have been documented (Martin et al. 2007; Mason et al. 2006; Mosconi 2005; Simpson et al. 1994; Sonnewald and Kondziella 2003). On the one hand, the metabolic impairment can be very clear as during ischemia, where the energy supply is acutely disrupted leading to death of brain cells. On the other hand, the defect can be as small as a single gene mutation causing the dysfunction of a key enzyme or transport step involved in brain metabolism leading to neuronal dysfunction, such as glycogen storage disease or pyruvate dehydrogenase deficiency. Research focusing on

mechanisms and effects of such diseases can profit from new approaches. In this respect, further research in a more clinical and disease-related environment can profit twofold from the present project. Firstly, the radiotracer kinetic measurements by the beta probe technology can be easily translated into a clinical setup by using positron emission tomography. This is an elegant example of accelerating the way from preclinical to clinical studies. Secondly, a better understanding of pathogenesis of the diseased brain may pave the way for new therapeutic approaches. Metabolic alterations often precede structural changes and the detection of these changes may prove critical in assessing disease progression and treatment. Based on our work, it is particularly interesting that many neurological diseases exhibit mitochondrial dysfunction (Beal 2000; Beal et al. 1993). Therefore the measurement of the astrocytic or neuronal $CMRO_2$ may prove beneficial for the investigation of such diseases.

In summary, the present project demonstrates the possibility to measure distinct parameters of separate metabolic compartments in the intact brain using radiotracer kinetics. The fact that radiotracer kinetic measurements are in principle smoothly transferable to humans further increases the relevance of this work. The application of radiotracer measurements using nuclear medicine devices may prove important in the future for both, a better understanding of neuron/astrocyte contribution to energy metabolism, and the ability to obtain novel insights into the pathomechanisms of various pathologies.

References

Abemayor E, Kovachich GB, Haugaard N. (1984) Effects of dichloroacetate on brain pyruvate dehydrogenase. *J Neurochem* 42:38-42.

Ackermann RF, Lear JL. (1989) Glycolysis-induced discordance between glucose metabolic rates measured with radiolabeled fluorodeoxyglucose and glucose. *J Cereb Blood Flow Metab* 9:774-785.

Alpert NM, Eriksson L, Chang JY, Bergstrom M, Litton JE, Correia JA, Bohm C, Ackerman RH, Taveras JM. (1984) Strategy for the measurement of regional cerebral blood flow using short-lived tracers and emission tomography. *J Cereb Blood Flow Metab* 4:28-34.

Armbrecht JJ, Buxton DB, Schelbert HR. (1990) Validation of [1-11C]acetate as a tracer for noninvasive assessment of oxidative metabolism with positron emission tomography in normal, ischemic, postischemic, and hyperemic canine myocardium. *Circulation* 81:1594-1605.

Attwell D, Laughlin SB. (2001) An energy budget for signaling in the grey matter of the brain. *J Cereb Blood Flow Metab* 21:1133-1145.

Aureli T, Di Cocco ME, Calvani M, Conti F. (1997) The entry of [1-13C]glucose into biochemical pathways reveals a complex compartmentation and metabolite trafficking between glia and neurons: a study by 13C-NMR spectroscopy. *Brain Res* 765:218-227.

Austin VC, Blamire AM, Allers KA, Sharp T, Styles P, Matthews PM, Sibson NR. (2005) Confounding effects of anesthesia on functional activation in rodent brain: a study of halothane and alpha-chloralose anesthesia. *Neuroimage* 24:92-100.

Badar-Goffer RS, Bachelard HS, Morris PG. (1990) Cerebral metabolism of acetate and glucose studied by 13C-n.m.r. spectroscopy. A technique for investigating metabolic compartmentation in the brain. *Biochem J* 266:133-139.

Bayer E, Bauer B, Eggerer H. (1981) Evidence from inhibitor studies for conformational changes of citrate synthase. *Eur J Biochem* 120:155-160.

Beal MF. (2000) Energetics in the pathogenesis of neurodegenerative diseases. *Trends Neurosci* 23:298-304.

Beal MF, Hyman BT, Koroshetz W. (1993) Do defects in mitochondrial energy metabolism underlie the pathology of neurodegenerative diseases? *Trends Neurosci* 16:125-131.

Berl S, Clarke DD, Nicklas WJ. (1970) Compartmentation of citric acid cycle metabolism in brain: effect of aminooxyacetic acid, ouabain and Ca2+ on the labelling of glutamate, glutamine, aspartate and gaba by [1-14C]acetate, [U-14C]glutamate and [U-14C]asparate. *J Neurochem* 17:999-1007.

Berl S, Frigyesi TL. (1968) Metabolism of [14C]leucine and [14C]acetate in sensorimotor cortex, thalamus, caudate nucleus and cerebellum of the cat. *J Neurochem* 15:965-970.

Berl S, Frigyesi TL. (1969) The turnover of glutamate, glutamine, aspartate and GABA labeled with [1-14C]acetate in caudate nucleus, thalamus and motor cortex (cat). *Brain Res* 12:444-455.

Berl S, Nicklas WJ, Clarke DD. (1968) Compartmentation of glutamic acid metabolism in brain slices. *J Neurochem* 15:131-140.

Bittar PG, Charnay Y, Pellerin L, Bouras C, Magistretti PJ. (1996) Selective distribution of lactate dehydrogenase isoenzymes in neurons and astrocytes of human brain. *J Cereb Blood Flow Metab* 16:1079-1089.

Bland JM, Altman DG. (1986) Statistical methods for assessing agreement between two methods of clinical measurement. *Lancet* 1:307-310.

Bonvento G, Charbonne R, Correze JL, Borredon J, Seylaz J, Lacombe P. (1994) Is alpha-chloralose plus halothane induction a suitable anesthetic regimen for cerebrovascular research? *Brain Res* 665:213-221.

Bonvento G, Herard AS, Voutsinos-Porche B. (2005) The astrocyte-neuron lactate shuttle: a debated but still valuable hypothesis for brain imaging. *J Cereb Blood Flow Metab* 25: 1394-1399.

Bouzier-Sore AK, Serres S, Canioni P, Merle M. (2003a) Lactate involvement in neuron-glia metabolic interaction: (13)C-NMR spectroscopy contribution. *Biochimie* 85:841-848.

Bouzier-Sore AK, Voisin P, Bouchaud V, Bezancon E, Franconi JM, Pellerin L. (2006) Competition between glucose and lactate as oxidative energy substrates in both neurons and astrocytes: a comparative NMR study. *Eur J Neurosci* 24:1687-1694.

Bouzier-Sore AK, Voisin P, Canioni P, Magistretti PJ, Pellerin L. (2003b) Lactate is a preferential oxidative energy substrate over glucose for neurons in culture. *J Cereb Blood Flow Metab* 23:1298-1306.

Bouzier AK, Thiaudiere E, Biran M, Rouland R, Canioni P, Merle M. (2000) The metabolism of [3-(13)C]lactate in the rat brain is specific of a pyruvate carboxylase-deprived compartment. *J Neurochem* 75:480-486.

Broer S, Broer A, Schneider HP, Stegen C, Halestrap AP, Deitmer JW. (1999) Characterization of the high-affinity monocarboxylate transporter MCT2 in Xenopus laevis oocytes. *Biochem J* 341 (Pt 3):529-535.

Broer S, Rahman B, Pellegri G, Pellerin L, Martin JL, Verleysdonk S, Hamprecht B, Magistretti PJ. (1997) Comparison of lactate transport in astroglial cells and monocarboxylate transporter 1 (MCT 1) expressing Xenopus laevis oocytes. Expression of two different monocarboxylate transporters in astroglial cells and neurons. *J Biol Chem* 272:30096-30102.

Brooks DJ, Lammertsma AA, Beaney RP, Leenders KL, Buckingham PD, Marshall J, Jones T. (1984) Measurement of Regional Cerebral Ph in Human-Subjects Using Continuous Inhalation of (Co2)-C-11 and Positron Emission Tomography. *Journal of Cerebral Blood Flow and Metabolism* 4:458-465.

Brooks GA. (2002) Lactate shuttles in nature. *Biochem Soc Trans* 30:258-264.

Brown AM, Ransom BR. (2007) Astrocyte glycogen and brain energy metabolism. *Glia* 55:1263-1271.

Buck A, Wolpers HG, Hutchins GD, Savas V, Mangner TJ, Nguyen N, Schwaiger M. (1991) Effect of carbon-11-acetate recirculation on estimates of myocardial oxygen consumption by PET. *J Nucl Med* 32:1950-1957.

Cangro CB, Sweetnam PM, Neale JH, Haser WG, Curthoys NP. (1984) Selective localization of glutaminase in spinal and sensory nerve cells. A potential marker for glutamate neurotransmission. *Jama* 251:797.

Chatziioannou AF. (2002) PET scanners dedicated to molecular imaging of small animal models. *Mol Imaging Biol* 4:47-63.

Chih CP, Lipton P, Roberts EL, Jr. (2001) Do active cerebral neurons really use lactate rather than glucose? *Trends Neurosci* 24:573-578.

Chih CP, Roberts Jr EL. (2003) Energy substrates for neurons during neural activity: a critical review of the astrocyte-neuron lactate shuttle hypothesis. *J Cereb Blood Flow Metab* 23:1263-1281.

Choi IY, Seaquist ER, Gruetter R. (2003) Effect of hypoglycemia on brain glycogen metabolism in vivo. *J Neurosci Res* 72:25-32.

Cremer JE. (1970) Selective inhibition of glucose oxidation by triethyltin in rat brain in vivo. *Biochem J* 119:95-102.

Cremer JE. (1982) Substrate utilization and brain development. *J Cereb Blood Flow Metab* 2:394-407.

Cremer JE, Cunningham VJ, Pardridge WM, Braun LD, Oldendorf WH. (1979) Kinetics of blood-brain barrier transport of pyruvate, lactate and glucose in suckling, weanling and adult rats. *J Neurochem* 33:439-445.

Crone C. (1963) THE PERMEABILITY OF CAPILLARIES IN VARIOUS ORGANS AS DETERMINED BY USE OF THE 'INDICATOR DIFFUSION' METHOD. *Acta Physiol Scand* 58:292-305.

Cruz NF, Lasater A, Zielke HR, Dienel GA. (2005) Activation of astrocytes in brain of conscious rats during acoustic stimulation: acetate utilization in working brain. *J Neurochem* 92:934-947.

Dalsgaard MK, Secher NH. (2007) The brain at work: a cerebral metabolic manifestation of central fatigue? *J Neurosci Res.* 85:3334-3339.

Danbolt NC. (2001) Glutamate uptake. *Prog Neurobiol* 65:1-105.

Debernardi R, Pierre K, Lengacher S, Magistretti PJ, Pellerin L. (2003) Cell-specific expression pattern of monocarboxylate transporters in astrocytes and neurons observed in different mouse brain cortical cell cultures. *J Neurosci Res* 73:141-155.

Desbree A, Pain F, Gurden H, Zimmer L, Pinot L, Laniece P, Mastrippolito R. (2004) Combining the radiosensitive Beta MicroProbe to nuclear magnetic resonance: theoretical approach for in vivo studies in small animals. *J Neurosci Methods* 140:47-52.

Desbree A, Rbah L, Langlois JB, Grenier D, Mastrippolito R, Pain F, Pinot L, Laniece P, Zimmer L, Gurden H. (2007) Simultaneous in vivo magnetic resonance imaging and radioactive measurements with the beta-MicroProbe. *Eur J Nucl Med Mol Imaging* 34:1868-1872.

Desbree A, Verdurand M, Godart J, Dubois A, Mastrippolito R, Pain F, Pinot L, Delzescaux T, Gurden H, Zimmer L, Laniece P. (2008) The Potential of a Radiosensitive Intracerebral Probe to Monitor 18F-MPPF Binding in Mouse Hippocampus In Vivo. *J Nucl Med* 49:1155-1161.

Dienel GA, Schmidt KC, Cruz NF. (2007) Astrocyte activation in vivo during graded photic stimulation. *J Neurochem* 103:1506-1522.

Dimmer KS, Friedrich B, Lang F, Deitmer JW, Broer S. (2000) The low-affinity monocarboxylate transporter MCT4 is adapted to the export of lactate in highly glycolytic cells. *Biochem J* 350 Pt 1:219-227.

Dombrowski GJ, Jr., Swiatek KR, Chao KL. (1989) Lactate, 3-hydroxybutyrate, and glucose as substrates for the early postnatal rat brain. *Neurochem Res* 14:667-675.

Drandarov K, Schubiger PA, Westera G. (2006) Automated no-carrier-added synthesis of [1-11C]-labeled D- and L-enantiomers of lactic acid. *Appl Radiat Isot* 64:1613-1622.

Duelli R, Kuschinsky W. (2001) Brain glucose transporters: relationship to local energy demand. *News Physiol Sci* 16:71-76.

Erlichman JS, Hewitt A, Damon TL, Hart M, Kurascz J, Li A, Leiter JC. (2008) Inhibition of monocarboxylate transporter 2 in the retrotrapezoid nucleus in rats: a test of the astrocyte-neuron lactate-shuttle hypothesis. *J Neurosci* 28:4888-4896.

Escartin C, Valette J, Lebon V, Bonvento G. (2006) Neuron-astrocyte interactions in the regulation of brain energy metabolism: a focus on NMR spectroscopy. *J Neurochem* 99:393-401.

Fox PT, Raichle ME. (1986) Focal physiological uncoupling of cerebral blood flow and oxidative metabolism during somatosensory stimulation in human subjects. *Proc Natl Acad Sci U S A* 83:1140-1144.

Fox PT, Raichle ME, Mintun MA, Dence C. (1988) Nonoxidative glucose consumption during focal physiologic neural activity. *Science* 241:462-464.

Froberg MK, Gerhart DZ, Enerson BE, Manivel C, Guzman-Paz M, Seacotte N, Drewes LR. (2001) Expression of monocarboxylate transporter MCT1 in normal and neoplastic human CNS tissues. *Neuroreport* 12:761-765.

Galineau L, Wilson AA, Garcia A, Houle S, Kapur S, Ginovart N. (2006) In vivo characterization of the pharmacokinetics and pharmacological properties of [11C]-(+)-PHNO in rats using an intracerebral beta-sensitive system. *Synapse.* 60:172-183.

Gerhart DZ, Enerson BE, Zhdankina OY, Leino RL, Drewes LR. (1998) Expression of the monocarboxylate transporter MCT2 by rat brain glia. *Glia* 22:272-281.

Gerhart DZ, Leino RL. (1999) Distribution of monocarboxylate transporters MCT1 and MCT2 in rat retina. *Neuroscience.* 92:367-375.

Ginovart N, Sun W, Wilson AA, Houle S, Kapur S. (2004) Quantitative validation of an intracerebral beta-sensitive microprobe system to determine in vivo drug-induced receptor occupancy using [11C]raclopride in rats. *Synapse* 52:89-99.

Gjedde A, Crone C. (1975) Induction processes in blood-brain transfer of ketone bodies during starvation. *Am J Physiol* 229:1165-1169.

Gjedde A, Marrett S, Vafaee M. (2002) Oxidative and nonoxidative metabolism of excited neurons and astrocytes. *J Cereb Blood Flow Metab* 22:1-14.

Haiss F, Schwarz C. (2005) Spatial segregation of different modes of movement control in the whisker representation of rat primary motor cortex. *J Neurosci* 25:1579-1587.

Halestrap AP, Price NT. (1999) The proton-linked monocarboxylate transporter (MCT) family: structure, function and regulation. *Biochem J* 343 Pt 2:281-299.

Hassel B, Brathe A. (2000) Cerebral metabolism of lactate in vivo: evidence for neuronal pyruvate carboxylation. *J Cereb Blood Flow Metab* 20:327-336.

Hassel B, Paulsen RE, Johnsen A, Fonnum F. (1992) Selective inhibition of glial cell metabolism in vivo by fluorocitrate. *Brain Res* 576:120-124.

Hawkins RA, Mans AM, Davis DW. (1986) Regional ketone body utilization by rat brain in starvation and diabetes. *Am J Physiol* 250:E169-178.

Hawkins RA, O'Kane RL, Simpson IA, Vina JR. (2006) Structure of the blood-brain barrier and its role in the transport of amino acids. *J Nutr* 136:218S-226S.

Hawkins RA, Williamson DH, Krebs HA. (1971) Ketone-body utilization by adult and suckling rat brain in vivo. *Biochem J* 122:13-18.

Hertz L. (2004) Intercellular metabolic compartmentation in the brain: past, present and future. *Neurochem Int* 45:285-296.

Hertz L, Drejer J, Schousboe A. (1988) Energy metabolism in glutamatergic neurons, GABAergic neurons and astrocytes in primary cultures. *Neurochem Res* 13:605-610.

Hertz L, Kala G. (2007) Energy metabolism in brain cells: effects of elevated ammonia concentrations. *Metab Brain Dis.* 22:199-218.

Hertz L, Peng L, Dienel GA. (2007) Energy metabolism in astrocytes: high rate of oxidative metabolism and spatiotemporal dependence on glycolysis/glycogenolysis. *J Cereb Blood Flow Metab.* 27:219-249.

Hosoi R, Okada M, Hatazawa J, Gee A, Inoue O. (2004) Effect of astrocytic energy metabolism depressant on 14C-acetate uptake in intact rat brain. *J Cereb Blood Flow Metab* 24:188-190.

Huang Y, Zielke CL, Tildon JT, Zielke HR. (1993) Monitoring in vivo oxidation of 14C-labelled substrates to 14CO2 by brain microdialysis. *Dev Neurosci* 15:233-239.

Hume SP, Gunn RN, Jones T. (1998) Pharmacological constraints associated with positron emission tomographic scanning of small laboratory animals. *Eur J Nucl Med* 25:173-176.

Hume SP, Myers R. (2002) Dedicated small animal scanners: a new tool for drug development? *Curr Pharm Des* 8:1497-1511.

Hyder F, Patel AB, Gjedde A, Rothman DL, Behar KL, Shulman RG. (2006) Neuronal-glial glucose oxidation and glutamatergic-GABAergic function. *J Cereb Blood Flow Metab* 26:865-877.

Ide K, Schmalbruch IK, Quistorff B, Horn A, Secher NH. (2000) Lactate, glucose and O2 uptake in human brain during recovery from maximal exercise. *J Physiol* 522 Pt 1:159-164.

Itoh Y, Esaki T, Shimoji K, Cook M, Law MJ, Kaufman E, Sokoloff L. (2003) Dichloroacetate effects on glucose and lactate oxidation by neurons and astroglia in vitro and on glucose utilization by brain in vivo. *Proc Natl Acad Sci U S A* 100:4879-4884.

Kasischke KA, Vishwasrao HD, Fisher PJ, Zipfel WR, Webb WW. (2004) Neural activity triggers neuronal oxidative metabolism followed by astrocytic glycolysis. *Science* 305:99-103.

Kety SS, Schmidt CF. (1948) The Nitrous Oxide Method for the Quantitative Determination of Cerebral Blood Flow in Man - Theory, Procedure and Normal Values. *Journal of Clinical Investigation* 27:476-483.

Kimelberg HK. (2004) The role of hypotheses in current research, illustrated by hypotheses on the possible role of astrocytes in energy metabolism and cerebral blood flow: from Newton to now. *J Cereb Blood Flow Metab* 24:1235-1239.

Knudsen GM, Paulson OB, Hertz MM. (1991) Kinetic analysis of the human blood-brain barrier transport of lactate and its influence by hypercapnia. *J Cereb Blood Flow Metab* 11:581-586.

Korf J. (2006) Is brain lactate metabolized immediately after neuronal activity through the oxidative pathway? *J Cereb Blood Flow Metab.* 26:1584-1586.

LaManna JC, Harrington JF, Vendel LM, Abi-Saleh K, Lust WD, Harik SI. (1993) Regional blood-brain lactate influx. *Brain Res* 614:164-170.

Landau WM, Freygang WH, Jr., Roland LP, Sokoloff L, Kety SS. (1955) The local circulation of the living brain; values in the unanesthetized and anesthetized cat. *Trans Am Neurol Assoc*:125-129.

Larrabee MG. (1983) Lactate uptake and release in the presence of glucose by sympathetic ganglia of chicken embryos and by neuronal and nonneuronal cultures prepared from these ganglia. *J Neurochem* 40:1237-1250.

Larrabee MG. (1995) Lactate metabolism and its effects on glucose metabolism in an excised neural tissue. *J Neurochem* 64:1734-1741.

Larrabee MG. (1996) Partitioning of CO2 production between glucose and lactate in excised sympathetic ganglia, with implications for brain. *J Neurochem* 67:1726-1734.

Laughton JD, Charnay Y, Belloir B, Pellerin L, Magistretti PJ, Bouras C. (2000) Differential messenger RNA distribution of lactate dehydrogenase LDH-1 and LDH-5 isoforms in the rat brain. *Neuroscience* 96:619-625.

Le Loirec C, Champion C. (2007) Track structure simulation for positron emitters of medical interest. Part I: The case of the allowed decay isotopes. *Nuclear Instruments & Methods in Physics Research Section a-Accelerators Spectrometers Detectors and Associated Equipment* 582:644-653.

Lear JL, Kasliwal RK. (1991) Autoradiographic measurement of cerebral lactate transport rate constants in normal and activated conditions. *J Cereb Blood Flow Metab* 11:576-580.

Lebon V, Petersen KF, Cline GW, Shen J, Mason GF, Dufour S, Behar KL, Shulman GI, Rothman DL. (2002) Astroglial contribution to brain energy metabolism in humans revealed by 13C nuclear magnetic resonance spectroscopy: elucidation of the dominant pathway for neurotransmitter glutamate repletion and measurement of astrocytic oxidative metabolism. *J Neurosci* 22:1523-1531.

Lindauer U, Villringer A, Dirnagl U. (1993) Characterization of CBF response to somatosensory stimulation: model and influence of anesthetics. *Am J Physiol* 264:H1223-1228.

Lindner O, Sorensen J, Vogt J, Fricke E, Baller D, Horstkotte D, Burchert W. (2006) Cardiac efficiency and oxygen consumption measured with 11C-acetate PET after long-term cardiac resynchronization therapy. *J Nucl Med* 47:378-383.

Loaiza A, Porras OH, Barros LF. (2003) Glutamate triggers rapid glucose transport stimulation in astrocytes as evidenced by real-time confocal microscopy. *J Neurosci* 23:7337-7342.

Lovatt D, Sonnewald U, Waagepetersen HS, Schousboe A, He W, Lin JHC, Han X, Takano T, Wang S, Sim FJ, Goldman SA, Nedergaard M. (2007) The transcriptome and metabolic gene signature of protoplasmic Astrocytes in the adult murine cortex. *Journal of Neuroscience* 27:12255-12266.

Magistretti PJ. (1999) Brain Energy Metabolism. In: *Fundamental Neuroscience* (J. ZM, Bloom FE, Landis SC et al., eds), New York: Academic Press, pp 389-413.

Magistretti PJ, Pellerin L. (1999) Astrocytes Couple Synaptic Activity to Glucose Utilization in the Brain. *News Physiol Sci* 14:177-182.

Magistretti PJ, Pellerin L, Rothman DL, Shulman RG. (1999) Energy on demand. *Science* 283:496-497.

Maher F, Vannucci SJ, Simpson IA. (1993) Glucose transporter isoforms in brain: absence of GLUT3 from the blood-brain barrier. *J Cereb Blood Flow Metab* 13:342-345.

Maher F, Vannucci SJ, Simpson IA. (1994) Glucose transporter proteins in brain. *Faseb J* 8:1003-1011.

Martin C, Martindale J, Berwick J, Mayhew J. (2006a) Investigating neural-hemodynamic coupling and the hemodynamic response function in the awake rat. *Neuroimage* 32:33-48.

Martin PM, Gopal E, Ananth S, Zhuang L, Itagaki S, Prasad BM, Smith SB, Prasad PD, Ganapathy V. (2006b) Identity of SMCT1 (SLC5A8) as a neuron-specific Na+-coupled transporter for active uptake of L-lactate and ketone bodies in the brain. *J Neurochem* 98:279-288.

Martin WR, Wieler M, Hanstock CC. (2007) Is brain lactate increased in Huntington's disease? *J Neurol Sci.* 263:70-74.

Martinez-Hernandez A, Bell KP, Norenberg MD. (1977) Glutamine synthetase: glial localization in brain. *Science* 195:1356-1358.

Mason GF, Petersen KF, Lebon V, Rothman DL, Shulman GI. (2006) Increased brain monocarboxylic acid transport and utilization in type 1 diabetes. *Diabetes* 55:929-934.

McEwen BS, Reagan LP. (2004) Glucose transporter expression in the central nervous system: relationship to synaptic function. *Eur J Pharmacol* 490:13-24.

McIlwain H. (1953) Substances which support respiration and metabolic response to electrical impulses in human cerebral tissues. *J Neurol Neurosurg Psychiatry* 16:257-266.

McKenna MC, Hopkins IB, Carey A. (2001) Alpha-cyano-4-hydroxycinnamate decreases both glucose and lactate metabolism in neurons and astrocytes: implications for lactate as an energy substrate for neurons. *J Neurosci Res* 66:747-754.

Mikolajczyk K, Szabatin M, Rudnicki P, Grodzki M, Burger C. (1998) A JAVA environment for medical image data analysis: initial application for brain PET quantitation. *Med Inform (Lond)* 23:207-214.

Millet P, Sallanon MM, Petit JM, Charnay Y, Vallet P, Morel C, Cespuglio R, Magistretti PJ, Ibanez V. (2004) In vivo measurement of glucose utilization in rats using a beta-microprobe: direct comparison with autoradiography. *J Cereb Blood Flow Metab.* 24:1015-1024.

Minchin MC, Beart PM. (1975a) Compartmentation of amino acid metabolism in the rat dorsal root ganglion; a metabolic and autoradiographic study. *Brain Res* 83:437-449.

Minchin MC, Beart PM. (1975b) Compartmentation of amino acid metabolism in the rat posterior pituitary. *J Neurochem* 24:881-884.

Mintun MA, Raichle ME, Martin WR, Herscovitch P. (1984) Brain oxygen utilization measured with O-15 radiotracers and positron emission tomography. *J Nucl Med* 25:177-187.

Morgello S, Uson RR, Schwartz EJ, Haber RS. (1995) The human blood-brain barrier glucose transporter (GLUT1) is a glucose transporter of gray matter astrocytes. *Glia* 14:43-54.

Mosconi L. (2005) Brain glucose metabolism in the early and specific diagnosis of Alzheimer's disease. FDG-PET studies in MCI and AD. *Eur J Nucl Med Mol Imaging* 32:486-510.

Muir D, Berl S, Clarke DD. (1986) Acetate and fluoroacetate as possible markers for glial metabolism in vivo. *Brain Res* 380:336-340.

Nakao Y, Itoh Y, Kuang TY, Cook M, Jehle J, Sokoloff L. (2001) Effects of anesthesia on functional activation of cerebral blood flow and metabolism. *Proc Natl Acad Sci U S A* 98:7593-7598.

Nehlig A, Pereira de Vasconcelos A. (1993) Glucose and ketone body utilization by the brain of neonatal rats. *Prog Neurobiol* 40:163-221.

Nehlig A, Wittendorp-Rechenmann E, Lam CD. (2004) Selective uptake of [14C]2-deoxyglucose by neurons and astrocytes: high-resolution microautoradiographic imaging by cellular 14C-trajectography combined with immunohistochemistry. *J Cereb Blood Flow Metab.* 24:1004-1014.

Norenberg MD, Martinez-Hernandez A. (1979) Fine structural localization of glutamine synthetase in astrocytes of rat brain. *Brain Res* 161:303-310.

Obrenovitch TP, Zilkha E. (2001) Microdialysis coupled to online enzymatic assays. *Methods* 23:63-71.

Ogawa S, Tank DW, Menon R, Ellermann JM, Kim SG, Merkle H, Ugurbil K. (1992) Intrinsic signal changes accompanying sensory stimulation: functional brain mapping with magnetic resonance imaging. *Proc Natl Acad Sci U S A* 89:5951-5955.

Okazawa H, Yamauchi H, Sugimoto K, Toyoda H, Kishibe Y, Takahashi M. (2001) Effects of acetazolamide on cerebral blood flow, blood volume, and oxygen metabolism: A positron emission tomography study with healthy volunteers. *Journal of Cerebral Blood Flow and Metabolism* 21:1472-1479.

Oz G, Berkich DA, Henry PG, Xu Y, LaNoue K, Hutson SM, Gruetter R. (2004) Neuroglial metabolism in the awake rat brain: CO2 fixation increases with brain activity. *J Neurosci* 24:11273-11279.

Pain F, Besret L, Vaufrey F, Gregoire MC, Pinot L, Gervais P, Ploux L, Bloch G, Mastrippolito R, Laniece P, Hantraye P, Zimmer L, Mauger G, Plenevaux A, Le Bars D, Pujol JF, Renaud B. (2002a) In vivo quantification of localized neuronal activation and inhibition in the rat brain using a dedicated high temporal-resolution beta +-sensitive microprobe. *Proc Natl Acad Sci U S A.* 99:10807-10812.

Pain F, Laniece P, Mastrippolito R, Charon Y, Comar D, Leviel V, Pajol JF, Valentin L. (2000) SIC, an intracerebral radiosensitive probe for *in vivo* neuropharmacology investigations in small laboratory animals. *IEEE Transactions on Nuclear Science* 47:25-32.

Pain F, Laniece P, Mastrippolito R, Pinot L, Charon Y, Glatigny A, Guillemin MT, Hantraye P, Leviel V, Menard L, Valentin L. (2002b) SIC, an intracerebral radiosensitive probe for *in vivo* neuropharmacology investigations in small laboratory animals: prototype design,

characterization, and in vivo evaluation. *IEEE Transactions on Nuclear Science* 49:822-826.

Paulson OB. (2002) Blood-brain barrier, brain metabolism and cerebral blood flow. *European Neuropsychopharmacology* 12:495-501.

Paxinos G, Watson C. (1998) *The Rat Brain in Stereotaxic Coordinates*. San Diego: Academic Press.

Pellerin L. (2003) Lactate as a pivotal element in neuron-glia metabolic cooperation. *Neurochem Int* 43:331-338.

Pellerin L, Bouzier-Sore AK, Aubert A, Serres S, Merle M, Costalat R, Magistretti PJ. (2007) Activity-dependent regulation of energy metabolism by astrocytes: An update. *Glia* 55:1251-1262.

Pellerin L, Magistretti PJ. (1994) Glutamate uptake into astrocytes stimulates aerobic glycolysis: a mechanism coupling neuronal activity to glucose utilization. *Proc Natl Acad Sci U S A* 91:10625-10629.

Pellerin L, Magistretti PJ. (2003) Food for thought: challenging the dogmas. *J Cereb Blood Flow Metab* 23:1282-1286.

Pellerin L, Pellegri G, Martin JL, Magistretti PJ. (1998) Expression of monocarboxylate transporter mRNAs in mouse brain: support for a distinct role of lactate as an energy substrate for the neonatal vs. adult brain. *Proc Natl Acad Sci U S A* 95:3990-3995.

Phelps ME, Hoffman EJ, Mullani NA, Ter-Pogossian MM. (1975) Application of annihilation coincidence detection to transaxial reconstruction tomography. *J Nucl Med* 16:210-224.

Phelps ME, Mazziotta JC, Huang SC. (1982) Study of cerebral function with positron computed tomography. *J Cereb Blood Flow Metab* 2:113-162.

Phelps ME, Mazziotta JC, Schelbert HR. (1986) *Positron Emission Tomography and Autoradiography: Principles and Applications for the Brain and the Heart*. New York: Raven Press.

Pierre K, Magistretti PJ, Pellerin L. (2002) MCT2 is a major neuronal monocarboxylate transporter in the adult mouse brain. *J Cereb Blood Flow Metab* 22:586-595.

Pierre K, Pellerin L. (2005) Monocarboxylate transporters in the central nervous system: distribution, regulation and function. *J Neurochem* 94:1-14.

Prichard JW, Shulman RG. (1986) NMR spectroscopy of brain metabolism in vivo. *Annu Rev Neurosci* 9:61-85.

Qu H, Haberg A, Haraldseth O, Unsgard G, Sonnewald U. (2000) (13)C MR spectroscopy study of lactate as substrate for rat brain. *Dev Neurosci* 22:429-436.

Raichle ME. (2003) Functional brain imaging and human brain function. *J Neurosci* 23:3959-3962.

Raichle ME, Mintun MA. (2006) Brain work and brain imaging. *Annu Rev Neurosci* 29:449-476.

Reivich M, Kuhl D, Wolf A, Greenberg J, Phelps M, Ido T, Casella V, Fowler J, Gallagher B, Hoffman E, Alavi A, Sokoloff L. (1977) Measurement of local cerebral glucose metabolism in man with 18F-2-fluoro-2-deoxy-d-glucose. *Acta Neurol Scand Suppl* 64:190-191.

Reivich M, Kuhl D, Wolf A, Greenberg J, Phelps M, Ido T, Casella V, Fowler J, Hoffman E, Alavi A, Som P, Sokoloff L. (1979) The [18F]fluorodeoxyglucose method for the measurement of local cerebral glucose utilization in man. *Circ Res.* 44:127-137.

Renkin EM. (1959) Transport of potassium-42 from blood to tissue in isolated mammalian skeletal muscles. *Am J Physiol* 197:1205-1210.

Rowland DJ, Cherry SR. (2008) Small-animal preclinical nuclear medicine instrumentation and methodology. *Semin Nucl Med* 38:209-222.

Roy CS, Sherrington CS. (1890) On the Regulation of the Blood-supply of the Brain. *J Physiol* 11:85-185.

Sakurada O, Kennedy C, Jehle J, Brown JD, Carbin GL, Sokoloff L. (1978) Measurement of local cerebral blood flow with iodo [14C] antipyrine. *Am J Physiol* 234:H59-66.

Savaki HE, Davidsen L, Smith C, Sokoloff L. (1980) Measurement of free glucose turnover in brain. *J Neurochem* 35:495-502.

Schurr A. (2005) Lactate: the ultimate cerebral oxidative energy substrate? *J Cereb Blood Flow Metab* 26:142.152.

Schurr A, Miller JJ, Payne RS, Rigor BM. (1999) An increase in lactate output by brain tissue serves to meet the energy needs of glutamate-activated neurons. *J Neurosci* 19:34-39.

Schurr A, Payne RS, Miller JJ, Tseng MT, Rigor BM. (2001) Blockade of lactate transport exacerbates delayed neuronal damage in a rat model of cerebral ischemia. *Brain Res* 895:268-272.

Schurr A, West CA, Rigor BM. (1988) Lactate-supported synaptic function in the rat hippocampal slice preparation. *Science* 240:1326-1328.

Serres S, Bezancon E, Franconi JM, Merle M. (2004) Ex vivo analysis of lactate and glucose metabolism in the rat brain under different states of depressed activity. *J Biol Chem* 279:47881-47889.

Serres S, Bezancon E, Franconi JM, Merle M. (2005) Ex vivo NMR study of lactate metabolism in rat brain under various depressed states. *J Neurosci Res* 79:19-25.

Serres S, Bouyer JJ, Bezancon E, Canioni P, Merle M. (2003) Involvement of brain lactate in neuronal metabolism. *NMR Biomed* 16:430-439.

Serres S, Raffard G, Franconi JM, Merle M. (2008) Close coupling between astrocytic and neuronal metabolisms to fulfill anaplerotic and energy needs in the rat brain. *J Cereb Blood Flow Metab* 28:712-724.

Shen J, Petersen KF, Behar KL, Brown P, Nixon TW, Mason GF, Petroff OA, Shulman GI, Shulman RG, Rothman DL. (1999) Determination of the rate of the glutamate/glutamine cycle in the human brain by in vivo 13C NMR. *Proc Natl Acad Sci U S A* 96:8235-8240.

Sibson NR, Dhankhar A, Mason GF, Rothman DL, Behar KL, Shulman RG. (1998) Stoichiometric coupling of brain glucose metabolism and glutamatergic neuronal activity. *Proc Natl Acad Sci U S A* 95:316-321.

Siesjo BK. (1978) *Brain Energy Metabolism*. New York.

Simpson IA, Chundu KR, Davies-Hill T, Honer WG, Davies P. (1994) Decreased concentrations of GLUT1 and GLUT3 glucose transporters in the brains of patients with Alzheimer's disease. *Ann Neurol* 35:546-551.

Smith D, Pernet A, Hallett WA, Bingham E, Marsden PK, Amiel SA. (2003) Lactate: a preferred fuel for human brain metabolism in vivo. *J Cereb Blood Flow Metab* 23:658-664.

Sokoloff. (1989) *Circulation and energy metabolism of the brain*. New York: Raven Press.

Sokoloff L, Reivich M, Kennedy C, Des Rosiers MH, Patlak CS, Pettigrew KD, Sakurada O, Shinohara M. (1977) The [14C]deoxyglucose method for the measurement of local cerebral glucose utilization: theory, procedure, and normal values in the conscious and anesthetized albino rat. *J Neurochem.* 28:897-916.

Sonnewald U, Kondziella D. (2003) Neuronal glial interaction in different neurological diseases studied by ex vivo 13C NMR spectroscopy. *NMR Biomed* 16:424-429.

Tabernero A, Vicario C, Medina JM. (1996) Lactate spares glucose as a metabolic fuel in neurons and astrocytes from primary culture. *Neurosci Res* 26:369-376.

Tyce GM, Ogg J, Owen CA, Jr. (1981) Metabolism of acetate to amino acids in brains of rats after complete hepatectomy. *J Neurochem* 36:640-650.

Tyson RL, Gallagher C, Sutherland GR. (2003) 13C-Labeled substrates and the cerebral metabolic compartmentalization of acetate and lactate. *Brain Res* 992:43-52.

Van den Berg CJ, Krzalic L, Mela P, Waelsch H. (1969) Compartmentation of glutamate metabolism in brain. Evidence for the existence of two different tricarboxylic acid cycles in brain. *Biochem J* 113:281-290.

Van den Berg CJ, Ronda G. (1976) The incorporation of double-labelled acetate into glutamate ad related amino acids from adult mouse brain: compartmentation of amino acid metabolism in brain. *J Neurochem* 27:1443-1448.

Vannucci SJ, Clark RR, Koehler-Stec E, Li K, Smith CB, Davies P, Maher F, Simpson IA. (1998) Glucose transporter expression in brain: relationship to cerebral glucose utilization. *Dev Neurosci* 20:369-379.

Vannucci SJ, Maher F, Simpson IA. (1997) Glucose transporter proteins in brain: delivery of glucose to neurons and glia. *Glia* 21:2-21.

Volterra A, Meldolesi J. (2005) Astrocytes, from brain glue to communication elements: the revolution continues. *Nat Rev Neurosci* 6:626-640.

Waniewski RA, Martin DL. (1998) Preferential utilization of acetate by astrocytes is attributable to transport. *J Neurosci* 18:5225-5233.

Watanabe H, Passonneau JV. (1973) Factors affecting the turnover of cerebral glycogen and limit dextrin in vivo. *J Neurochem* 20:1543-1554.

Weber B, Burger C, Biro P, Buck A. (2002a) A femoral arteriovenous shunt facilitates arterial whole blood sampling in animals. *Eur J Nucl Med Mol Imaging* 29:319-323.

Weber B, Fouad K, Burger C, Buck A. (2002b) White matter glucose metabolism during intracortical electrostimulation: a quantitative [(18)F]Fluorodeoxyglucose autoradiography study in the rat. *Neuroimage* 16:993-998.

Weber B, Spath N, Wyss M, Wild D, Burger C, Stanley R, Buck A. (2003) Quantitative cerebral blood flow measurements in the rat using a beta-probe and H2 15O. *J Cereb Blood Flow Metab* 23:1455-1460.

Weber S, Bauer A. (2004) Small animal PET: aspects of performance assessment. *Eur J Nucl Med Mol Imaging* 31:1545-1555.

Whitehouse S, Cooper RH, Randle PJ. (1974) Mechanism of activation of pyruvate dehydrogenase by dichloroacetate and other halogenated carboxylic acids. *Biochem J* 141:761-774.

Wolfe RR, Jahoor F. (1990) Recovery of labeled CO2 during the infusion of C-1- vs C-2-labeled acetate: implications for tracer studies of substrate oxidation. *Am J Clin Nutr* 51:248-252.

Wyss MT, Ametamey SM, Treyer V, Bettio A, Blagoev M, Kessler LJ, Burger C, Weber B, Schmidt M, Gasparini F, Buck A. (2007) Quantitative evaluation of 11C-ABP688 as PET ligand for the measurement of the metabotropic glutamate receptor subtype 5 using autoradiographic studies and a beta-scintillator. *Neuroimage* 35:1086-1092.

Wyss MT, Weber B, Treyer V, Heer S, Pellerin L, Magistretti PJ, Buck A. (2009) Stimulation-induced increases of astrocytic oxidative metabolism in rats and humans investigated with 1-11C-acetate. *J Cereb Blood Flow Metab* 29:44-56.

Yee SH, Lee K, Jerabek PA, Fox PT. (2006) Quantitative measurement of oxygen metabolic rate in the rat brain using microPET imaging of briefly inhaled 15O-labelled oxygen gas. *Nucl Med Commun* 27:573-581.

Zielke HR, Collins RM, Jr., Baab PJ, Huang Y, Zielke CL, Tildon JT. (1998) Compartmentation of [14C]glutamate and [14C]glutamine oxidative metabolism in the rat hippocampus as determined by microdialysis. *J Neurochem* 71:1315-1320.

Zielke HR, Zielke CL, Baab PJ. (2007) Oxidation of (14)C-labeled compounds perfused by microdialysis in the brains of free-moving rats. *J Neurosci Res.*

List of Publications

Articles in peer reviewed journals *during* the MD PhD program

Wyss M.T., Hofer S., Brühlmeyer M., Hefti M., Uhlmann C., Bärtschi E., Buettner U.W. and Roelcke U. (2009) Early metabolic responses in temozolomide treated low-grade glioma patients. *J Neurooncology, in revision.*

Zakharov P., Völker A.C., **Wyss M.T.**, Haiss F., Calcinaghi N., Zunzunegui C., Buck A., Scheffold F. and Weber B. (2009) Dynamic laser speckle imaging of cerebral blood flow. *Submitted to J Cereb Blood Flow and Metab.*

Gosh A., Haiss F., Sydekum E., Schneider R., Gullo M., **Wyss M.T.**, Mueggler T., Rudin M., Weber B. and Schwab M.E. (2009) Rewiring of axotomised hindlimb corticospinal neurons in paraparetic adult rats. *Nat Neurosci, in revision.*

Haiss F., Jolivet R.*, **Wyss M.T**.*, Reichold J., Braham N.B., Scheffold F., Krafft M.P. and Weber B. (2009) Lifting the curtain: Improved In vivo two-photon imaging after blood replacement by perfluorocarbon. *Submitted to J Physiol*.
(* = contributed equally)

Wyss M.T., Obrist N.M., Haiss F., Eckert R., Stainley R., Burger C., Buck A. and Weber B. (2009) Novel high sensitivity beta-scintillator for cortical measurements of radiotracer kinetics in the rodent brain. *Submitted J Nucl Med.*

Wyss M.T., Weber B., Treyer V., Heer S., Pellerin L., Magistretti P.J. and Buck A. (2009) Stimulation-induced Increases of Astrocytic oxidative metabolism in rats and humans investigated with 1-^{11}C-acetate. *J Cereb Blood Flow Metab;* 29; 44-56.

Treyer V., Streffer J., **Wyss M.T.**, Bettio A., Ametamey S.M., Fischer U., Schmidt M., Gasparini F., Hock C. and Buck A. (2007) Evaluation of the metabotropic glutamate receptor subtype 5 using PET and ^{11}C-ABP688, assessment of methods, *J Nucl Med*; 48; 1207-1215.

Wyss M.T., Hofer S., Hefti M., Bärtschi E., Uhlmann C., Treyer V. and Roelcke U. (2007) Spatial heterogeneity of low-grade gliomas at the capillary level. A PET study on tumor blood flow and amino acid uptake, *J Nucl Med*; 48; 1047-1052.

Wyss M.T., Spaeth N., Biollaz G., Pahnke J., Alessi P., Trachsel E., Treyer V., Weber B., Neri D. and Buck A. (2007) Uptake of ^{18}F-fluorocholine, ^{18}F-fluoro-ethyl-L-tyrosine and ^{18}F-fluoro-2-deoxyglucose in C6 gliomas and correlation with ^{131}I-labeled SIP(L19), a marker of angiogenesis, *J Nucl Med*; 48; 608-614.

Roelcke U., **Wyss M.**, Bärtschi E., Hofer S. (2007) Metabolic deactivation of low-grade glioma during chemotherapy, *J Neurology*; 254; 668-669.

Von Lukowicz T., Silacci M., **Wyss M.T.**, Trachsel E., Lohmann C., Buck A., Lüscher T.F., Neri D. and Matter C.M. (2007) The human antibody against the C Domain of Tenascin-C images murine atherosclerotic plaques ex vivo, *J Nucl Med*; 48; 582-587.

Ametamey S.M., Treyer V., Streffer J., **Wyss M.T.**, Schmidt M., Blagoev M., Hintermann S., Auberson Y., Gasparini F., Fischer U.C. and Buck A. (2007) Human PET Studies of Metabotropic Glutamate Receptor Subtype 5 with 11C-ABP688, *J Nucl Med*; 48; 247-252.

Wyss M.T., Ametamey S.M., Treyer V., Bettio A., Blagoev M., Kessler L.J., Burger C., Weber B., Schmidt M., Gasparini F. and Buck A. (2007) Quantitative evaluation of ^{11}C-ABP688 as PET ligand for the measurement of the metabotropic glutamate receptor subtype 5 using autoradiographic studies and a beta-Scintillator, *Neuroimage*; 35; 1086-1092.

Matter C.M., **Wyss M.T.**, Meier P., Späth N., von Lukowicz T., Lohmann C., Weber B., de Molina A.R., Lacal J.C., Ametamey S.M., von Schulthess G.K., Lüscher T.F., Kaufmann P.A. and Buck A. (2006) ^{18}F-Choline images murine atherosclerotic plaques ex vivo, *ATVB*; 26: 584-589.

Späth N, **Wyss M.T.**, Pahnke J., Biollaz G., Lutz A., Goepfert K., Westera G., Treyer V., Weber B. and Buck A. (2006) Uptake of ^{18}F-fluorocholine, ^{18}F-fluoro-ethyl-L-tyrosine and ^{18}F-fluoro-2-deoxyglucose in F98 gliomas in the rat, *Eur J Nucl Med Mol Imaging*; 33: 673-682.

Wyss M.T., Honer M., Schubiger P.A. and Ametamey S.M. (2006) NanoPET imaging of [^{18}F]Fluoromisonidazole uptake in experimental mouse tumours, *Eur J Nucl Med Mol Imaging*; 33; 311-318.

Späth N., **Wyss M.T.**, Pahnke J., Biollaz G., Trachsel E., Drandarov K., Treyer V., Weber B., Neri D. and Buck A. (2006) Radioimmunotherapy targeting the extra domain B of fibronectin in C6 rat gliomas: a preliminary study about the therapeutic efficacy of iodine-131-labeled SIP(L19), *Nucl Med Biol*; 33(5); 661-666.

Ametamey S.M., Kessler L.J., Honer M., **Wyss M.T.**, Buck A., Hintermann S., Auberson Y.P., Gasparini F. and Schubiger P.A. (2006) Radiosynthesis and preclinical evaluation of 11C-ABP688 as a probe for imaging the metabotropic glutamate receptor subtype 5, *J Nucl Med*; 47(4); 698-705.

Allemann K., **Wyss M.T.**, Wergin M., Ohlerth S., Rohrer-Bley C., Evans S.M., Schubiger A.P., Ametamey S.M. and Kaser-Hotz B (2005) Measurements of hypoxia ([^{18}F]-FMISO, [^{18}F]-EF5) with positron emission tompgraphy (PET) and perfusion using PET ([^{15}O]-H_2O) and power Doppler ultrasonography in feline fibrosarcomas, *Veterinary and Comparative Oncology*; 3: 211-221. :

Articles in peer reviewed journals *before* the MD PhD program

Wyss M.T., Weber B., Honer M., Späth N., Ametamey S.M., Westera G., Bode B., Kaim A.H. and Buck A. (2004) 18F-choline in experimental soft tissue infection assessed with autoradiography and high-resolution PET, *Eur J Nucl Med Mol Imaging*; 31; 312-316.

Wyss M.T., Honer M., Späth N., Gottschalk J., Ametamey S.M., Weber B., von Schulthess G.K., Buck A. and Kaim A.H. (2004) Influence of ceftriaxone treatment on FDG uptake – An in vivo [^{18}F]-fluorodeoxyglucose imaging study in soft tissue infections in rats, *Nucl Med Biol*; 31: 875-882.

Späth N., **Wyss M.T.**, Weber B., Scheidegger S., Lutz A., Verwey J., Radovanovic I., Pahnke J., Wild D., Westera G., Weisshaupt D., Hermann D.M., Kaser-Hotz B., Aguzzi A.and Buck A. (2004) Uptake of [^{18}F]-fluorocholine, [^{18}F]-Fluoro-ethyl-L-tyrosine and [^{18}F]-fluoro-2-deoxyglucose in acute cerebral radiation injury in the rat: implications for the separation of radiation necrosis from tumor recurrence, *J Nucl Med*; 45: 1931-1938.

Allemann K., **Wyss M.T.**, Wergin M., Bley C.R., Ametamey S., Brühlmeier M. and Kaser-Hotz B. (2004) Positron emission tomography: diagnostic imaging on a molecular level, *Schweiz Arch Tierheilkd*; 146: 359-364.

Weber B., Burger C., **Wyss M.T**., von Schulthess G.K., Scheffold F. and Buck A. (2004) Optical imaging of the spatiotemporal dynamics of cerebral blood flow and oxidative metabolism in the rat barrel cortex, *Eur J Neuroscience*; 20: 2664-2670.

Kamel E.M., Zwahlen D., **Wyss M.T.**, Stumpe K.D., von Schulthess G.K. and Steinert H.C. (2003) Whole-body [^{18}F]FDG PET improves the management of patients with small cell lung cancer, *J Nucl Med*; 44: 1911-1917.

Kamel E.M., **Wyss M.T.**, Fehr M.K., von Schulthess G.K. and Goerres G.W. (2003)

[^{18}F]-Fluorodeoxyglucose positron emission tomography in patients with suspected recurrence of breast cancer. *J Cancer Res Clin Oncol*; 129; 147-153.

Weber B., Späth N., **Wyss M**., Wild D., Burger C., Stanley R. and Buck A. (2003) Quantitative cerebral blood flow measurements in the rat using a Beta-probe and $H_2{}^{15}O$, *J Cereb Blood Flow Metab*; 23: 1455-1460.

Thesis

Wyss M.T. (2003) Glukosestoffwechsel und Vaskularisierung des Rattenhirns mit besonderer Berücksichtigung des Corpus callosum. MD Thesis, University of Zürich, Medical Faculty.

Poster presentations and talks

Wyss M.T., Obrist N., Aznavour N., Magistretti P.J., Buck A., Weber B. (2009) Cerebral glucose utilization measurements using a beta probe and ^{18}F-fluorodeoxyglucose: Impact of lactate. SSN Annual Meeting 2009, Fribourg, Switzerland.

Calcinaghi N.*, Jolivet R.*, **Wyss M.T.***, Zunzunegui C., Gasparini F., Buck A., Weber B. (2009) Blockade of the metabotropic glutamate receptor mGluR5 does not affect neurovascular coupling in adult Sprague-Dawley rats. SSN Annual Meeting 2009, Fribourg, Switzerland.
(* these authors contributed equally to this work)

Lanz B., **Wyss M.T.**, Weber B., Buck A., Gruetter R. (2009) Measurements of glial metabolic fluxes with 11C-acetate using positron emission and an adapted NMR-based metabolic modeling approach. XXXIVth International Symposium on Cerebral Blood Flow, Metabolism and Function and the IXth International Conference on Quantification of Brain Function 2009, Chicago, Illinois, USA.

Lanz B., Xin L., **Wyss M.T.**, Weber B., Buck A., Gruetter R. (2008) Measurements of glial metabolic fluxes with ^{11}C-acetate using positron emission and ^{1}H{^{13}C}NMR spectroscopy. ISMRM 17th scientific meeting, Honolulu, Hawai'i.

Aznavour N., **Wyss M.**, Weber B., Buck A., Magistretti P.J. (2008) In vivo measurement of cerebral metabolic rate of glucose using beta microprobes and [^{18}F]FDG: Preliminary results. CIBM seminar, Lausanne, Switzerland.

Wyss M.T., Obrist N., Haiss F., Buck A., Weber B. (2008) Novel high-sensitivity beta-probe for quantitative modelling of radiotracer kinetics in the rodent brain, ZNZ Symposium, Zürich, Switzerland.

Hasler F., Quednow B.B., Treyer V., **Wyss M.T.**, Schubiger P.A., Buck A., Vollenweider F.X. (2008) Hallucinogenic drug effects of psilocybin are mediated by serotonin-2A receptors in the human anterior cingulated and medial prefrontal cortex. ZNZ, Zürich, Switzerland.

Quednow B.B., Hasler F., Treyer V., **Wyss M.T.**, Schubiger P.A., Buck A., Vollenweider F.X. (2008) Assessment of serotonin release capacity in the human brain using dexfenfluramine challenge and [^{18}F]altanserin PET. ZNZ, Zürich, Switzerland.

Glatthar R., Vranesic I., Desrayaud S., Fendt M., Hoyer D., Auberson Y., McAllister K., **Wyss M.T.**, Buck A. (2008) Correlation of efficacy, PK and central receptor occupancy of three mGluR5 antagonists. 4th Modern Drug Discovery & Development Summit, San Diego, CA, USA.

Vranesic I., Glatthar R., Desravaud S., Fendt M., Hoyer D., Auberson Y., McAllister K.H., **Wyss M.**, Buck A. (2008) Quantitative evaluation of central mGlu5 receptor occupancy in vivo by a novel mGluR5 antagonist in the rat. 6th international Meeting on Metabotropic Glutamate Receptors 2008. Taormina, Italy.

Wyss M.T. (2008) Radiotracer perspective on cerebral metabolic compartmentation. Pharma Day, Zürich, Switzerland.

Wyss M.T., Obrist N., Haiss F., Buck A., Weber B. (2008) Novel high-sensitivity beta-probe for quantitative modelling of radiotracer kinetics in the rodent brain, Pharma Day, Zürich, Switzerland.

Weber B., Jolivet R., **Wyss M.T.**, Reichold J., Krafft P.M., Haiss F. (2008) Improved in-vivo 2-photon imaging after blood replacement by perfluorocarbon transfusion, SNF, Washington, USA.

Wyss M.T., Obrist N., Haiss F., Buck A., Weber B. (2008) Novel high-sensitivity beta-probe for quantitative modelling of radiotracer kinetics in the rodent brain, FENS, Geneva, Switzerland.

Wyss M., Hofer S., Bruehlmeier M., Hefti M., Uhlmann C., Bärtschi E., Buettner U, Roelcke U. (2008) Early metabolic response in temozolomide treated low-grade glioma patients. Schweiz. Arch. Neurol Psych. 2008, 159, 282.

Wyss M., Weber B., Pellerin L., Magistretti P., Buck A. (2007) Marker for a better understanding of astrocytic oxidative metabolism: Kinetics of 1-^{11}C-acetate, SSN Joint Meeting, Berne, Switzerland.

Geissler E., Ametamey S., Bodenmann S., Treyer V., **Wyss M.**, Rétey J, Achermann P., Schubiger A., Landolt H. (2007) Electroencephalographic alpha activity reflects cerebral adenosine A1 receptor occupancy in humans, SSN Joint Meeting, Berne, Switzerland.

Weber B., **Wyss M.**, Haiss F., Zakharov P., Voelker A., Scheffold F., Buck A. (2007) Optical imaging of blood flow and metabolism in the rat somatosensory cortex, SSN Joint Meeting, Berne, Switzerland.

Hasler F., Quednow B. B., Treyer V., **Wyss M.T.**, Schubiger P.A., Vollenweider F.X. (2007) Assessment of serotonin release capacity in the human brain using dexfenfluramine challenge and [18F]altanserin positron emission tomography. Proof of concept, Congress of European College of Neuropsychopharmacology, Vienna, Austria.

Wyss M.T., Uhlmann C., Bärtschi E., Brühlmeier M., Hofer S., Hefti M., Treyer V., Roelcke U. (2007) FET PET imaging as a response marker of low-gradeglioma to low-dose temozolomide chemotherapy in MR stable disease patients. Nuklearmedizin, 46: A140.

Voelker A., Zakharov P., **Wyss M.T**., Haiss F., Buck A., Scheffold, Weber B. (2007) Improved laser speckle contrast imaging of cerebral blood flow. 8. ZNZ Symposium, Zürich, Switzerland.

Wyss M.T., Obrist N., Buck A., Weber B. (2007) Novel high-sensitivity beta-probe for quantitative modelling of radiotracer kinetics in the brain. 8. ZNZ Symposium, Zürich, Switzerland.

Wyss M, Hofer S, Hefti M, Bärtschi E, Uhlmann C, Roelcke U. (2006) Patterns of microvessel density (MVD) and blood flow (CBF) in low-grade gliomas (LGG). A PET study. *J Neurol,* 253, S2:59.

Wyss M, Uhlmann C, Bärtschi E, Bruehlmeier M, Hofer S, Hefti M, Roelcke U. (2006) Low-dose continuous chemotherapy produces pronounced metabolic responses in MR stable disease patients with low-grade glioma (LGG). *J Neurol,* 253, S2:60.

Wyss M. T., Bärtschi E., Hofer S., Roelcke U. (2006) Monitoring chemotherapy response in low-grade glioma using ^{18}F-FET and positron emission tomography. *Nuklearmedizin*, 45; A143.

Wyss M.T., Treyer V., Heer S., Drandarov K. and Buck A. (2006) Investigation of the astrocytic oxidative metabolism using ^{11}C-acetate, Jahrestreffen der Swiss Society of Neuroscience, Basel

Wyss M.T., Hofer, S., Hefti M., Bärtschi E., Uhlmann C. and Roelcke U. (2006) Patterns of microvessel density and blood flow in low-grade gliomas: A PET study, 16. Meeting of the European Neurological Society, Lausanne

Wyss M.T., Uhlmann C., Bärtschi E., Brühlmeier M., Hofer S., Hefti M and Roelcke U. (2006) Low-dose chemotherapy produces pronounced metabolic responses in MR stable disease patients with low-grade glioma (LGG), 16 Meeting of the European Neurological Society, Lausanne

Wyss M.T., Uhlmann C., Bärtschi E., Treyer V., Brühlmeier M., Hofer S., Hefti M. and Roelcke U. (2006) Monitoring chemotherapy response in low-grade glioma using ^{18}F-FET and positron emission tomography, 7. Jahreskongress der Schweiz. Gesellschaft für Nuklearmedizin, Lausanne.

von Lukowicz T., Silacci M., Trachsel E., Lohmann C., **Wyss M.T.**, Buck A., Lüscher T.F., Neri D., Matter C.M. (2006).The human antibody against the C domain of Tenascin-C images murine

atherosclerotic plaques *ex vivo,* Accepted for presentation at the American Heart Association Scientific Sessions 2006, November 12-15, Chicago, USA.

Wyss M.T., Drandarov K., Pellerin L., Magistretti P.-J., Weber B., Buck A. (2006) Using 11C-acetate for the assessment of oxidative astrocytic metabolism, 7th International Conference on Brain Energy Metabolism, Lausanne, Switzerland.

Wyss M.T., Drandarov K., Treyer V., Weber B., Buck A. (2006) Radiolabeled lactate enantiomers: New PET tracers for the investigation of neuronal metabolism in vivo? 6. Gordon Research Conference, Oxford, United Kingdom.

Wyss M.T., Weber B., Pellerin L., Magistretti P.-J., Buck A. (2006)
Astrocytes increase their oxidative energy metabolism during raised neuronal activity – A study using radiolabeled acetate, 7. ZNZ Symposium, Zürich, Switzerland.

Weber B., Zakharov P., Völker A.C., Burger C., **Wyss M.T.**, Scheffold F., Buck A. (2006) High resolution mapping of CBF and oxidative metabolism using laser speckle and flavoprotein imaging in vivo, 7. ZNZ Symposium, Zürich, Switzerland.

Geissler E., Ametamey S.M., Treyer V., **Wyss M.**, Bodenmann S., Rétey J.V., Achermann P. Schubiger P.A., Landolt H.P. (2006) Adenosine A1 receptor occupancy and sleep deprivation: a PET study, 7. ZNZ Symposium, Zürich, Switzerland.

Geissler E., Landolt H., Achermann P., **Wyss M.**, Schubiger P.A., Ametamey S. (2006) Radiosynthesis of [18F] CPFPX as a PET tracer for imaging of adenosine A1 receptor subtype. ZNZ Symposium, Zürich, Switzerland.

Drandarov K., **Wyss M**., Westera G., Schubiger P. and Buck A. (2005) 1-[^{11}C]-D- and L-lactic acid, potential markers of neuronal lactate metabolism, *Eur J Nucl Med Mol Imaging*, 32; Supp. 1 (P756).

Drandarov K., Westera G., **Wyss M**. and Schubiger P.A. (2005) Radiosynthesis of 1-[^{11}C]-D- and L-lactic acid as potential markers of neuronal lactate metabolism, *J Label Compd Radiopharm*, 48; Supp. 1 (S154).

Blagoev M., Ametamey S.M., Bettio A., Mu L., Keller C., Westera G., **Wyss M.**, Buck A., Treyer V., Streffer J., Hock C., Auberson Y., Hintermann S., Schmidt M., Waldvogel E., Moussaoni S., Wiederhold K.H. and Schubiger A.P. (2005) Radiosynthesis and evaluation of 18F-AGC393 as a biological marker of beta-amyloid deposits, *J Label Compd Radiopharm*, 48; Supp. 1 (S319).

Wyss M.T., Bärtschi E., Hofer S., Roelcke U. (2005) Metabolic deactivation of low-grade glioma during chemotherapy, *Schweiz Archiv Neurol Psych*, 156; 391.

Wyss M.T., Drandarov K., Spaeth N., Weber B., Treyer V. and Buck A. (2005) ^{11}C-labeled D- and L-lactate: PET tracers for studies of neuronal energy metabolism? ZNZ Symposium, Zürich, Switzerland.

Geissler E., Landolt H.P., **Wyss M.**, Treyer V., Rétey J., Adam M., Achermann P., Schubiger P.A., Ametamey S. (2005) Investigations of the role of adenosine A1 receptors in human sleep regulation with positron emission tomography (PET), ZNZ Symposium, Zürich, Switzerland.

Wyss M.T., Bärtschi E., Hofer S. and Roelcke U. (2005) Metabolic deactivation of low-grade glioma during low-dose temozolomide chemotherapy, 176. Tagung der SNG, St. Gallen, Switzerland

Wyss M.T., Blagoev M., Allemann K., Bruehlmeier M., Keller C., Rohner Bley C., Wergin M., Koch C.J., Evans S.M., Ametamey S.M., Schubiger P.A. und Kaser-Hotz B. (2004) Hypoxie und Perfusion in spontanen, bösartigen Tumoren bei Hunden gemessen mit ^{18}F-FMISO-, ^{18}F-EF5- und ^{15}O-H_20-PET, *Nuklearmedizin*; 43; A5.

Wyss M., Weber B., Burger C., Scheffold F. and Buck A. (2004) Optical Imaging of CBF and Metabolism in the rat Barrel Cortex, ZNZ Symposium 2004, Zürich, Switzerland